

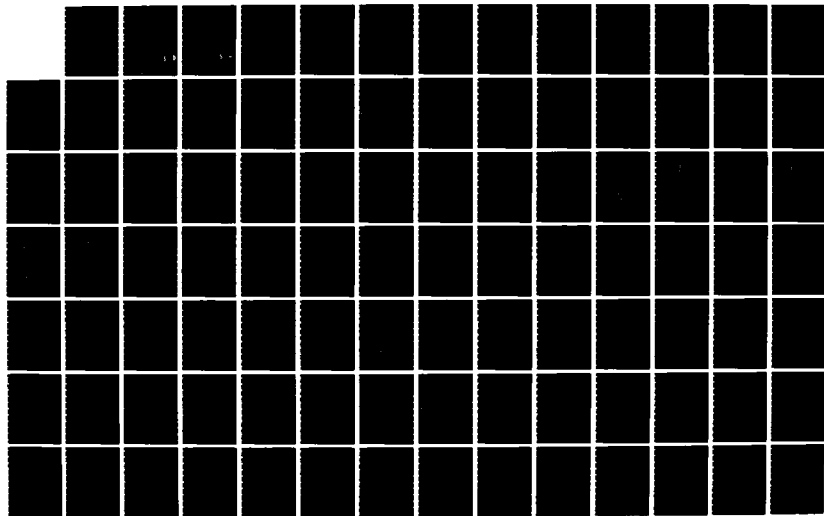
AD-A136 913

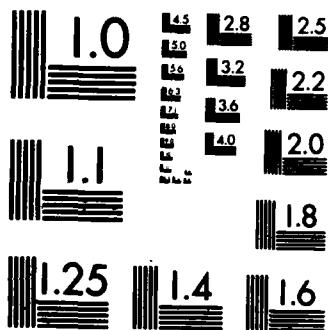
THE EFFECT OF CONSTANT VERSUS OSCILLATORY RATES ON  
DYNAMIC STABILITY DERIVATIVES(U) AIR FORCE INST OF TECH  
WRIGHT-PATTERSON AFB OH SCHOOL OF ENGI... M S LARSON  
DEC 83 AFIT/GAE/ENV/83D-11 F/G 20/4

1/2

UNCLASSIFIED

NL





MICROCOPY RESOLUTION TEST CHART  
NATIONAL BUREAU OF STANDARDS-1963-A

1

ADA136913



THE EFFECT OF CONSTANT VS OSCILLATORY  
 RATES ON DYNAMIC STABILITY  
 DERIVATIVES

THESIS

Michael S. Larson  
 Captain, USAF

DTIC FILE COPY

DTIC  
 ELECTE  
 JAN 18 1984  
 S D E

DEPARTMENT OF THE AIR FORCE  
 AIR UNIVERSITY  
**AIR FORCE INSTITUTE OF TECHNOLOGY**

Wright-Patterson Air Force Base, Ohio

This document has been approved  
 for public release and sales dis-  
 count is authorized.

84 01 17 134

①

THE EFFECT OF CONSTANT VS OSCILLATORY  
RATES ON DYNAMIC STABILITY  
DERIVATIVES

THESIS

Michael S. Larson  
Captain, USAF

AFIT/GAE/ENY/83D-11

**S** DTIC  
ELECTE **D**  
JAN 18 1984  
**E**

Approved for public release; distribution unlimited

AFIT/GAE/ENY/83D-11

THE EFFECT OF CONSTANT VS OSCILLATORY RATES  
ON DYNAMIC STABILITY DERIVATIVES

THESIS

Presented to the Faculty of the School of Engineering  
of the Air Force Institute of Technology

Air University

In Partial Fulfillment of the  
Requirements for the Degree of

Master of Science in Aeronautical Engineering



Michael S. Larson, B.S.

Captain, USAF

December 1983

Accession For	
NTIS GRA&I	<input checked="" type="checkbox"/>
DTIC TAB	<input type="checkbox"/>
Unannounced	<input type="checkbox"/>
Justification	
By _____	
Distribution/	
Availability Codes	
Dist	Avail and/or Special
A-1	

Approved for public release; distribution unlimited

## Acknowledgements

In accomplishing the work connected with this thesis I received extensive help from a large number of people. First and foremost, I am indebted to my advisor, Dr. Robert Calico, for patience and guidance throughout. I also want to thank Jim Schmiesing and Wayne Thor of the F-15 System Program Office and James Bowman of the NASA-Langley Research Center along with the personnel of ASD/ENFTC for their outstanding support in getting information and answering questions in a timely manner. Thanks also goes to my committee, Lt Col Michael Smith and Lt Sal Leone, along with Capt James Hodge for their assistance. Finally, I want to thank my family, Pat, Janelle, and Toni, for their understanding and patience during the disruption, tension, and pain associated with the last twenty months.

Michael S. Larson

## Table of Contents

	Page
Acknowledgements	ii
List of Figures	v
List of Tables	viii
Abstract	ix
I. Introduction	1
Historical Survey	1
Determining the Dynamic Derivatives	4
Purpose of This Thesis	5
II. Topic Discussion	6
Aerodynamic Test Data	6
Oscillatory Rate Phenomena	8
Rotary Balance Force and Moment Data	9
The Dynamic Derivatives	10
III. Approach	12
Data Set Selection	12
Choice of Comparisons	12
IV. Data Analysis	16
The Data Sets	16
Computing the Comparison Parameters	17
Presentation of the Comparison Parameters	18
V. Results	19
Rolling Moment Derivative ( $C_{l_n}$ ) Plots	19
Yawing Moment Derivative ( $C_{n_n}$ ) Plots	21
VI. Conclusions	24
Appendix A: Data from NASA CR 3478	A-1
Appendix B: Data from MDC A0502	B-1
Appendix C: Data from MDC A4172	C-1

	Page
Appendix D: Derivation of the Relation for $C_{i_n}$	D-1
Appendix E: Tabulations and Plots for Each Parameter/Mach Number/Data Set Combination	E-1
Bibliography	Bib-1
Vita	V-1



### List of Figures

Figure		Page
1.	Combined Plot: $C_{1n}$ vs $\alpha$	20
2.	Combined Plot: $C_{nn}$ vs $\alpha$	23
3.	Rotary Balance Data: $C_Y$ vs $nb/2V$ for $8^\circ < \alpha < 16^\circ$ SR = 6 ft	A-2
4.	Rotary Balance Data: $C_Y$ vs $nb/2V$ for $18^\circ < \alpha < 35^\circ$ SR = 6 ft	A-2
5.	Rotary Balance Data: $C_Y$ vs $nb/2V$ for $30^\circ < \alpha < 50^\circ$ SR = 0 ft	A-3
6.	Rotary Balance Data: $C_Y$ vs $nb/2V$ for $55^\circ < \alpha < 90^\circ$ SR = 0 ft	A-3
7.	Rotary Balance Data: $C_1$ vs $nb/2V$ for $8^\circ < \alpha < 16^\circ$ SR = 6 ft	A-4
8.	Rotary Balance Data: $C_1$ vs $nb/2V$ for $18^\circ < \alpha < 35^\circ$ SR = 6 ft	A-4
9.	Rotary Balance Data: $C_1$ vs $nb/2V$ for $30^\circ < \alpha < 50^\circ$ SR = 0 ft	A-5
10.	Rotary Balance Data: $C_1$ vs $nb/2V$ for $55^\circ < \alpha < 90^\circ$ SR = 0 ft	A-5
11.	Rotary Balance Data: $C_n$ vs $nb/2V$ for $8^\circ < \alpha < 16^\circ$ SR = 6 ft	A-6
12.	Rotary Balance Data: $C_n$ vs $nb/2V$ for $18^\circ < \alpha < 35^\circ$ SR = 6 ft	A-6
13.	Rotary Balance Data: $C_n$ vs $nb/2V$ for $30^\circ < \alpha < 50^\circ$ SR = 0 ft	A-7
14.	Rotary Balance Data: $C_n$ vs $nb/2V$ for $55^\circ < \alpha < 90^\circ$ SR = 0 ft	A-7
15.	Design Phase Data: $C_{Yp}$ vs $\alpha$ for 0.2M	B-2
16.	Design Phase Data: $C_{Yr}$ vs $\alpha$ for 0.2M	B-3
17.	Design Phase Data: $C_{1p}$ vs $\alpha$ for 0.2M	B-4

Figure		Page
18.	Design Phase Data: $C_{1_r}$ vs $\alpha$ for 0.2M	B-5
19.	Design Phase Data: $C_{n_p}$ vs $\alpha$ for 0.2M	B-6
20.	Design Phase Data: $C_{n_r}$ vs $\alpha$ for 0.2M	B-7
21.	Design Phase Data: $C_{Y_p}$ vs $\alpha$ for 0.6M	B-8
22.	Design Phase Data: $C_{Y_r}$ vs $\alpha$ for 0.6M	B-9
23.	Design Phase Data: $C_{1_p}$ vs $\alpha$ for 0.6M	B-10
24.	Design Phase Data: $C_{1_r}$ vs $\alpha$ for 0.6M	B-11
25.	Design Phase Data: $C_{n_p}$ vs $\alpha$ for 0.6M	B-12
26.	Design Phase Data: $C_{n_r}$ vs $\alpha$ for 0.6M	B-13
27.	Production Phase Data: $C_{Y_p}$ vs $\alpha$ for 0.3M	C-1
28.	Production Phase Data: $C_{Y_p}$ vs $\alpha$ for 0.6M	C-2
29.	Production Phase Data: $C_{Y_r}$ vs $\alpha$ for 0.3M	C-3
30.	Production Phase Data: $C_{Y_r}$ vs $\alpha$ for 0.6M	C-4
31.	Production Phase Data: $C_{1_p}$ vs $\alpha$ for 0.3M	C-5
32.	Production Phase Data: $C_{1_p}$ vs $\alpha$ for 0.6M	C-6
33.	Production Phase Data: $C_{1_r}$ vs $\alpha$ for 0.3M	C-7
34.	Production Phase Data: $C_{1_r}$ vs $\alpha$ for 0.6M	C-8
35.	Production Phase Data: $C_{n_p}$ vs $\alpha$ for 0.3M	C-9
36.	Production Phase Data: $C_{n_p}$ vs $\alpha$ for 0.6M	C-10
37.	Production Phase Data: $C_{n_r}$ vs $\alpha$ for 0.3M	C-11
38.	Production Phase Data: $C_{n_r}$ vs $\alpha$ for 0.6M	C-12
39.	Rotary Balance Data: $C_{1_n}$ vs $\alpha$	E-4
40.	Rotary Balance Data: $C_{n_n}$ vs $\alpha$	E-7
41.	Design Phase Data: $C_{1_n}$ vs $\alpha$ for 0.2M	E-9

Figure		Page
42.	Design Phase Data: $C_{n_{\Omega}}$ vs $\alpha$ for 0.2M	E-11
43.	Design Phase Data: $C_{1_{\Omega}}$ vs $\alpha$ for 0.6M	E-13
44.	Design Phase Data: $C_{n_{\Omega}}$ vs $\alpha$ for 0.6M	E-15
45.	Production Phase Data: $C_{1_{\Omega}}$ vs $\alpha$ for 0.3M	E-17
46.	Production Phase Data: $C_{n_{\Omega}}$ vs $\alpha$ for 0.3M	E-19
47.	Production Phase Data: $C_{1_{\Omega}}$ vs $\alpha$ for 0.6M	E-21
48.	Production Phase Data: $C_{n_{\Omega}}$ vs $\alpha$ for 0.6M	E-23
49.	Rotary Balance Data: $C_{1_{\Omega}}$ vs $\alpha$ ( $8^{\circ}$ - $90^{\circ}$ )	E-24
50.	Rotary Balance Data: $C_{n_{\Omega}}$ vs $\alpha$ ( $8^{\circ}$ - $90^{\circ}$ )	E-25

List of Tables

Table		Page
I.	Reynolds Number vs Altitude for $M = 0.1$ and $l = 1$ ft	14
II.	Data Set Mach and Reynolds Numbers	15
III.	Rotary Balance Data: $C_1$ vs $b/2V$ for $8^\circ < \alpha < 90^\circ$	E-2
IV.	Rotary Balance Data: $C_{1\Omega}$ vs $\alpha$ ( $8^\circ - 90^\circ$ )	E-3
V.	Rotary Balance Data: $C_n$ vs $b/2V$ for $8^\circ < \alpha < 90^\circ$	E-5
VI.	Rotary Balance Data: $C_{n\Omega}$ vs $\alpha$ ( $8^\circ - 90^\circ$ )	E-6
VII.	Design Phase Data: Computation of $C_{1\Omega}$ vs $\alpha$ ( $8^\circ - 35^\circ$ ) for $0.2M$	E-8
VIII.	Design Phase Data: Computation of $C_{n\Omega}$ vs $\alpha$ ( $8^\circ - 35^\circ$ ) for $0.2M$	E-10
IX.	Design Phase Data: Computation of $C_{1\Omega}$ vs $\alpha$ ( $8^\circ - 35^\circ$ ) for $0.6M$	E-12
X.	Design Phase Data: Computation of $C_{n\Omega}$ vs $\alpha$ ( $8^\circ - 35^\circ$ ) for $0.6M$	E-14
XI.	Production Phase Data: Computation of $C_{1\Omega}$ vs $\alpha$ ( $8^\circ - 35^\circ$ ) for $0.3M$	E-16
XII.	Production Phase Data: Computation of $C_{n\Omega}$ vs $\alpha$ ( $8^\circ - 35^\circ$ ) for $0.3M$	E-18
XIII.	Production Phase Data: Computation of $C_{1\Omega}$ vs $\alpha$ ( $8^\circ - 35^\circ$ ) for $0.6M$	E-20
XIV.	Production Phase Data: Computation of $C_{n\Omega}$ vs $\alpha$ ( $8^\circ - 35^\circ$ ) for $0.6M$	E-22

## ABSTRACT

The purpose of this thesis was to determine whether or not there are phenomenological differences between dynamic derivatives calculated from F-15A rotary balance data and data from other sources.

To make this determination, two additional data sets were obtained: (1) the F-15A design phase stability derivative data, and (2) the F-15A production phase stability derivative data. The lateral dynamic derivatives were then compared through derivatives of the lateral moments with respect to the rotation rate about the velocity vector (wind vector).

The conclusion of the project was that differences exist between the data sets, but that the dominant characteristics were the same for all of the data sets; the differences in the data were not indicative of basic (phenomenological) differences in the data itself. Therefore, the contention that oscillatory rates affect determination of the dynamic derivatives was not substantiated by this study.

## THE EFFECT OF CONSTANT VS OSCILLATORY RATES

### ON DYNAMIC STABILITY DERIVATIVES

#### I. INTRODUCTION

##### Historical Survey

Traditionally, aircraft stability and control is determined from a linearized system of differential equations of motion. The linearization is obtained by expanding the force and moment terms (as functions of the motion and control variables) in truncated Taylor series about an equilibrium point. The partial derivatives of the force and moment coefficients with respect to the motion variables are called aerodynamic stability derivatives and have been commonly used over the years to predict aircraft stability characteristics.

The stability derivatives are often further subdivided into "static" and "dynamic" stability derivatives. The static derivatives are those taken with respect to  $V$ ,  $\alpha$ , and  $\beta$ . All other derivatives are considered "dynamic". Basically, the static derivatives are relatively "easy and inexpensive" to determine from wind tunnel tests while dynamic derivatives are relatively "difficult and expensive" to determine.

Because of the difficulty and expense involved in the extensive dynamic testing required to obtain the dynamic derivatives empirically (a requirement necessary for their accurate determination over a broad range of flight conditions), the aviation industry has shied away from doing this testing. The industry uses flight test data to determine them instead. Prior to the mid-1930's, a combination of the inaccuracy of then-current test equipment, the relatively low cost of full scale aircraft prototypes, and the relatively conventional designs produced encouraged the designers to estimate, or in some cases ignore, the dynamic derivatives during the design phase. Stability problems attributable to the inaccuracies in their estimates were corrected through modifications during or after the production phase.

With the advent of the more sophisticated, high performance designs introduced as a result of the Second World War, increased emphasis was placed on predicting the stability and performance characteristics of new aircraft prior to production (or even first flight). But the cost of dynamic testing, was still prohibitive. In response to the need for data, a myraid of new estimation techniques was developed and put into use by the industry (1).

The techniques developed for WWII prevailed through the following decade. In the mid-1950's, two new factors

emerged to discourage the use of dynamic testing to determine the dynamic derivatives in the design phase: (1) analysis of air operations in the Korean War indicated tremendous U.S. supremacy over U.S.S.R. aircraft as demonstrated by the 12-1 kill ratio achieved in air to air combat (2: 110), and (2) the increasingly rapid development of electro-mechanical automatic control devices. The combination of these two factors made it easier and cheaper, and therefore more attractive, to modify new designs during (or after) production, if necessary, to make them meet required stability and performance criteria.

In the last decade, a combination of several factors has reawakened interest in dynamic testing: (1) analysis of air operations in Viet Nam showed a narrowing of U.S. supremacy as indicated by the 2.5-1 kill ratio achieved (2: 110), (2) the reduction in excess capability available in the automatic control systems to correct inherent design problems (due in large part to the expanded use of flexible structures throughout modern aircraft), and (3) the development of high speed/low cost computers which provide a relatively low cost, easy way to acquire and reduce the large amounts of data required by dynamic testing.

Without the technological superiority enjoyed in the past, mistakes in the design phase can no longer be corrected in the production phase and still achieve acceptable



performance. Therefore, new means of acquiring the information necessary in the design phase in a cost effective manner must be evaluated.

#### Determining the Dynamic Derivatives

There is a variety of techniques currently in use to determine the dynamic derivatives. These techniques range from the relatively simple and inexpensive estimation methods contained in the DATCOM (3) and similar sources (1, 4) to the very complex and expensive experimental procedures developed by various research facilities throughout the world (5).

Over the last decade, the NASA-Langley Research Center has been developing a technique for predicting spins using a rotary balance installed in the NASA-Langley Vertical Wind Tunnel. Birhle (6), in outlining the history of spin related research, points out the difficulty past investigators have had in predicting spins and the trajectories of spinning aircraft. He goes on to say that the reason the former investigators were unsuccessful was that the data necessary to compute the forces and moments due to the steady state components of the body angular rates -  $p$ ,  $q$ , and  $r$  - must come from a constant rotation dynamic test device, like the rotary balance, which was not formerly available. For accurate trajectory calculation, he contends, the rotational velocities must be broken up into

steady state and oscillatory components and the contributions of each to the forces and moments determined by tests in steady state facilities (e.g., rotary balance) and facilities that are not solely steady state, respectively.

#### Purpose of This Thesis

If it is true that steady state and oscillatory components of the body angular rates contribute to the forces and moments, other than in proportion to their magnitudes and directions, then the dynamic derivatives computed from steady state sources and sources other than solely steady state will be different. Further, these differences must be able to be explained due to phenomenological differences in the flows of the source data testing apparatus. The purpose of this thesis is to examine dynamic derivatives computed from a data set acquired from a solely steady state source and some data sets acquired from non solely steady state sources to determine any significant differences, and, if they exist, the phenomological reasons for these differences.

## II. Topic Discussion

This section introduces and discusses topics necessary for the analysis carried out in subsequent sections. The first subsection looks at the characteristics of aerodynamic test data to determine guidelines for comparing data sets. Next, the phenomena that affect the forces and moments due to oscillatory motion are examined and their probable contributions due to oscillatory rotation rates analyzed. The nature of rotary balance force and moment coefficient data is examined in the third subsection. And, finally, the dynamic derivatives taken with respect to the body angular rates are analyzed.

### Aerodynamic Test Data

Collection and analysis of aerodynamic test data is necessary to experimentally determine the values of aerodynamic parameters. A persistent problem with this process, however, has been that the data collected often shows significant scatter. This scatter shows in a limited manner for successive trials of a single test and more dramatically for tests conducted under a variety of conditions or for dissimilar tests designed to determine a certain parameter. As a result of the scatter, then, the existence of differences between parameters calculated from different data sets has come to be expected.

When the objective changes from determining the values of aerodynamic parameters to comparing data sets through parameters calculated from these data sets, some different implications are drawn from the scatter. Simple differences in the parameters may represent scatter rather than differences in the underlying data and therefore are not sufficient to demonstrate significant differences in the data sets. To demonstrate such differences, variations between the major characteristics of the parameters must be shown.

There are many characteristics of such parameters that can be usefully compared. Among them are slopes and magnitudes, points of change of slope, and consistency (or linearity). The choice of the most appropriate characteristic to use is dependent on the particular parameter under consideration.

Once the characteristics to be compared have been chosen, demonstration of similarity or dissimilarity is based on two criteria: (1) the parameters compared must predominantly exhibit the major characteristics, and (2) the similarities or dissimilarities identified must be consistent throughout the data sets. The key, then, to establishing similarity or dissimilarity rests with showing consistency. Without consistency, demonstrations of similarity or dissimilarity become mere demonstrations of scatter.

### Oscillatory Rate Phenomena

There are two phenomena which may affect the aerodynamic forces and moments as a result of oscillatory rotation rates. These phenomena are unsteady aerodynamics and aeroelasticity.

Unsteady aerodynamic effects result from the delays in the response of the flow field about an aircraft to motions of the aircraft. When the aircraft motions are rapid compared to the response of the flow field, transient forces and moments are applied to the aircraft while the flow field adjusts to the changing conditions. These forces and moments can be very pronounced when the motion is due to the structural modes of the aircraft.

These same structural modes can cause large forces and moments due to changes in the incidence of the wing. When triggered by unsteady forces of the proper frequency on the aircraft surfaces, the surfaces vibrate, sometimes with relatively large amplitude deflections. These deflections can cause changes in the incidence of the wing leading to additional forces. (If these additional forces are of the proper frequency, resonance results in very large amplitude deflections.)

The body angular rates are rigid body modes of the aircraft. The characteristic frequencies are on the order of 6-8 rad/sec (7). The characteristic frequencies for un-

steady aerodynamic phenomena and aeroelastic phenomena are in the range 20 rad/sec and up (8). Since both of these phenomena require excitation frequencies of the same order as their own frequencies, they will not be excited by the body angular rates. As a result, these phenomena will not contribute to the forces and moments.

#### Rotary Balance Force and Moment Data

The rotary balance used at the NASA-Langley Research Center provides for an aircraft model to be mounted in the spin tunnel at any desired angles of attack and sideslip and then spun about an axis parallel to the velocity vector while the forces and moments are measured and recorded (6). In normal mountings, the bank angle is zero. The angle of pitch is preset so it is unaffected by the spin; thus the pitching velocity is zero. This means that the spinning velocity, and therefore the force and moment data, is a function of the rolling and yawing body rates,  $p$  and  $r$ , only.

The spinning velocity of the aircraft is the overall rotation rate,  $\Omega$ . In general,  $\Omega$  is a combination of the roll and yaw rates,  $p$  and  $r$ , which cannot be independently controlled. Therefore, the resulting force and moment data can only be given as a function of this combination. It is not possible to use the spin tunnel force and moment data to find the rates of change (partial derivatives) of

the forces and moments with respect to the roll and yaw rates individually.

### The Dynamic Derivatives

As stated before, the dynamic derivatives are all of the stability derivatives except those taken with respect to  $V$ ,  $\alpha$ , and  $\beta$ . However, only those derivatives taken with respect to the body angular rates -  $p$ ,  $q$ , and  $r$  - are applicable to this report.

The combination of the six force and moment coefficients and the three angular body rates has the potential to produce 18 derivatives. The uncoupling of the longitudinal and lateral modes reduces this by half to nine, however, and the fact that the rotary balance data is not a function of the pitching rates reduces this number still further to six.

The yawing moment coefficient is normally larger in magnitude than and proportional to the side force coefficient. Therefore, the information provided by the two coefficients is redundant. Since the lateral modes are normally more dependent on the moments than the forces, this report will not examine the side force derivatives. This leaves the four moment coefficient derivatives.

Finally, since these four derivatives cannot be independently derived from rotary balance data, only the combined derivatives (the derivatives of the moment coeffi-

icients with respect to the overall rotation rate) can be used in this analysis.



### III. APPROACH

To accomplish the thesis' objective, three things needed to be done: (1) choose data sets, (2) choose the comparisons to make between the data sets, and (3) make the comparisons. This section deals with the first two activities.

#### Data Set Selection

The F-15 was chosen as the aircraft to use as the test case because it is the only operational Air Force aircraft to have been tested on the rotary balance (10). An operational aircraft was desired because a larger data base exists for operational aircraft than for most other aircraft.

Two data sets were chosen for comparison with the rotary balance data. The first set (11) was one for which the dynamic derivatives were estimated (12 - 14). The second set (15) was derived from production phase flight test data. (Note: It would have been desirable to have a data set derived from oscillatory wind tunnel testing - to be a source of solely oscillatory data - but because the Air Force policy for the last three decades has been to forego this type of testing, the data is not available.)

#### Choice of Comparisons

The rotary balance data set provides force and moment

coefficient data as a function of rotation rate (from which stability derivative parameters can be computed) for one Mach/Reynolds number combination and a wide range of angles of attack. The design phase and production phase data sets provide the stability derivatives for a large number of Mach/Reynolds number combinations but for a limited angle of attack range.

Reynolds number ( $R_e$ ) is determined by the relation:

$$R_e = \rho V l / \mu \quad (1)$$

which, when written in terms of Mach number, becomes:

$$R_e = \rho M a l / \mu \quad (2)$$

The quantity  $\rho/\mu$  decreases with increasing altitude, so for a given Mach number, Reynolds number decreases with increases in altitude (see Table I).

The stability derivative data in the design and production phase data sets are either independent of altitude (Reynolds number) or tend toward a limiting value with increasing altitude (decreasing Reynolds number). For Mach numbers of 0.6 and below this limiting value is very nearly reached by 80,000 ft. Therefore, this altitude value was used to compute Reynolds numbers for the design phase rigid data following the example of the production phase data (but note was taken that the Reynolds number for the rigid data can be an arbitrarily lower value; in the limit it is zero). A summary of Reynolds numbers for the data sets is

TABLE I

Reynolds Number vs Altitude for 0.1M and l=1 ft

<u>h(ft)</u>	<u><math>R_e \times 10^{-6}</math></u>
SL	7.133
5K	6.210
10K	5.379
15K	4.636
20K	3.976
25K	3.390
30K	2.872
35K	2.415
40K	1.920
50K	1.190
60K	0.738
70K	0.457
80K	0.284

given in Table II.

The most meaningful comparisons are those for comparable Mach numbers, Reynolds numbers, and angles of attack. For this analysis, the comparisons were limited to data for incompressible Mach numbers (0.6 and less), Reynolds numbers within approximately one order of magnitude, and the common angle of attack range.

TABLE II

Data Set Mach and Reynolds Numbers

<u>Report</u>	<u>Mach Number</u>	<u>Reynolds Number</u>
NASA CR 3478	0.022	$0.211 \times 10^6$
MDC A0502	0.2	$0.908 \times 10^6$
	0.6	$2.725 \times 10^6$
MDC A4172	0.3	$1.363 \times 10^6$
	0.6	$2.725 \times 10^6$

#### IV. DATA ANALYSIS

##### The Data Sets

The three data sets were produced over a period of approximately twelve years (roughly 1969-1981). As a result, the reports represent tests of slightly different configurations of the F-15A. (Some of the more noticeable changes were the addition of the leading edge snag on the horizontal stabilizer and downsizing of the speed brake which occurred in the early seventies.) In addition, some of the tests configured the aircraft differently, for example, including or not including air to air missiles. The effects of these variations in the configuration are small, however, having a negligible affect on this analysis.

Rotary Balance Data (Appendix A). The rotary balance data is raw moment coefficient data plotted as a function of angle of attack, non-dimensional spin rate, and spin radius. The portion of the data package used for the comparison was limited to the data for the basic configuration with no controls deflected and for the angle of attack range  $8^{\circ}$ -  $35^{\circ}$  which has a spin radius equivalent to six feet on the full scale aircraft. (Note: The data for angles of attack greater than  $35^{\circ}$  was taken with the spin radius set to zero.)

Design Phase Data (Appendix B). The design phase data consists of plots of the stability derivatives as a function

of angle of attack, Mach number, and altitude. (Note: Only the data for a rigid aircraft was used.)

Low angle of attack (less than approximately  $26^\circ$ ) and high angle of attack (approximately  $26^\circ$  to  $35^\circ$ ) data are presented separately and there are some inconsistencies in the data in the interface range. These inconsistencies, while noticeable, do not appreciably affect the results.

The data used for comparison was limited to the two Mach numbers 0.2 and 0.6 and the angle of attack range  $8^\circ$  to  $35^\circ$ .

Production Phase Data (Appendix C). The production phase data is presented in basically the same format as the design phase data. The data is not presented differently for two angle of attack ranges, so it doesn't suffer from the inconsistencies of the other data set.

The data used for comparison was limited to the two subsonic Mach numbers 0.3 and 0.6, the angle of attack range  $8^\circ$  to  $35^\circ$ , and 80,000 ft altitude.

#### Computing the Comparison Parameters

As stated earlier, the rotary balance force and moment coefficient data is a function of a combination of the roll rate,  $p$ , and the yaw rate,  $r$ . As a result, the individual stability derivatives with respect to these rates cannot, in general, be determined from the rotary balance data, while the derivatives with respect to the overall rotation

rate can. The appropriate parameters for comparison, then, are the derivatives with respect to:

$$C_{l_{\Omega}} \quad C_{n_{\Omega}}$$

Rotary Balance Comparison Parameters. The comparison parameters were calculated from the rotary balance moment coefficient data in Appendix A for the entire angle of attack range ( $8^{\circ} - 90^{\circ}$ ) using a linear least squares curve fit.

Design and Production Phase Comparison Parameters.

These stability derivatives were calculated from the stability derivative data in Appendices B and C using the relation:

$$C_{i_{\Omega}} = C_{i_p} \cos \alpha + C_{i_r} \sin \alpha \quad i = 1, n \quad (3)$$

which is developed in Appendix D.

Presentation of the Comparison Parameters

The computations of the comparison parameters along with the results were tabulated and the results plotted (see Appendix E). Plots for the angle of attack range  $8^{\circ}$  to  $35^{\circ}$  were made for each data set/Mach number/parameter combination; in addition, a plot of each parameter was made for the rotary balance data for the entire angle of attack range. The results for each parameter for all of the data set/Mach Number combinations for the angle of attack range  $8^{\circ}$  to  $35^{\circ}$  are summarized in Figures 1 and 2.

## V. Results

This section analyzes the plots discussed in Section IV. It looks at the plots of  $C_{1\Omega}$  analyzing the similarities and differences of the rotary balance, design phase, and production phase data. It then analyzes the plots of  $C_{n\Omega}$  in the same manner.

Rolling Moment Derivative ( $C_{1\Omega}$ ) Plots. The overall trends of the plots of  $C_{1\Omega}$  in Figure 1 show that the magnitude of the derivative increases from a large negative value at 8° angle of attack to a slightly negative value at 25° angle of attack and then stays relatively constant from 25° to 35°. This dominant trend is seen for all the plots.

The rotary balance data taken with a six foot spin radius does not show the bend at 25°, but shows it delayed to 30°. However, the data taken with zero spin radius (Figure 49) shows the bend at the expected 25°.

The design phase data shows the trend change at 25° as noticeably as the rotary balance data but does not show the remarkable linearity from 8° to 25° that the rotary balance data does. Since  $C_{1\Omega}$  is predominantly  $C_{1p}$  for low angles of attack, the nature of  $C_{1p}$  should account for the difference. The plots of  $C_{1p}$  (Figures 17 and 23) show that it does not change uniformly with angle of attack but shows a sharp increase from 10° to 15° for the 0.2M data and from



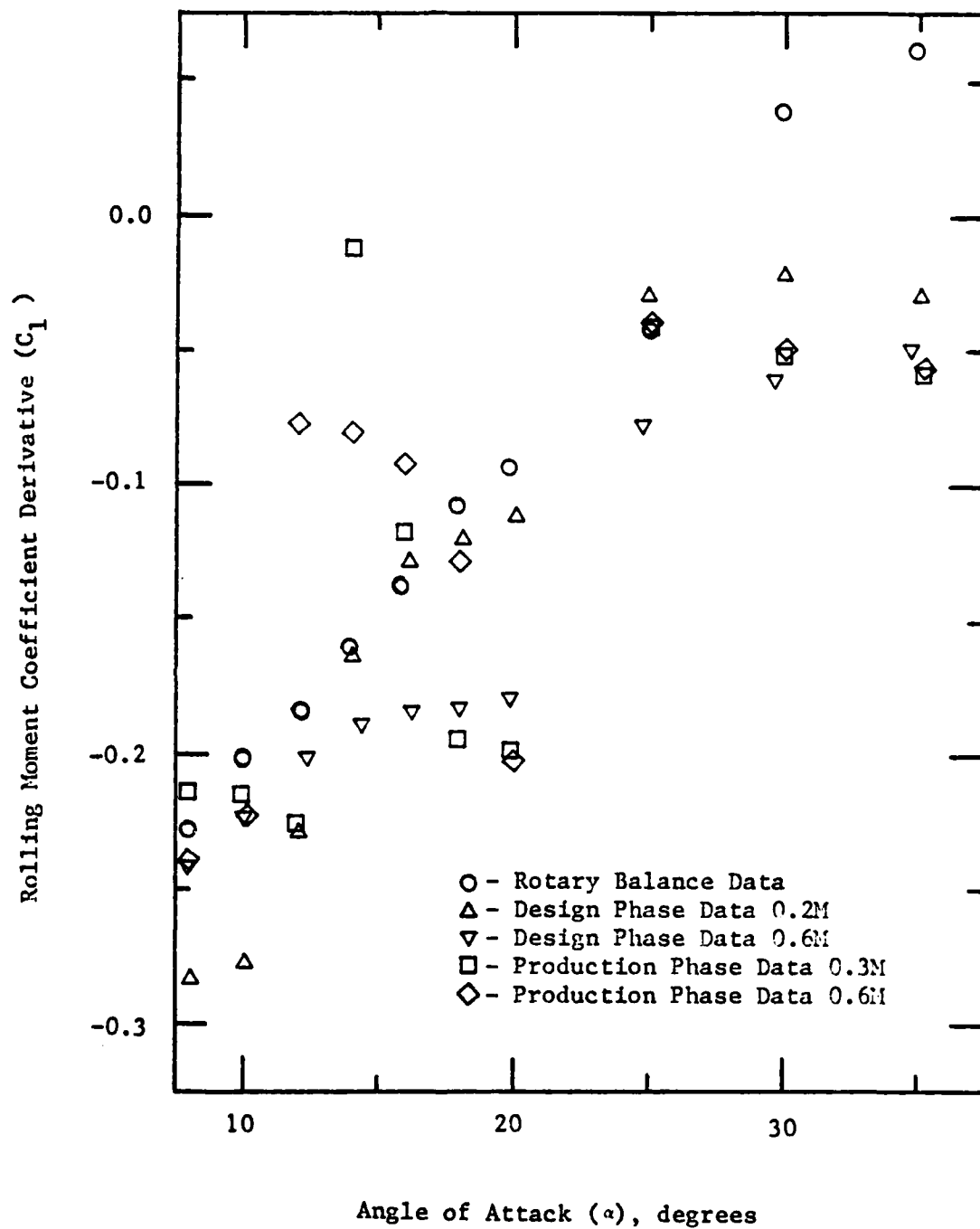


Figure 1. Combined Plot:  $C_1$  vs

20° to 25° for the 0.6M data. This step function nature is not reflected in the rotary balance data; the step shifts to lower angle of attack ranges for lower Mach/Reynolds number combinations and may have shifted out of the comparison range for the data in this report.

The production phase data once again change in trend at 25° angle of attack. The range from 8° to 25°, however, is characterized by peaks and valleys in stark contrast to both the rotary balance data and the design phase data. Both  $C_{1p}$  and  $C_{1r}$  (Figures 31 - 34) are highly nonlinear and the nonlinearity of  $C_{1p}$  again dominates  $C_{1r}$  for both 0.3M and 0.6M although the contribution of  $C_{1r}$  is readily detectable from 8° to 12° for 0.3M.

Yawing Moment Derivative ( $C_{n\Omega}$ ) Plots. Following the pattern seen with  $C_{1\Omega}$ , the plots of  $C_{n\Omega}$  in Figure 2 show a change in trend at approximately 25°. While the trend following 25° is not as consistent or obvious for  $C_{n\Omega}$  as it was for  $C_{1\Omega}$ , it is a pronounced change, immediately seen in all but one data set.

Paralleling the data for  $C_{1\Omega}$ , the rotary balance  $C_{n\Omega}$  data for the range 8° to 25° is surprisingly linear. It follows a negative trend from 8° to 20°, bottoms out from 20° - 25°, and increases slightly from 25° - 35°.

The design phase data show a peak between 8° and 25° at 15° for 0.2M and at 12° for 0.6M before picking up the

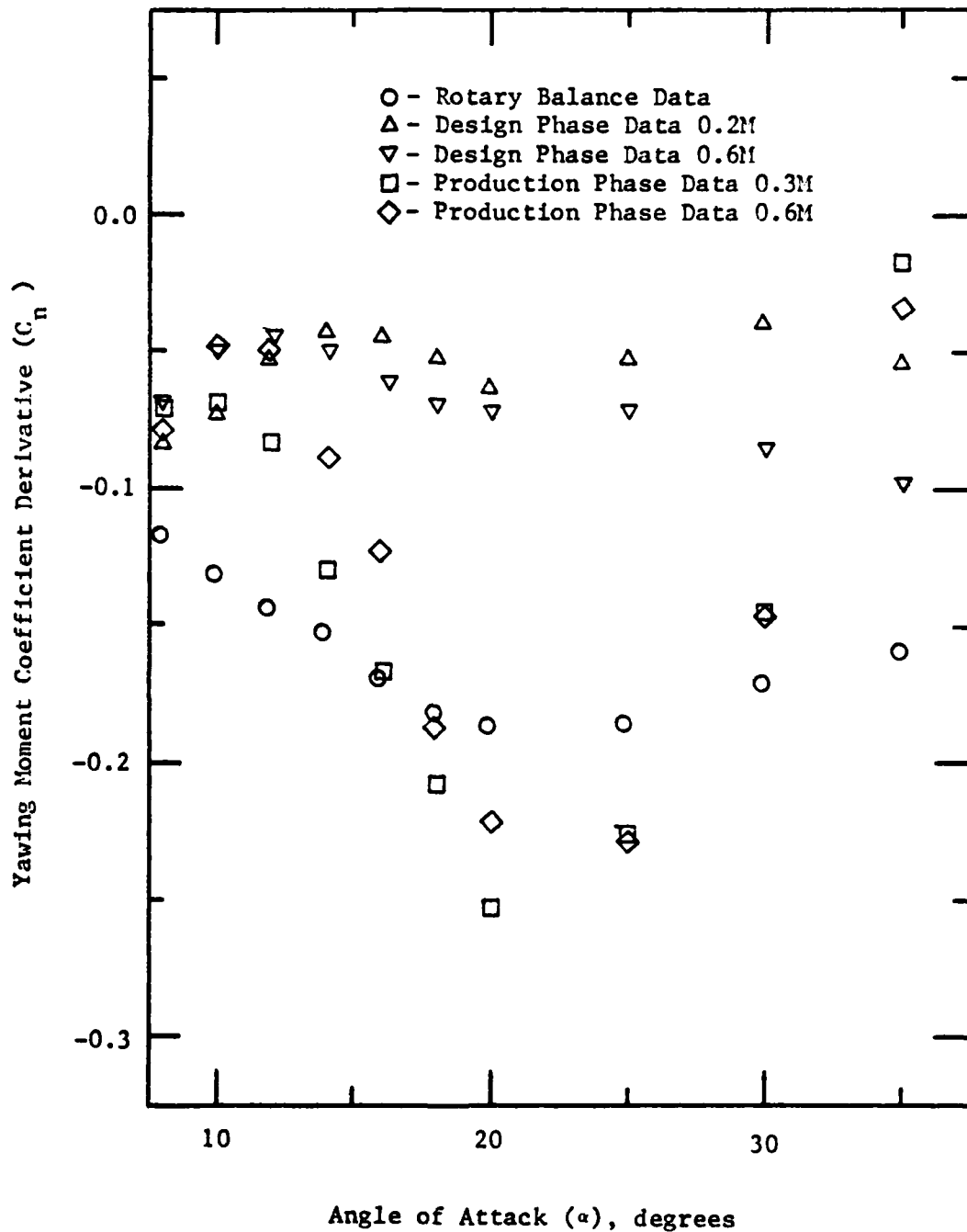


Figure 2. Combined Plot:  $C_n$  vs

the downward trend of the rotary balance data. Both bottom out between 20° and 25° before the 0.2M data picks up a neutral trend and the 0.6M data picks up a negative trend. The break at 25° is not as pronounced for the 0.6M data but is noticeable. The trends after 25° for both 0.2M and 0.6M differ from that for the rotary balance data.

The peak between 8° and 25° for both sets of data is a result of following  $C_{np}$ , whose behavior from 0° to 16° (Figures 19 and 25) is not reflected in the rotary balance data. The production phase data show the same trends as the design phase data for the range 8° to 25° but the downward trend from 12° to 20° is much more pronounced (it plunges). As a result of being so much more negative at 25° than the other data sets, the trend from 25° to 35° is strongly positive in order to return to the range near zero of the other data sets.

Overall, the outstanding characteristic of all the data is that the data shows one trend from 8° to 25° and another trend after 25°. This occurs regardless of the Mach and Reynolds number of the data set and the parameter looked at. The dominant trend prior to 25° is positive for  $C_l$  and negative for  $C_n$ ; after 25°,  $C_l$  and  $C_n$  both tend toward a nearly constant value.

## VI. Conclusions

The analysis has shown that there are both similarities and differences between the three data sets. The dominant trends are exhibited by all three data sets but the characteristics of these trends differ within each set to a greater or lesser degree.

The analysis does not show a phenomenological difference between the data taken on the rotary balance and the other data sets. Differences exist, but the differences are not consistent; the rotary balance data for  $C_{1\Omega}$  for  $8^\circ - 25^\circ$  is very similar to the design phase data but very different for the production data for this range while all three are similar for the range from  $25^\circ$  to  $35^\circ$ . For  $C_{n\Omega}$  it is just the opposite.

In summary, significant differences in the lateral dynamic derivatives were neither predicted by the theory nor seen in the actual test results. Therefore, this report concludes that the contention that there is a significant difference between data taken for steady state rotation rates and oscillatory rotation rates is not substantiated by this analysis.

Appendix A: Data from NASA CR 3478

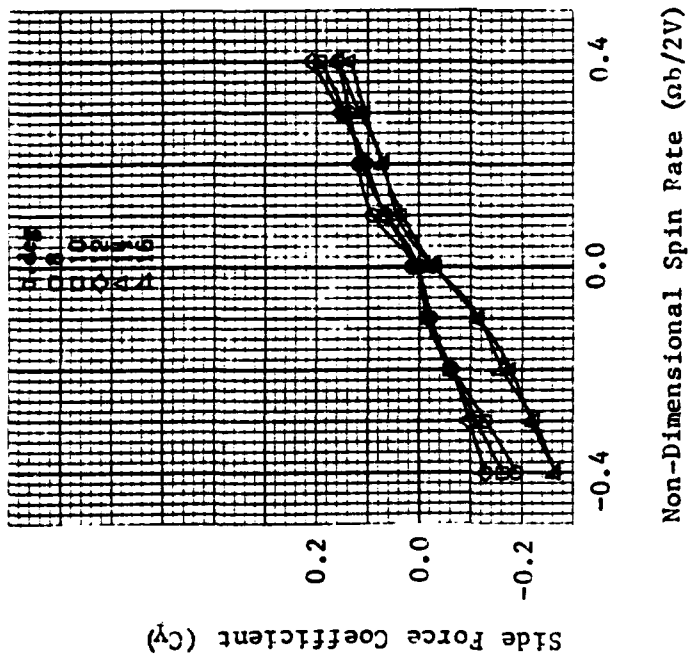


Figure 3.  $8^\circ - 16^\circ$

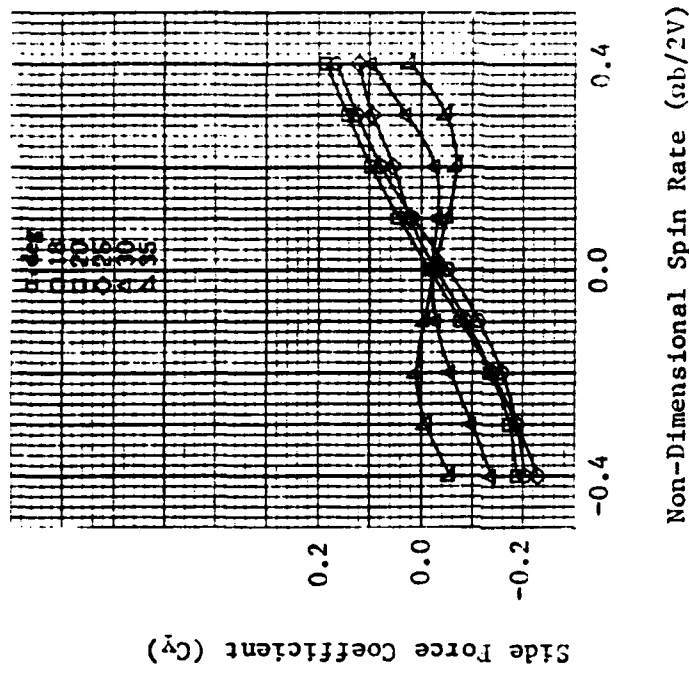


Figure 4.  $18^\circ - 35^\circ$

Rotary Balance Data:  $C_y$  vs  $nb/2V$  for  $SR = 6$  ft

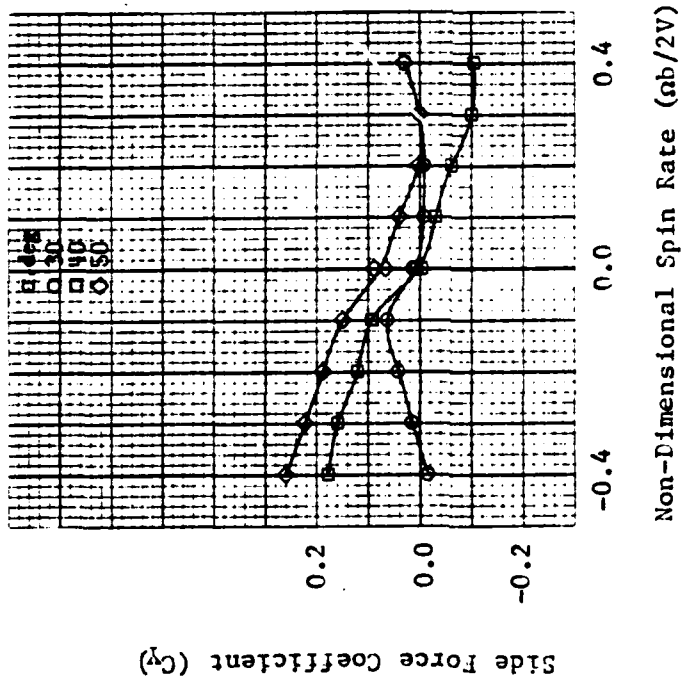


Figure 5. 30° - 50°

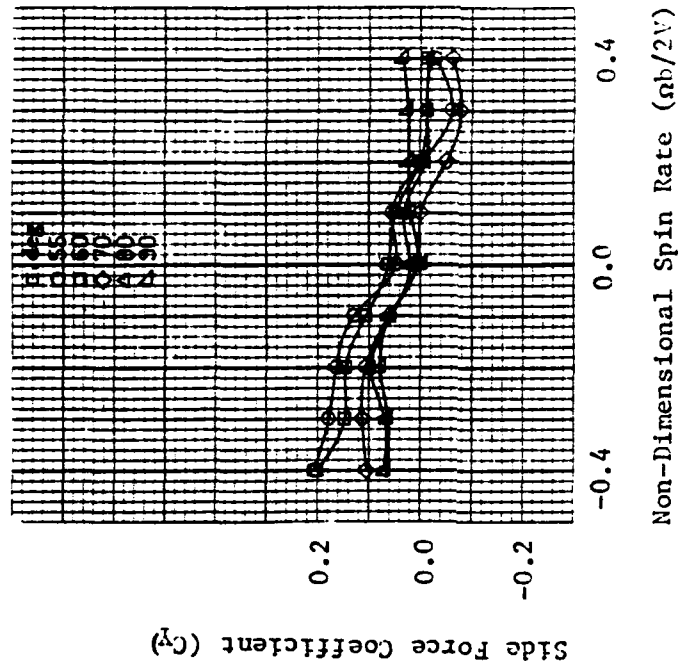


Figure 6. 55° - 90°

Rotary Balance Data:  $C_y$  vs  $nb/2V$  for  $SR = 0$  ft



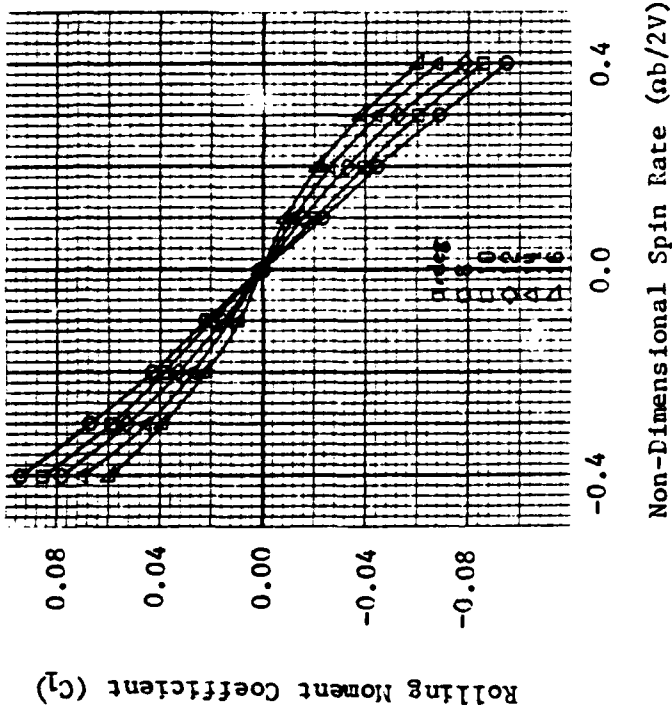


Figure 7.  $8^\circ$  -  $16^\circ$

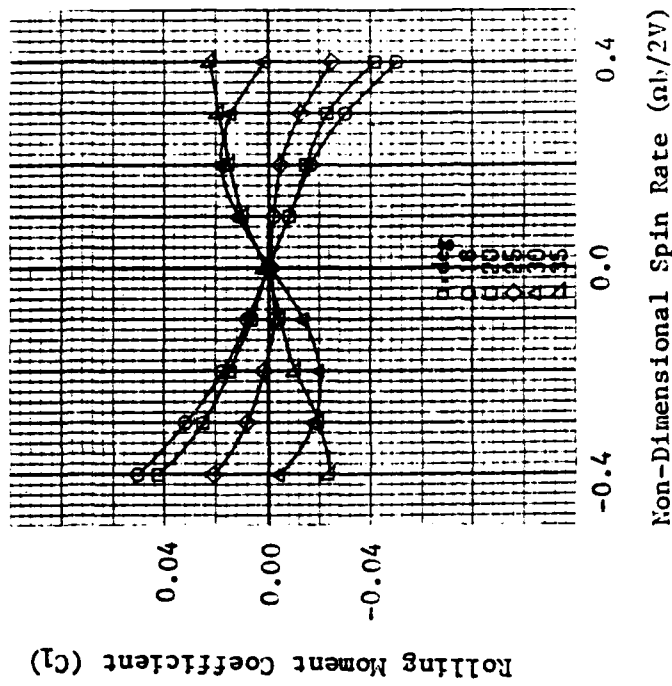


Figure 8.  $18^\circ$  -  $35^\circ$

Rotary Balance Data:  $C_l$  vs  $nb/2V$  for SR = 6 ft

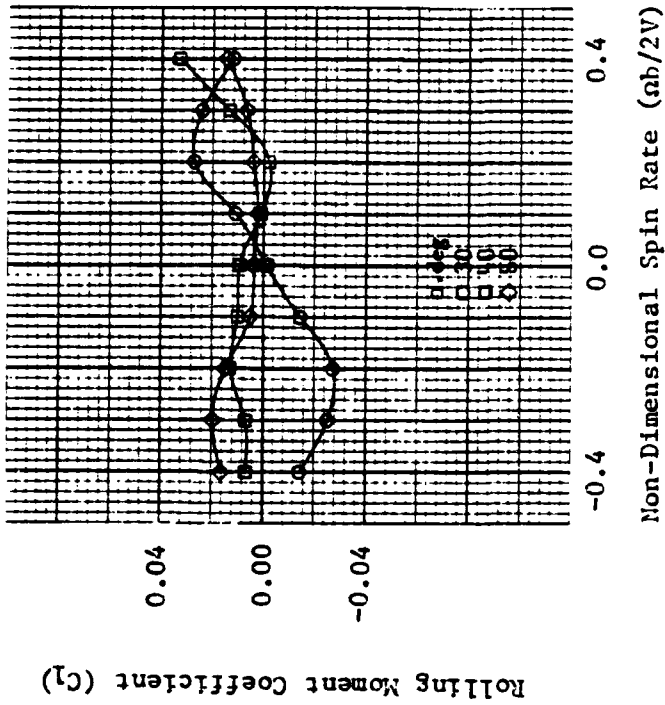


Figure 9. 30° - 50°

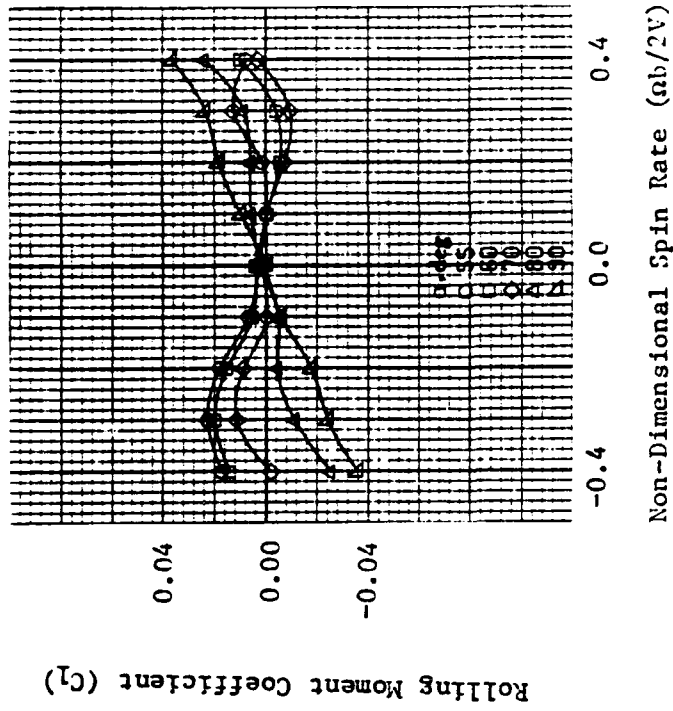


Figure 10. 55° - 90°

Rotary Balance Data:  $C_l$  vs  $nb/2V$  for  $SR = 0$  ft

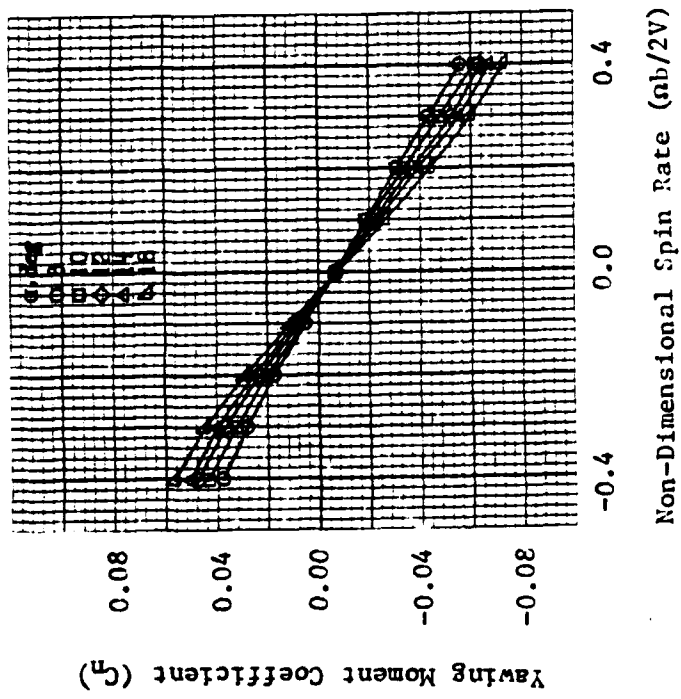


Figure 11. 8° - 16°

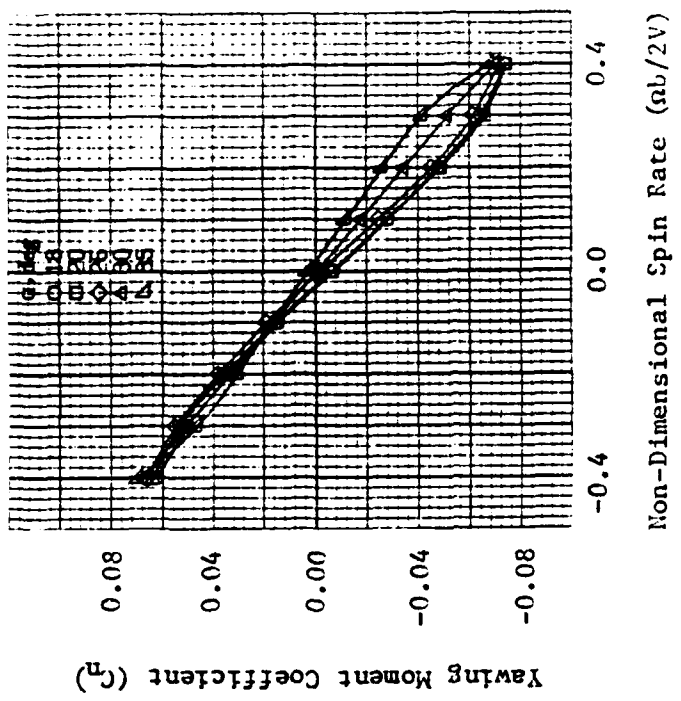


Figure 12. 18° - 35°

Rotary Balance Data:  $C_n$  vs  $nb/2V$  for SR = 6 ft

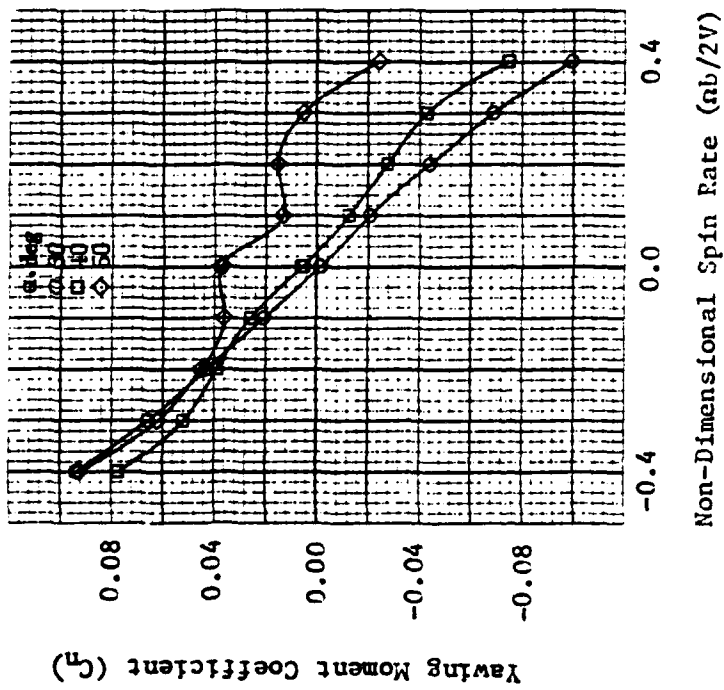


Figure 13. 30° - 50°

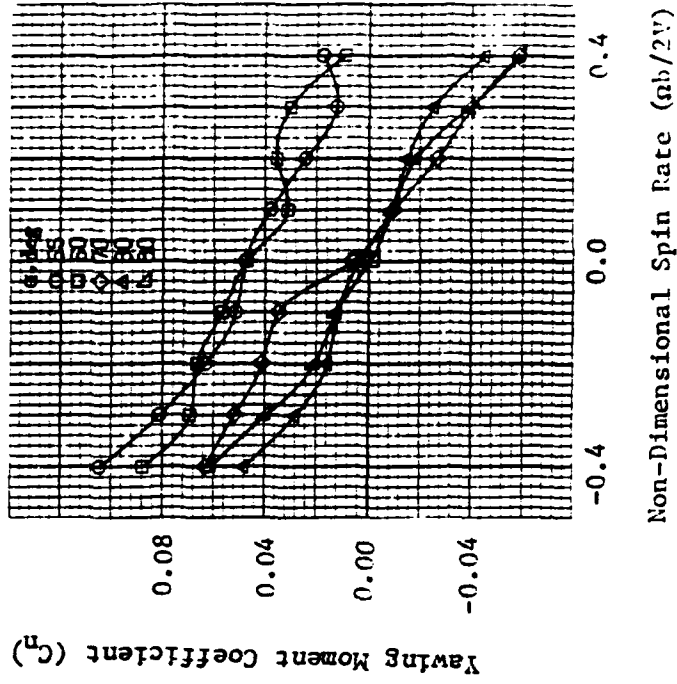
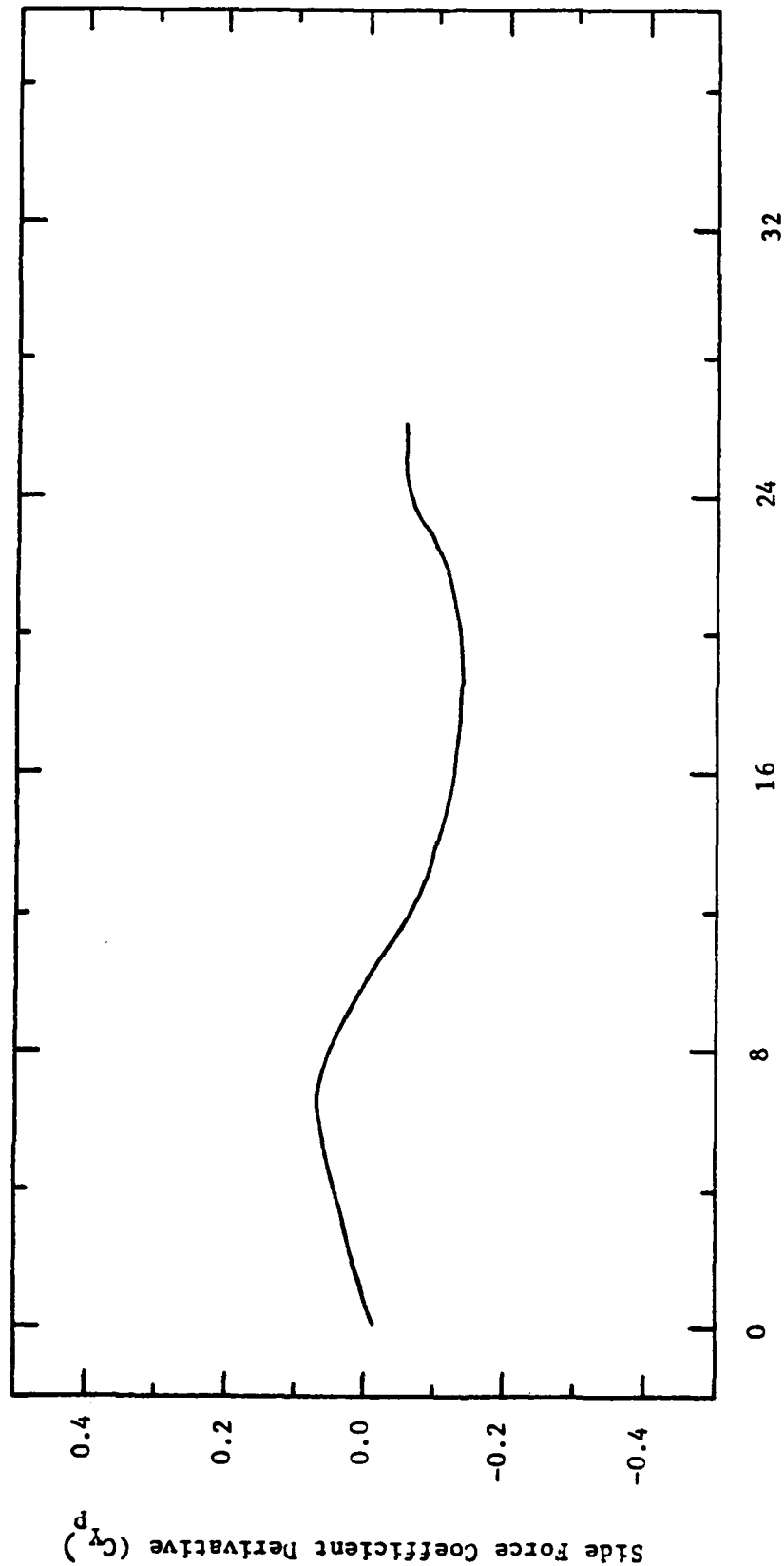


Figure 14. 55° - 90°

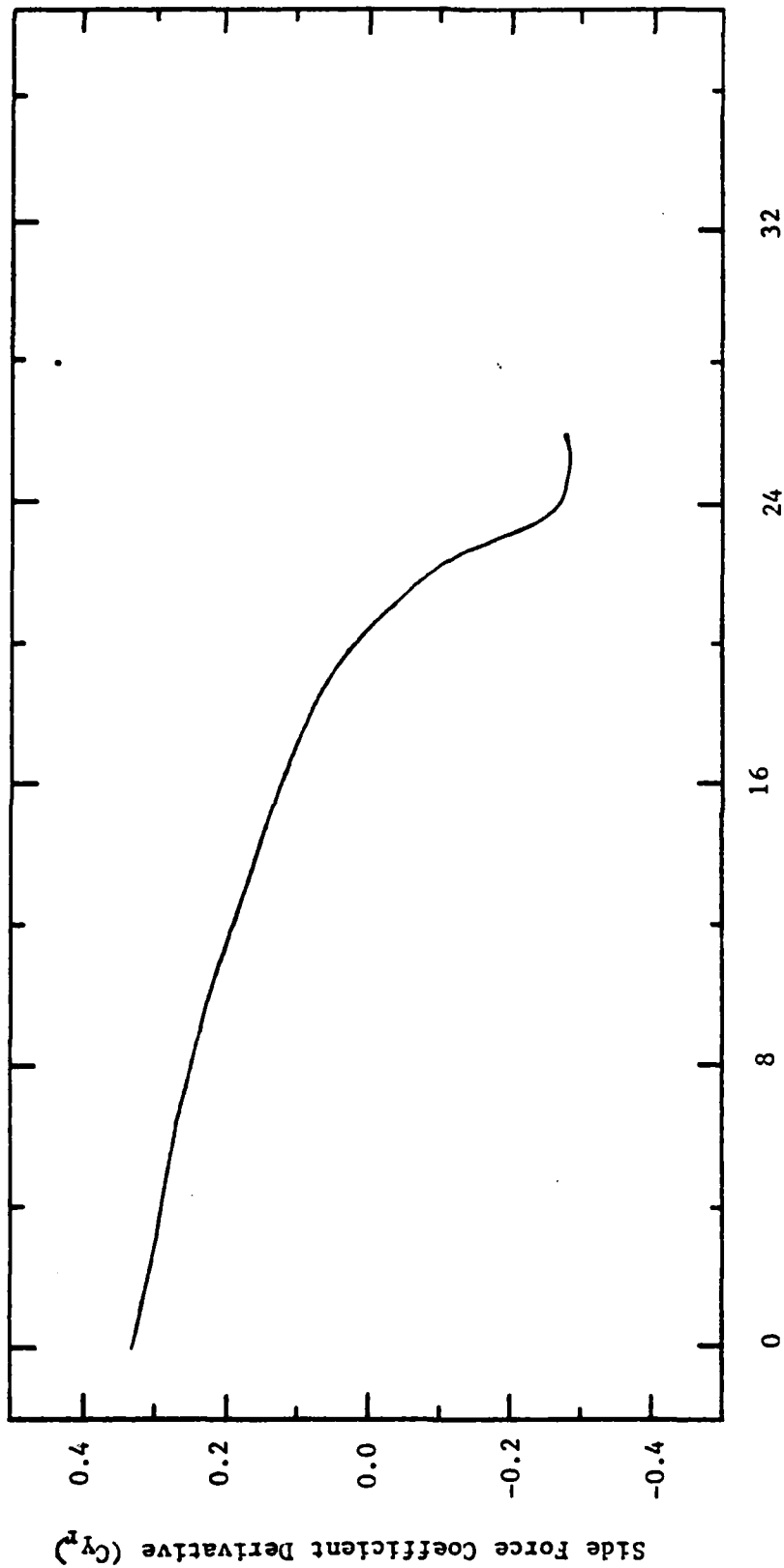
Rotary Balance Data:  $C_n$  vs  $nb/2V$  for  $SR = 0$  ft

Appendix B: Data from MDC A0502



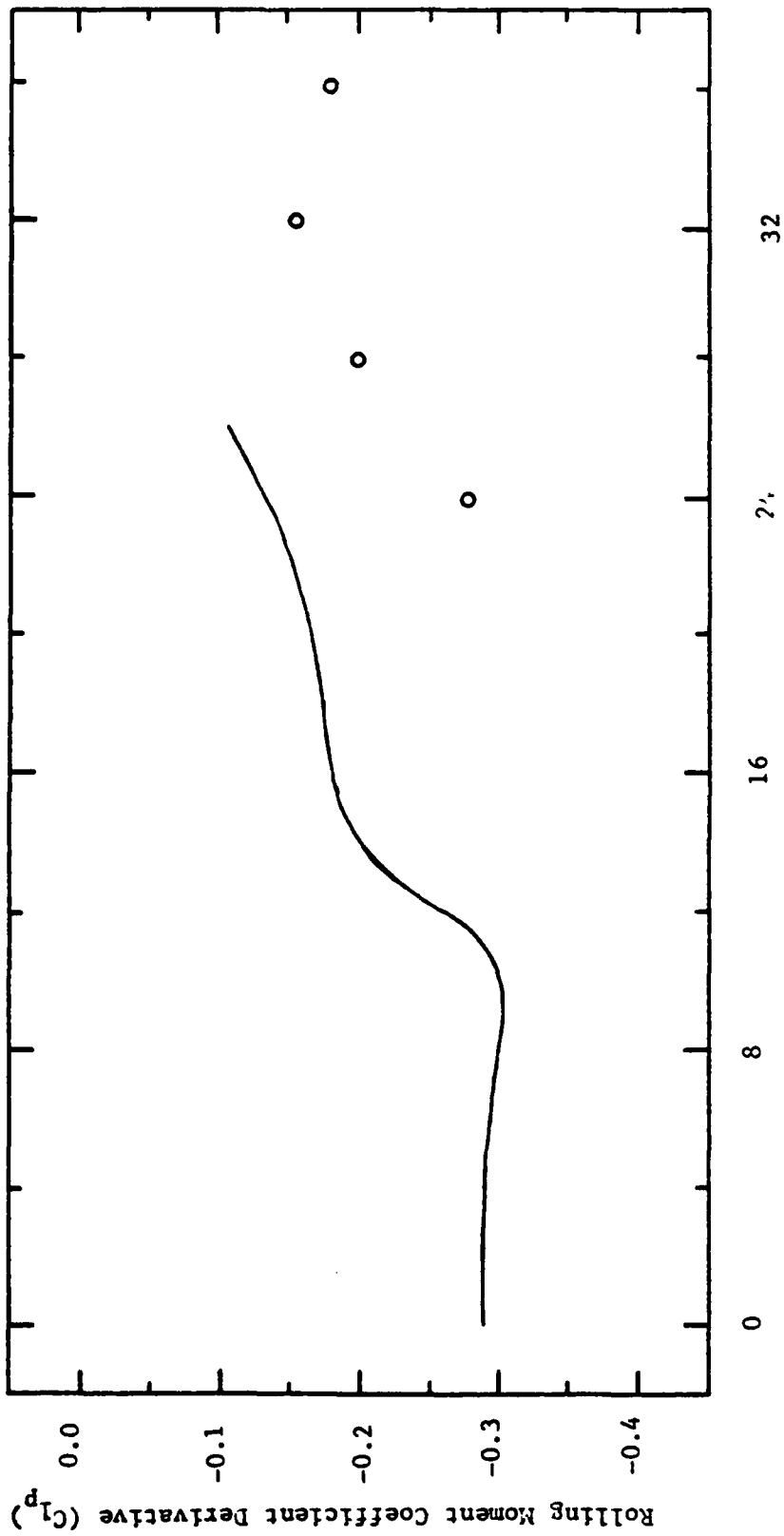
Angle of Attack ( $\alpha$ ), degrees

Figure 15. Design Phase Data:  $C_y^p$  vs  $\alpha$  for 0.2M



Angle of Attack ( $\alpha$ ), degrees

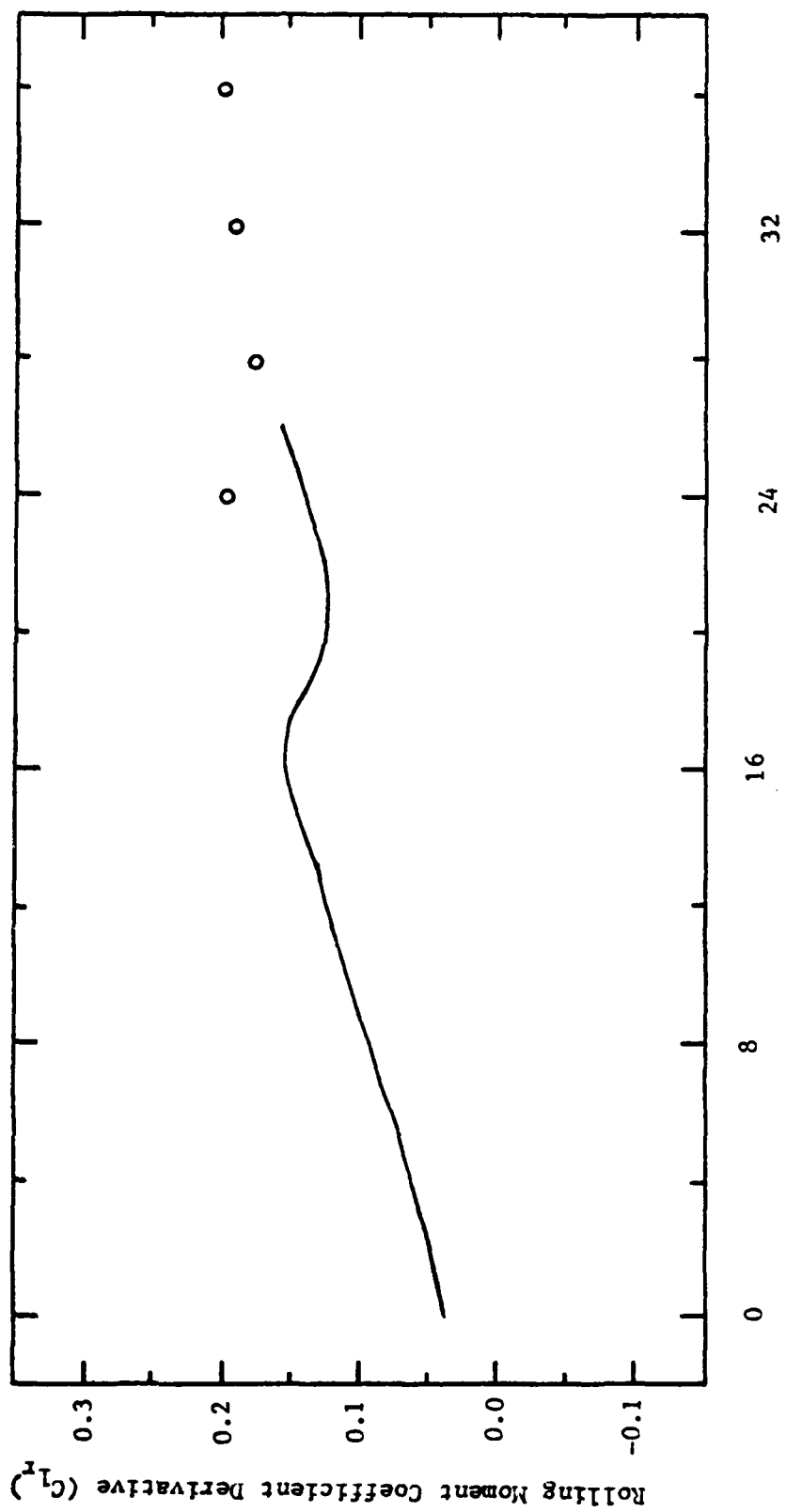
Figure 16. Design Phase Data:  $C_{Yr}$  vs  $\alpha$  for 0.2M



Angle of Attack ( $\alpha$ ), degrees

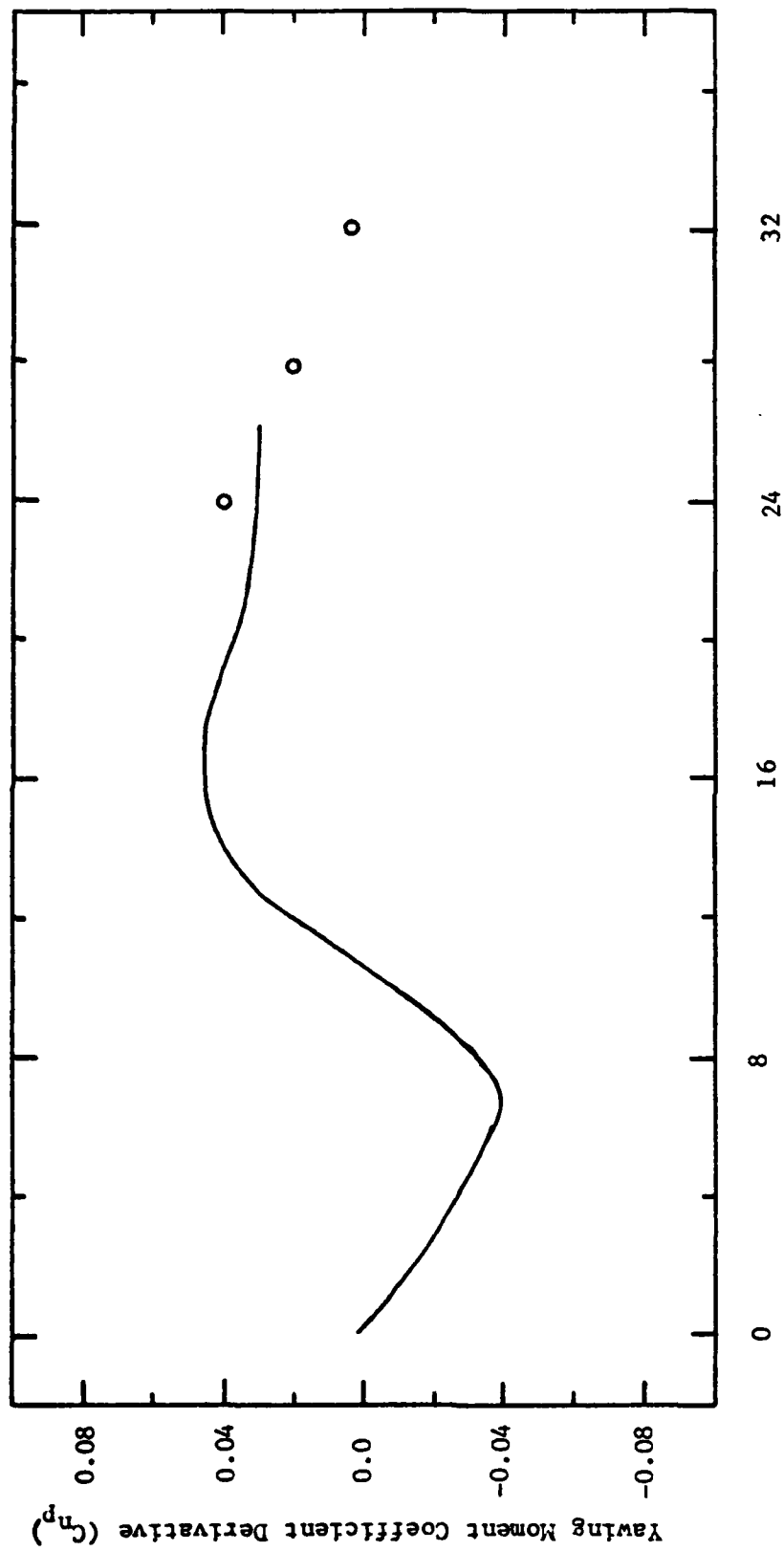
Figure 17. Design Phase Data:  $C_{1p}$  vs  $\alpha$  for 0.211





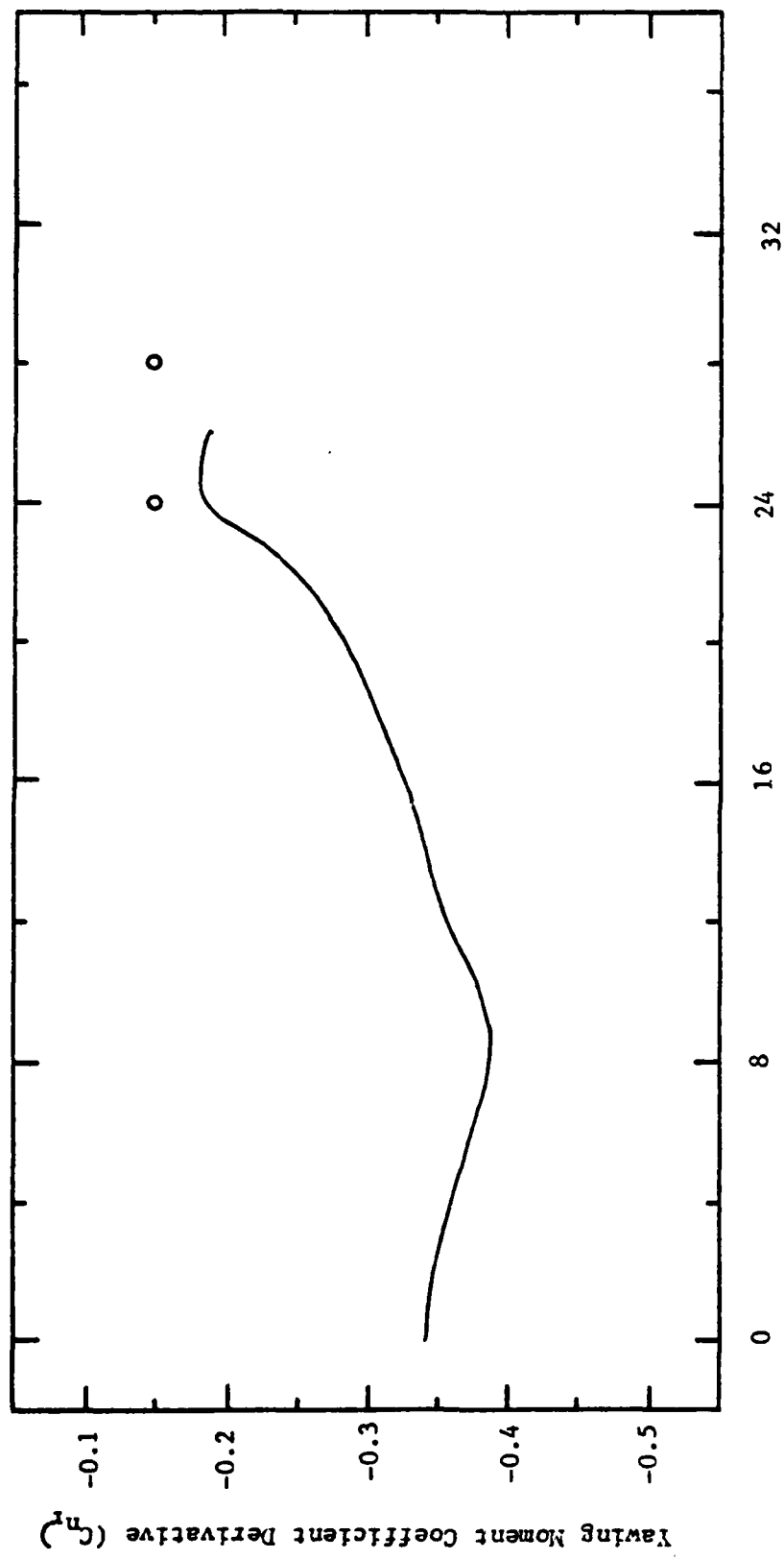
Angle of Attack ( $\alpha$ ), degrees

Figure 13. Design Phase Data:  $C_{l_r}$  vs  $\alpha$  for 0.2M



Angle of Attack ( $\alpha$ ), degrees

Figure 19. Design Phase Data:  $C_{np}$  vs  $\alpha$  for 0.2M



Angle of Attack ( $\alpha$ ), degrees

Figure 20. Design Phase Data:  $C_{nr}$  vs  $\alpha$  for 0.2M

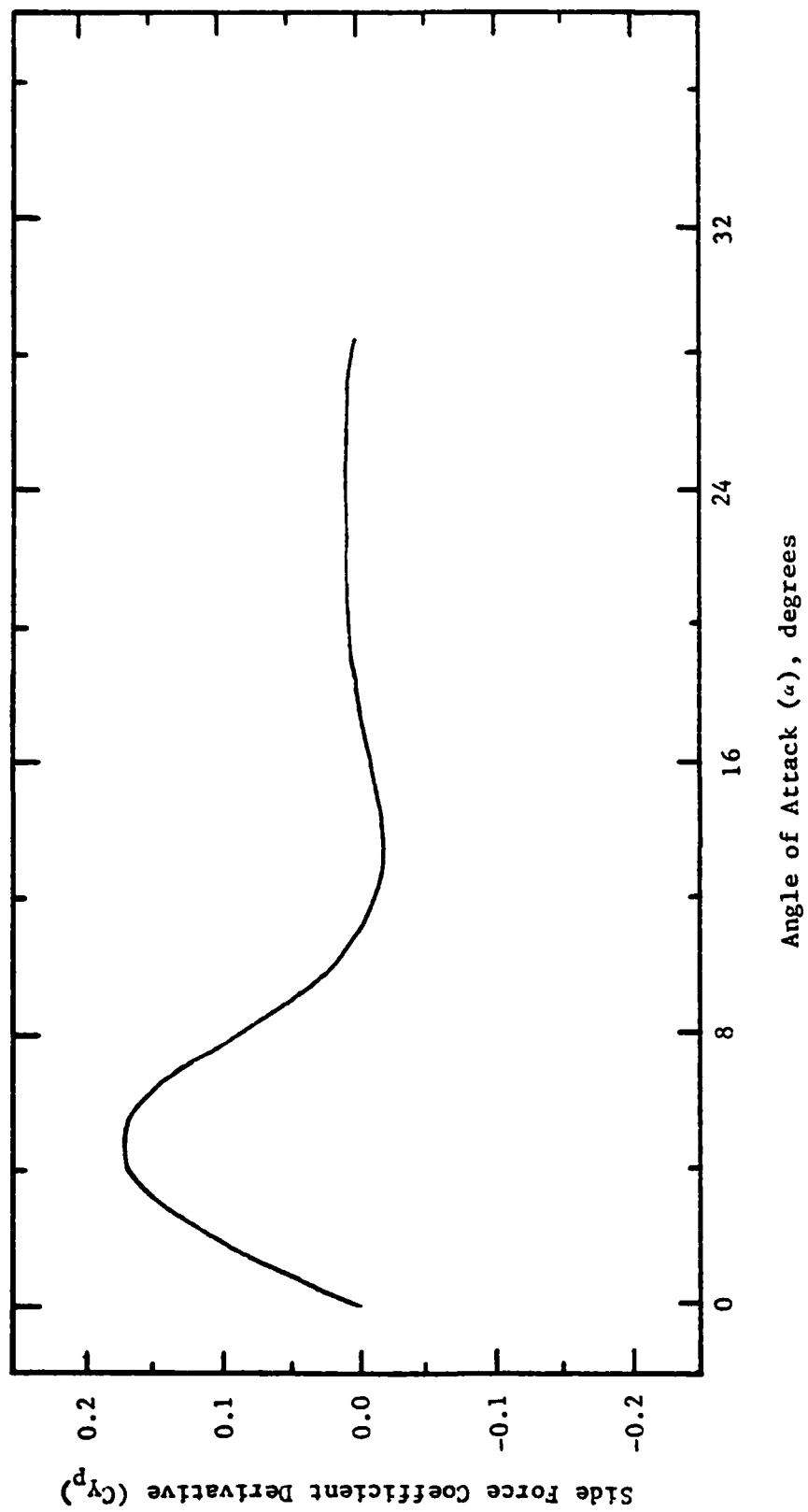


Figure 31. Design Phase data:  $C_{y_p}$  vs  $\alpha$  for 0.6M

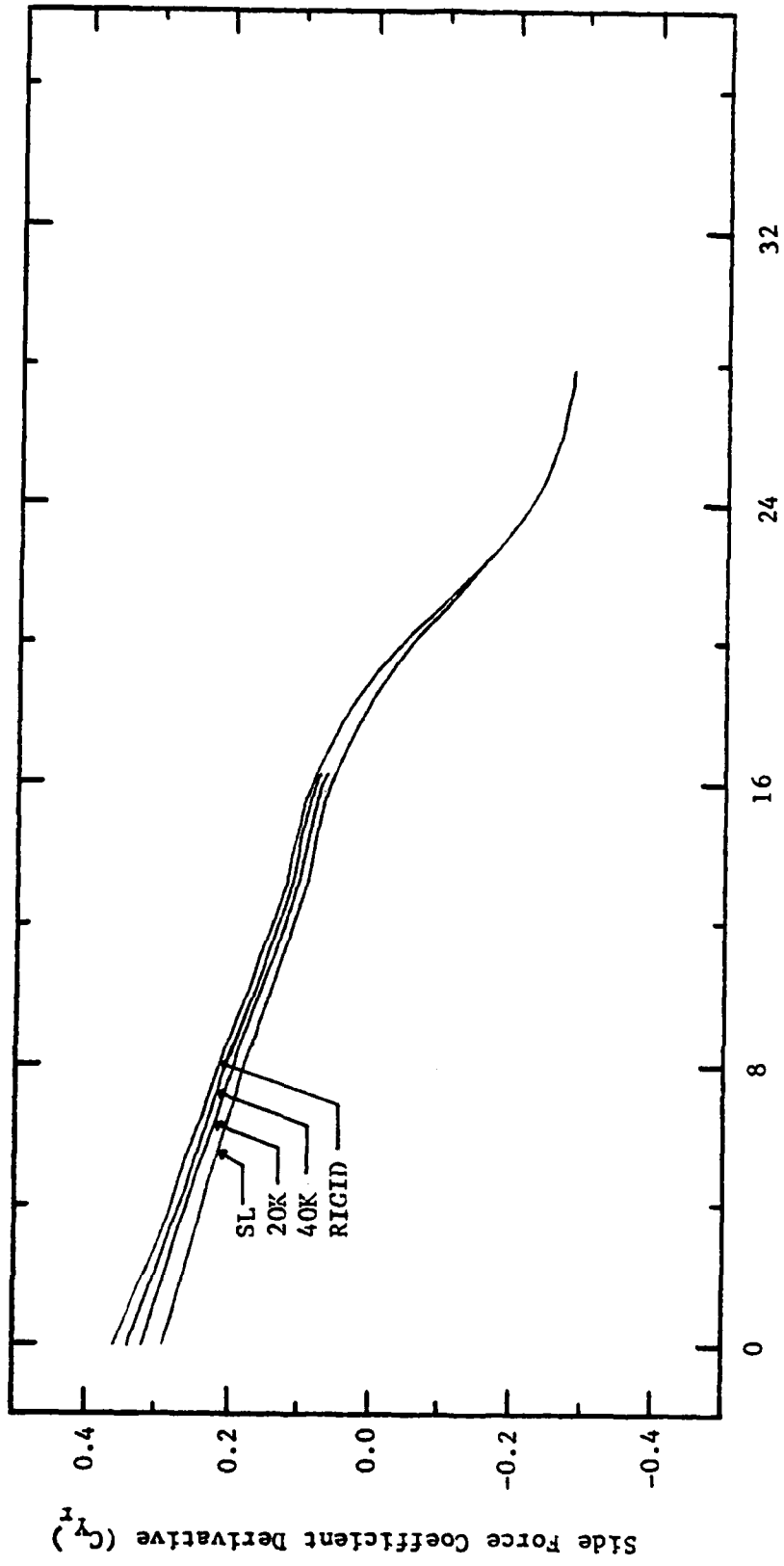


Figure 22. Design Phase Data:  $C_{Y_r}$  vs  $\alpha$  for 0.6M

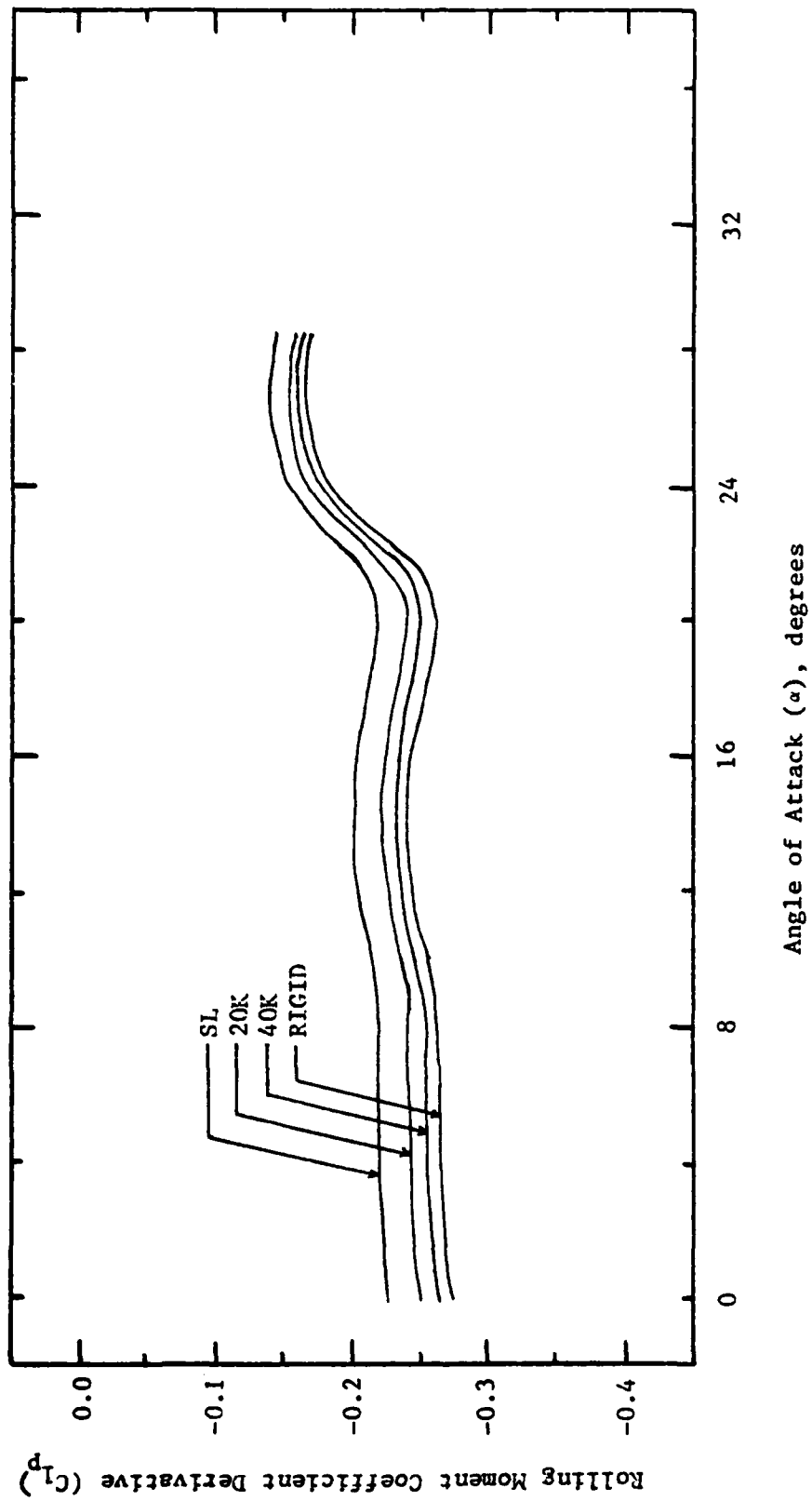


Figure 23. Design Phase Data:  $C_{l_p}$  vs  $\alpha$  for 0.6M

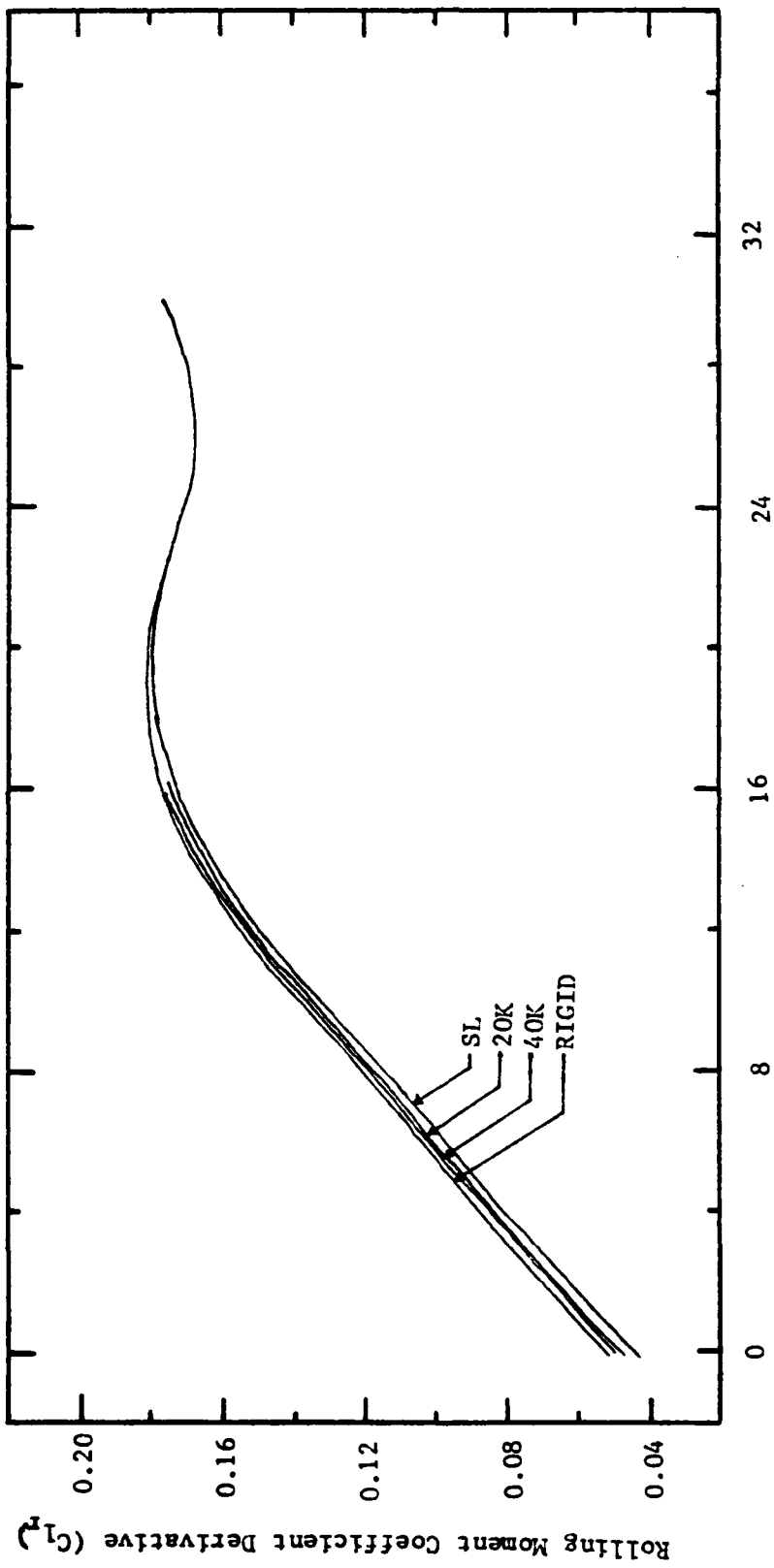
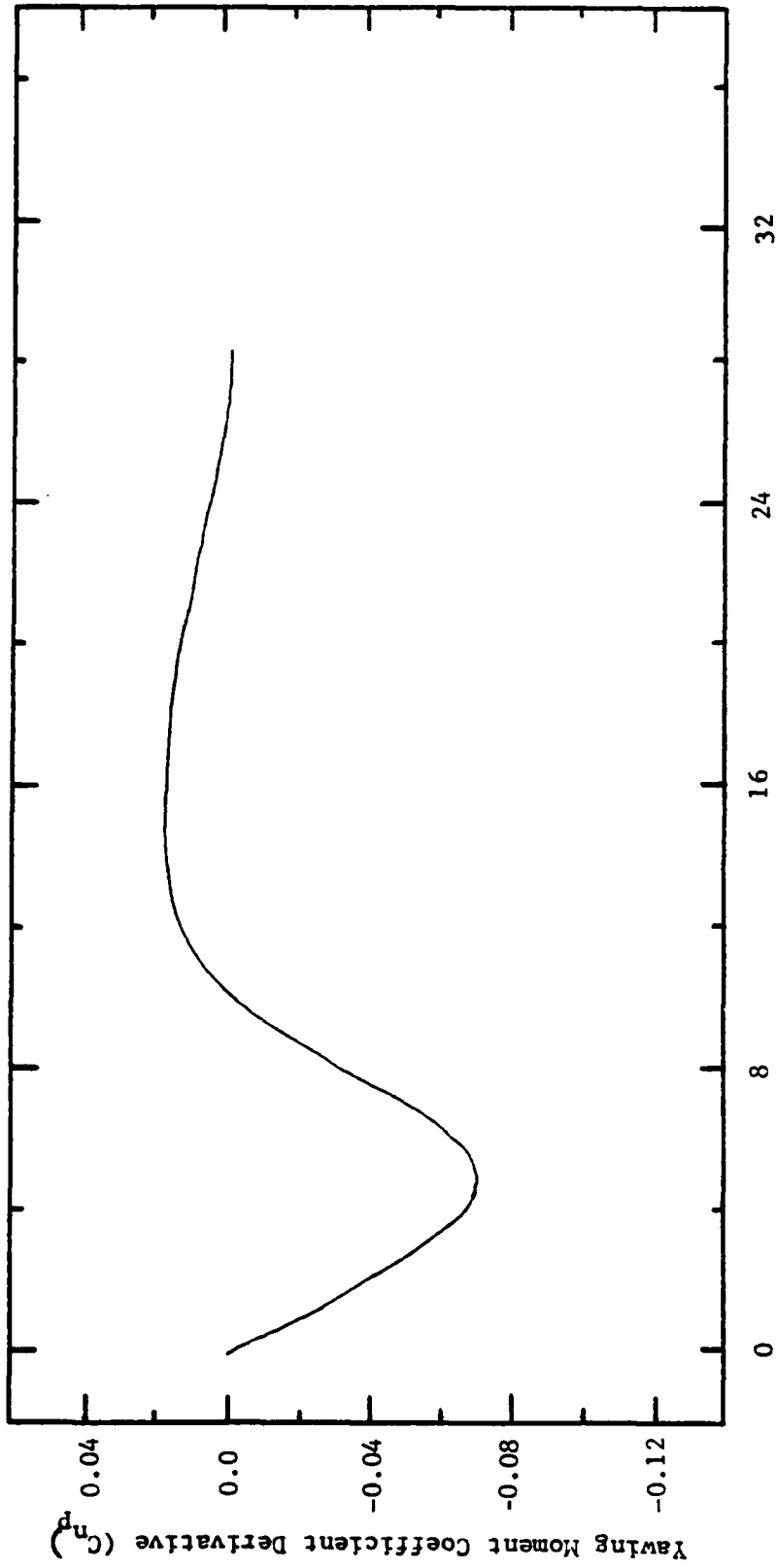


Figure 24. Design Phase Data:  $C_{l_r}$  vs  $\alpha$  for 0.6M



Angle of Attack ( $\alpha$ ), degrees

Figure 25. Design Phase Data:  $C_{np}$  vs  $\alpha$  for 0.6M



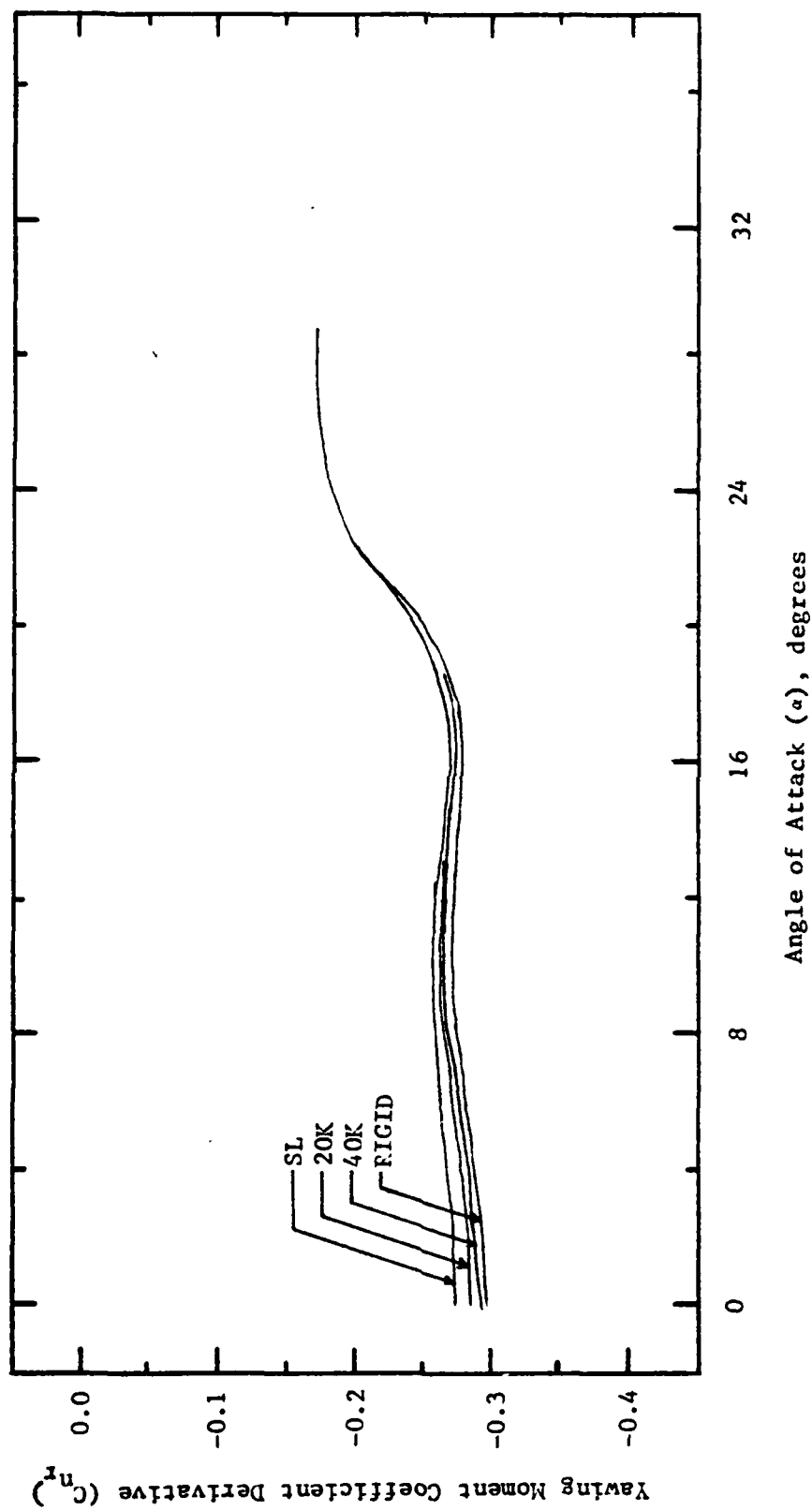


Figure 26. Design Phase Data:  $C_{n_r}$  vs  $\alpha$  for 0.6M

Appendix C: Data from MDC A4172

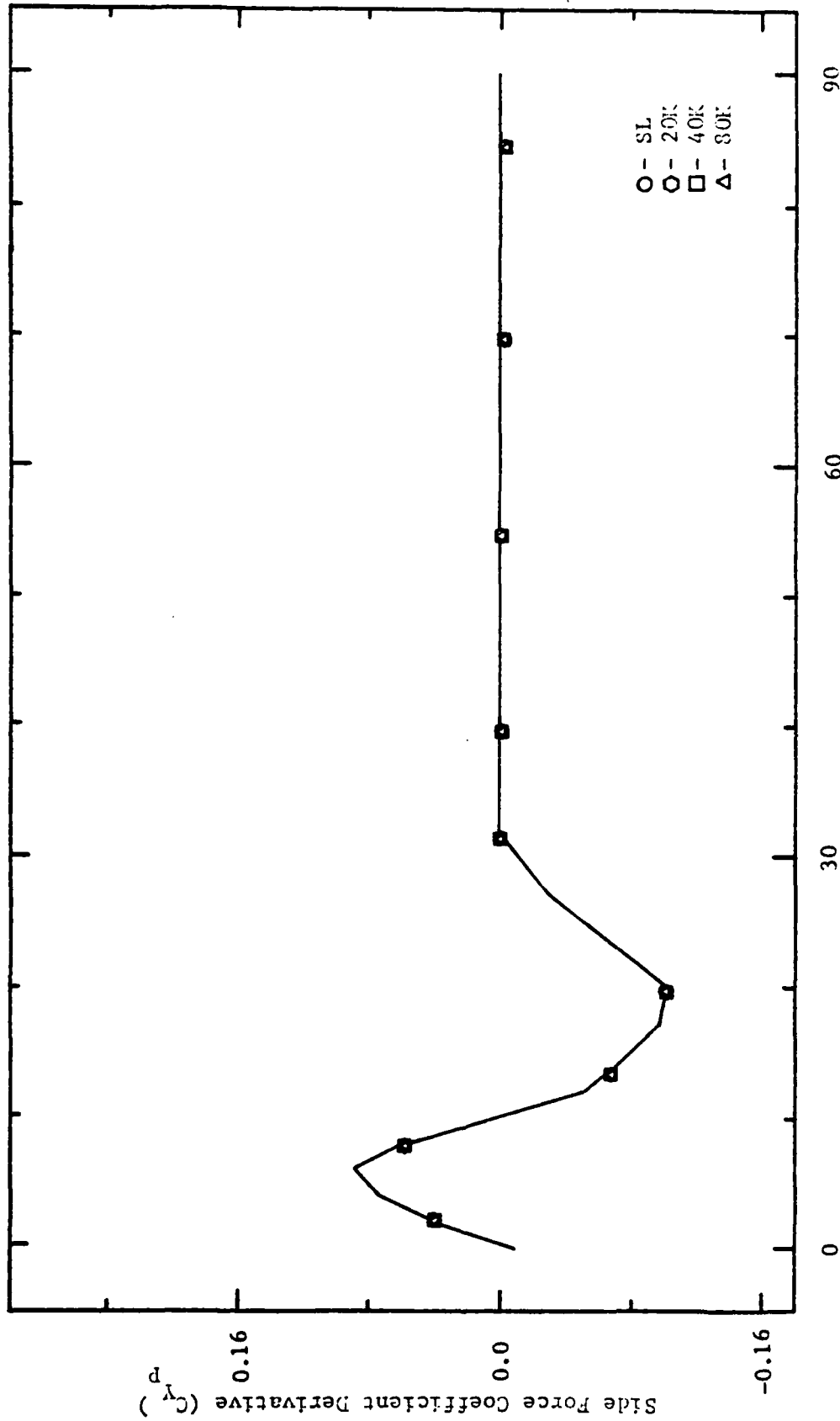


Figure 27. Production Phase Data:  $C_{Y_p}$  vs  $\alpha$  for 0.3M

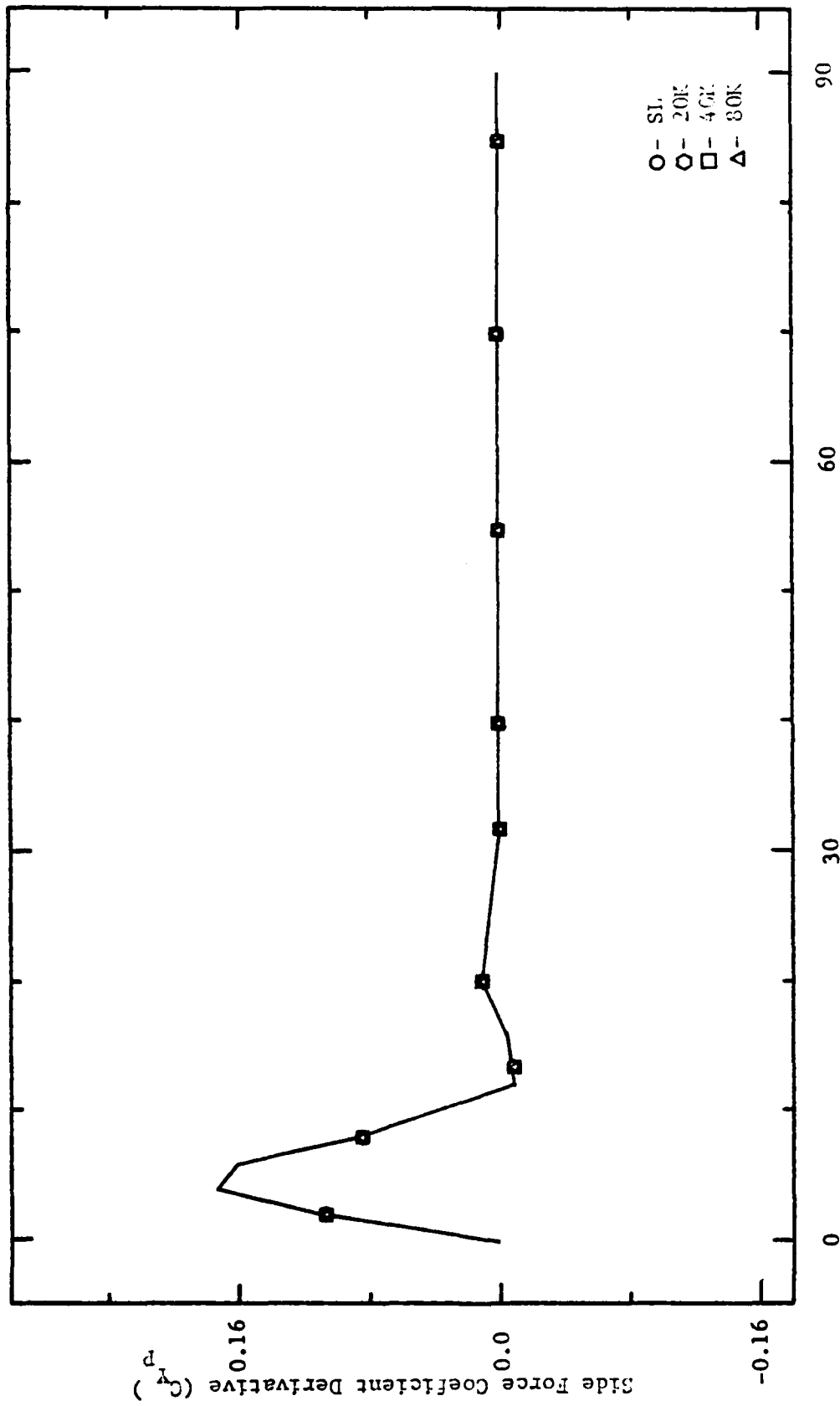


Figure 28. Production Phase Data:  $C_{Y_p}$  vs  $\alpha$  for 0.6M

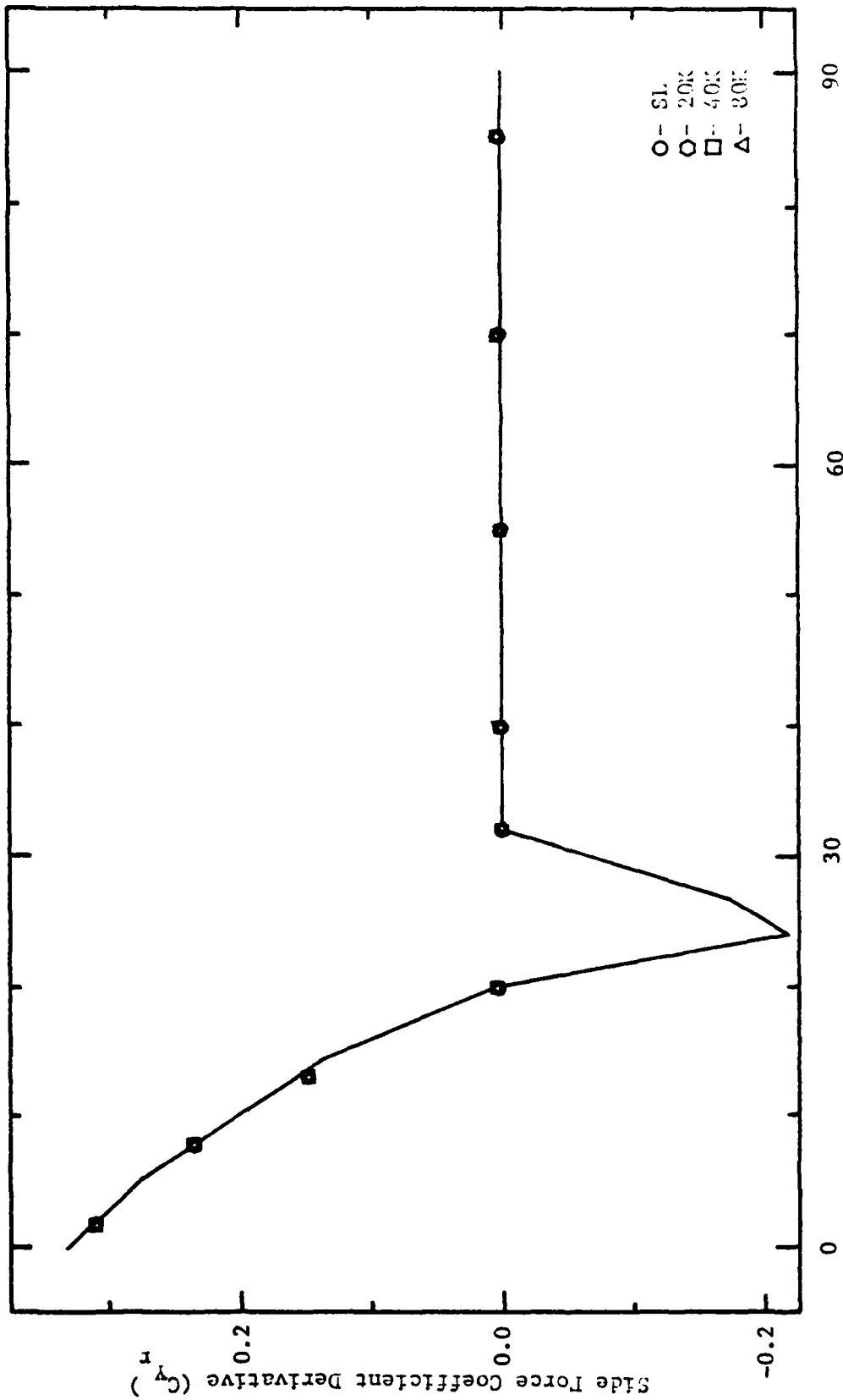
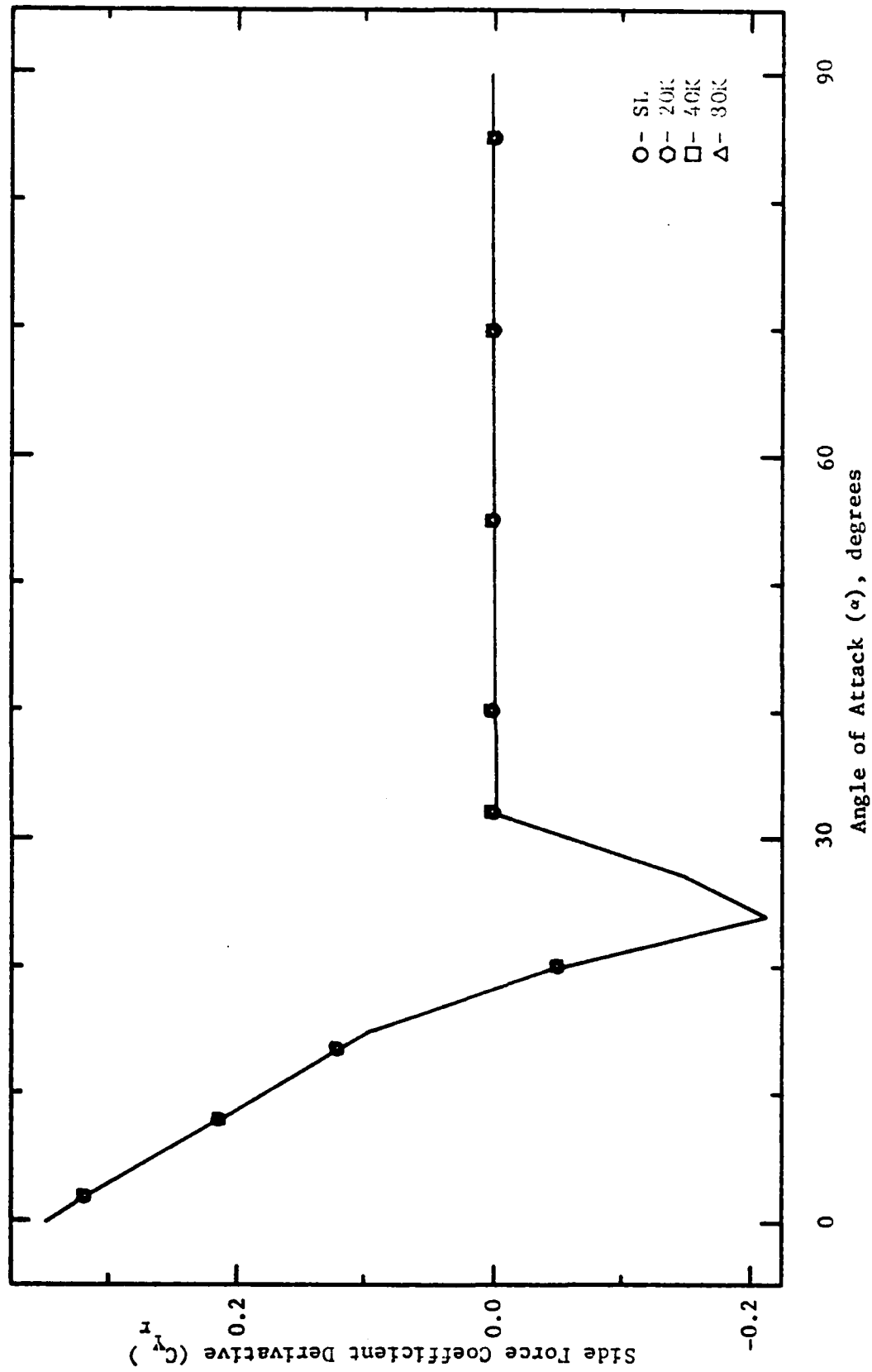


Figure 29. Production Phase Data:  $C_{Yr}$  vs  $\alpha$  for 0.3M



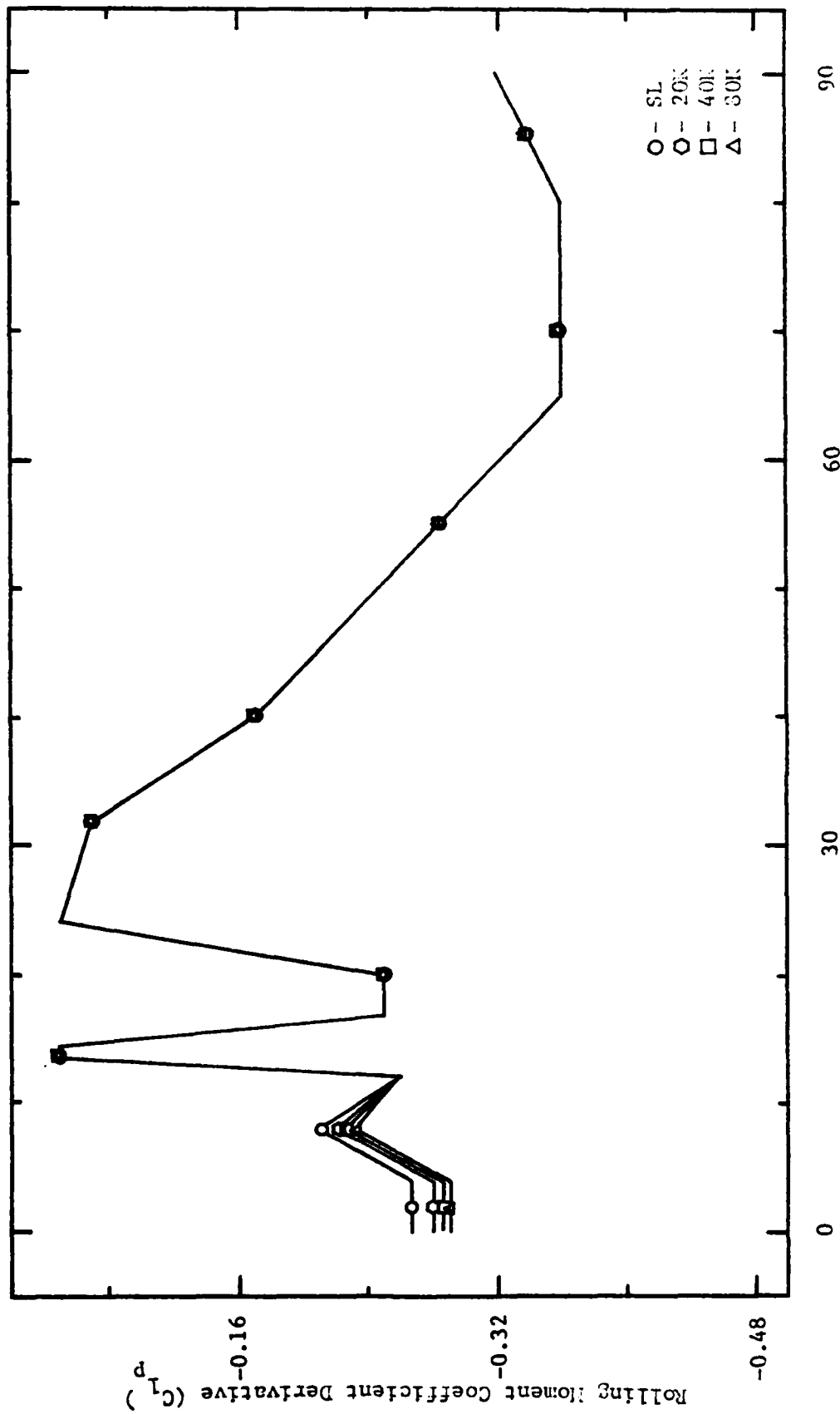


Figure 31. Production Phase Data:  $C_{1p}$  vs  $\alpha$  for 0.3M

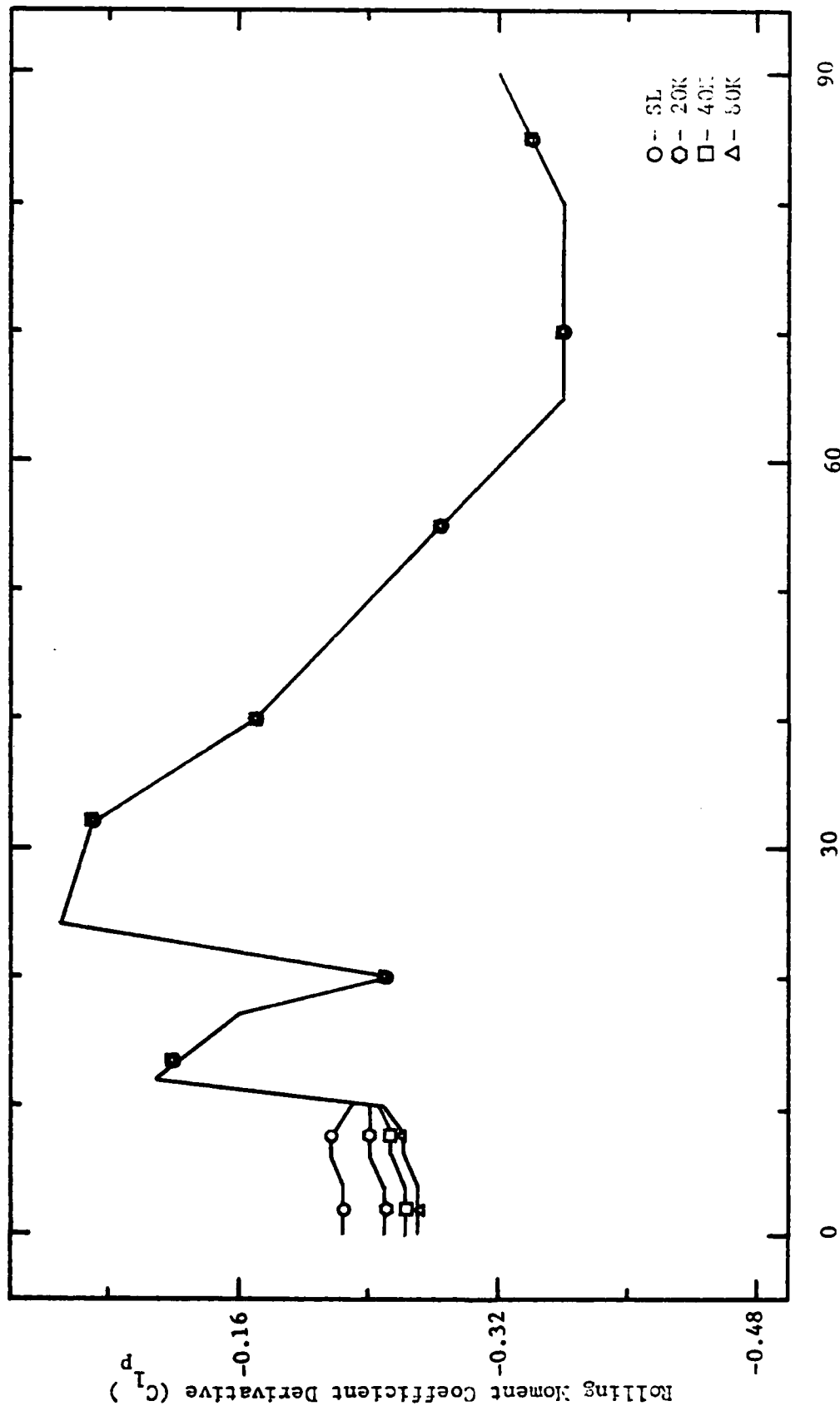


Figure 32. Production Phase Data:  $C_{l_p}$  vs  $\alpha$  for 0.6M



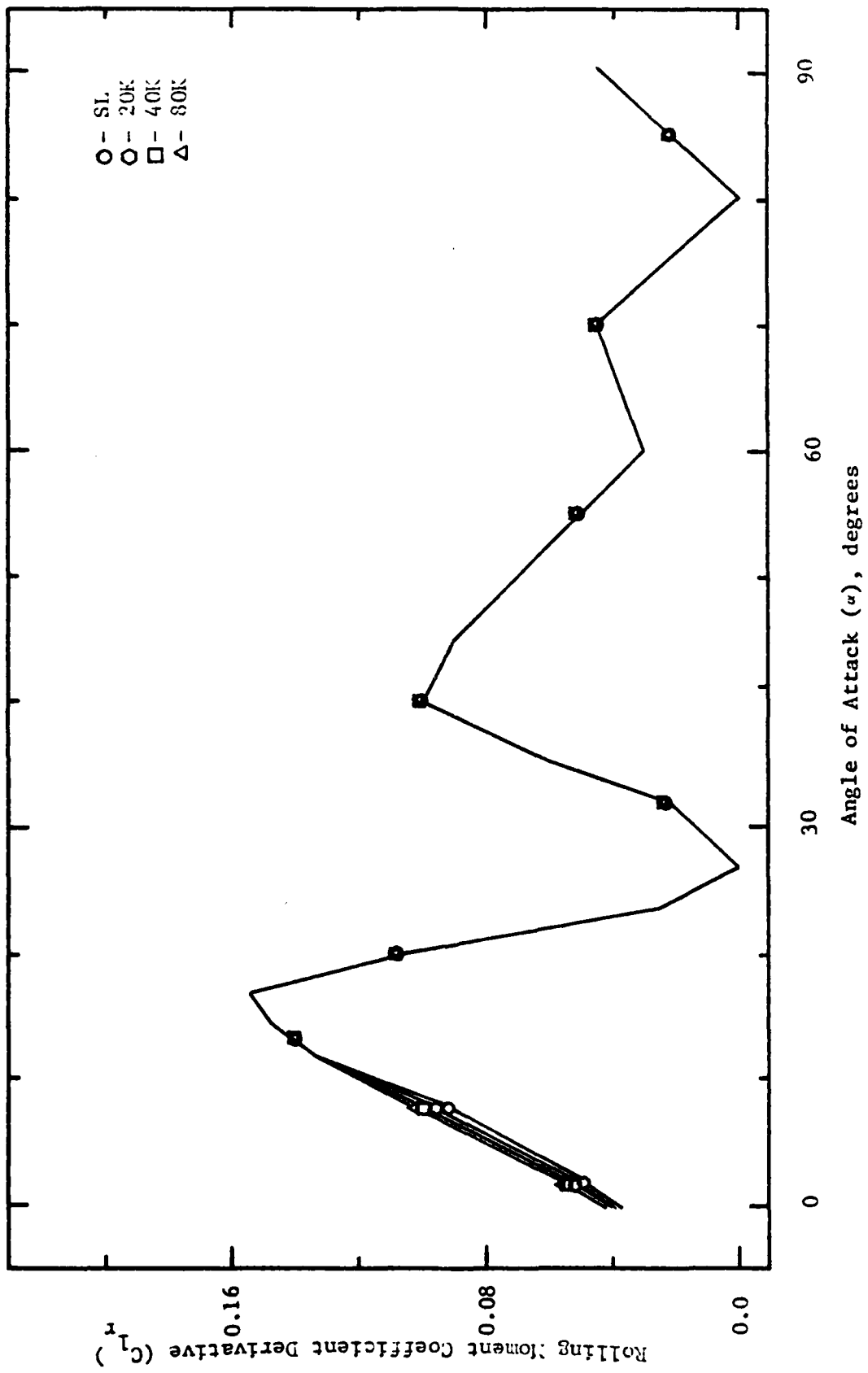


Figure 33. Production Phase Data:  $C_{l_r}$  vs  $\alpha$  for 0.3M

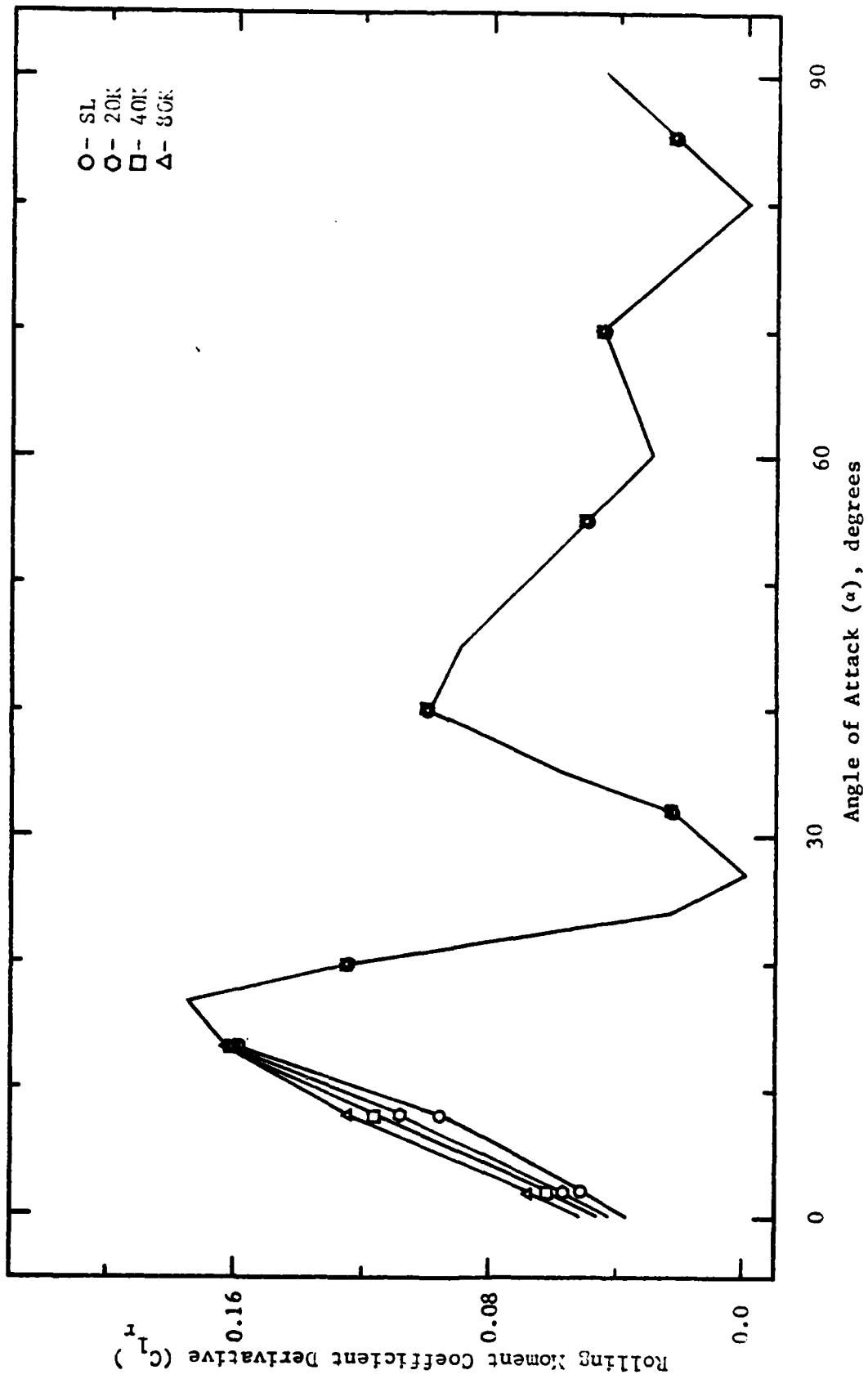
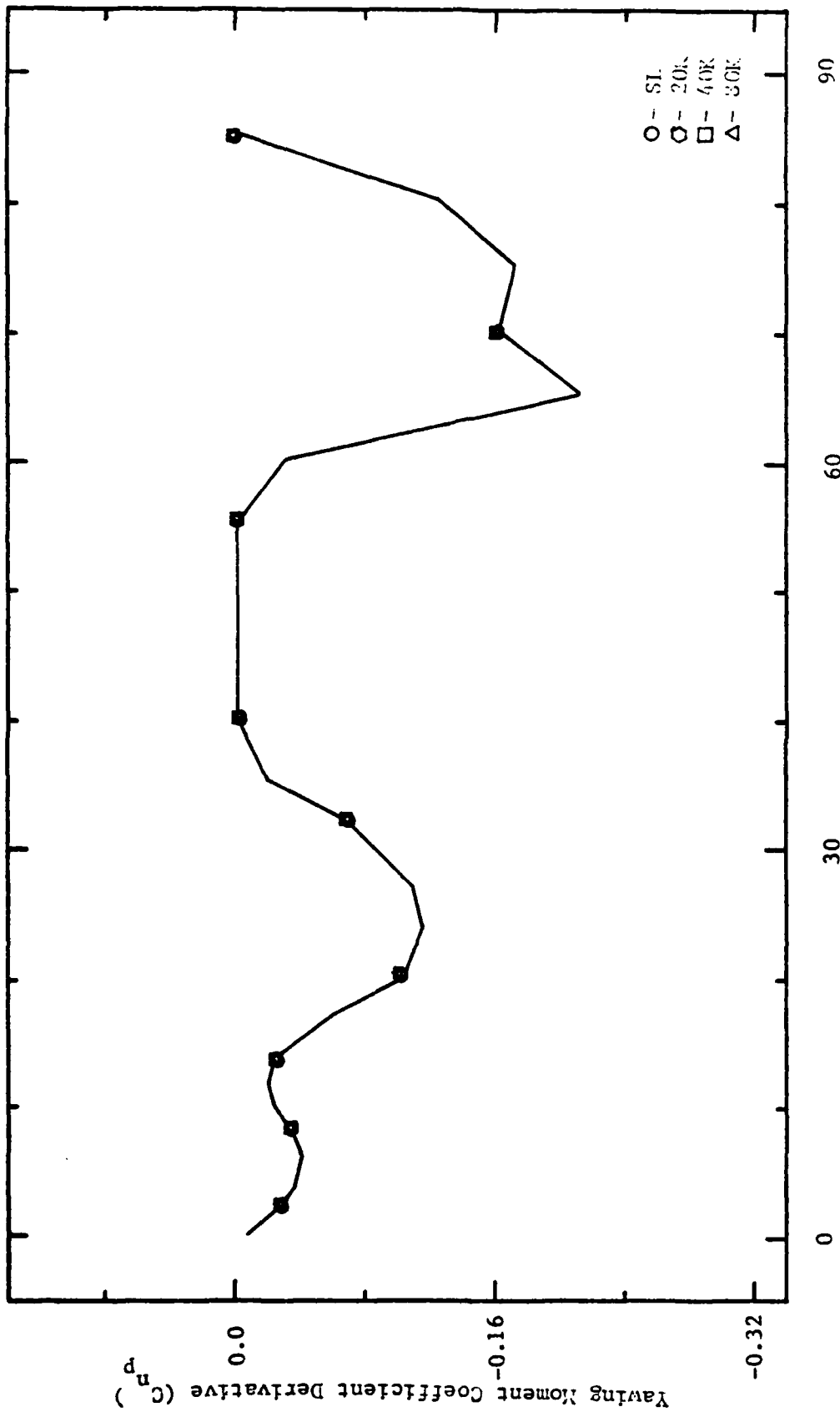


Figure 34. Production Phase Data:  $C_{lr}$  vs  $\alpha$  for 0.6M



90

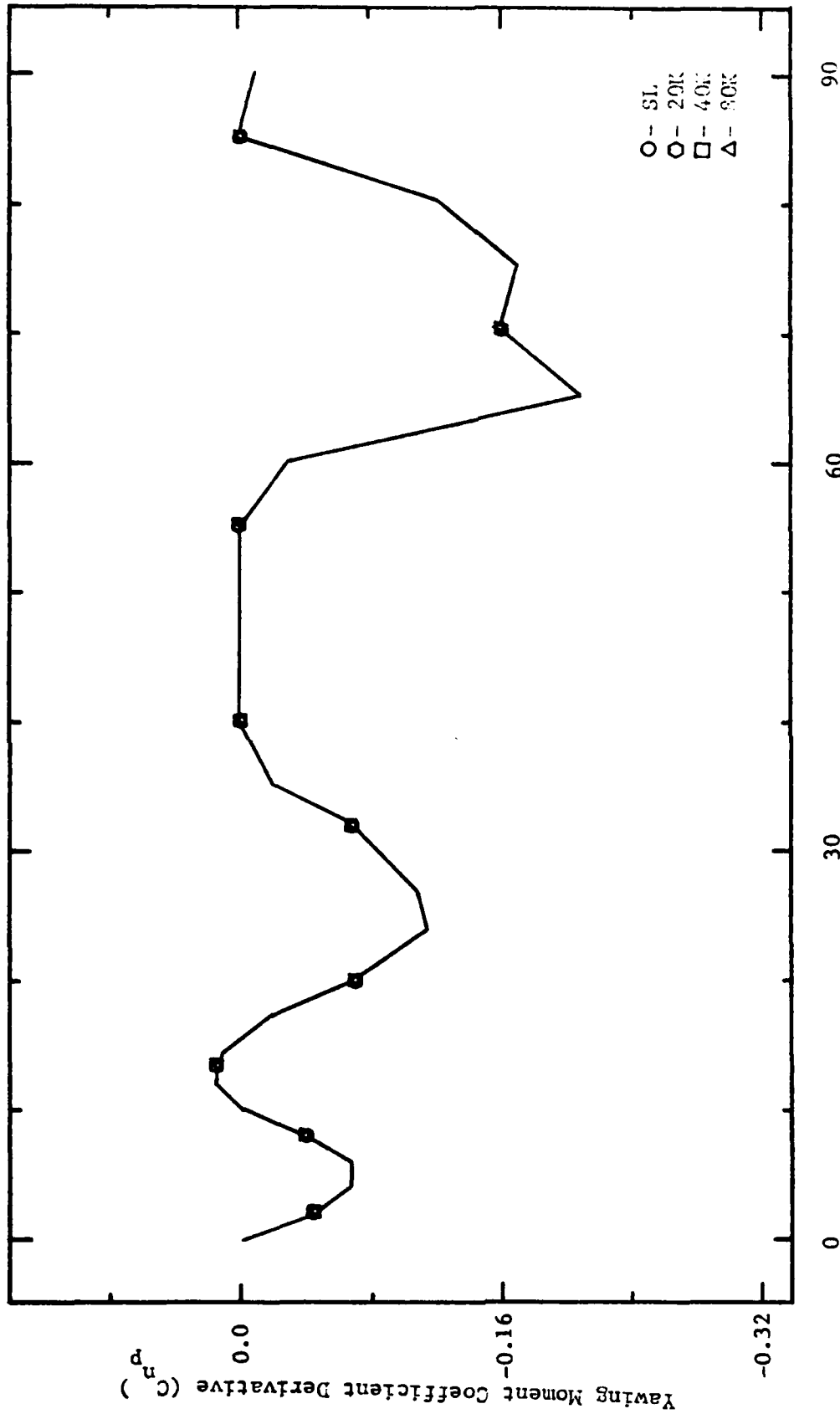
60

30

0

Angle of Attack ( $\alpha$ ), degrees

Figure 35. Production Phase Data:  $C_{np}$  vs  $\alpha$  for 0.3M



Angle of Attack ( $\alpha$ ), degrees

Figure 36. Production Phase Data:  $C_{np}$  vs  $\alpha$  for 0.6M

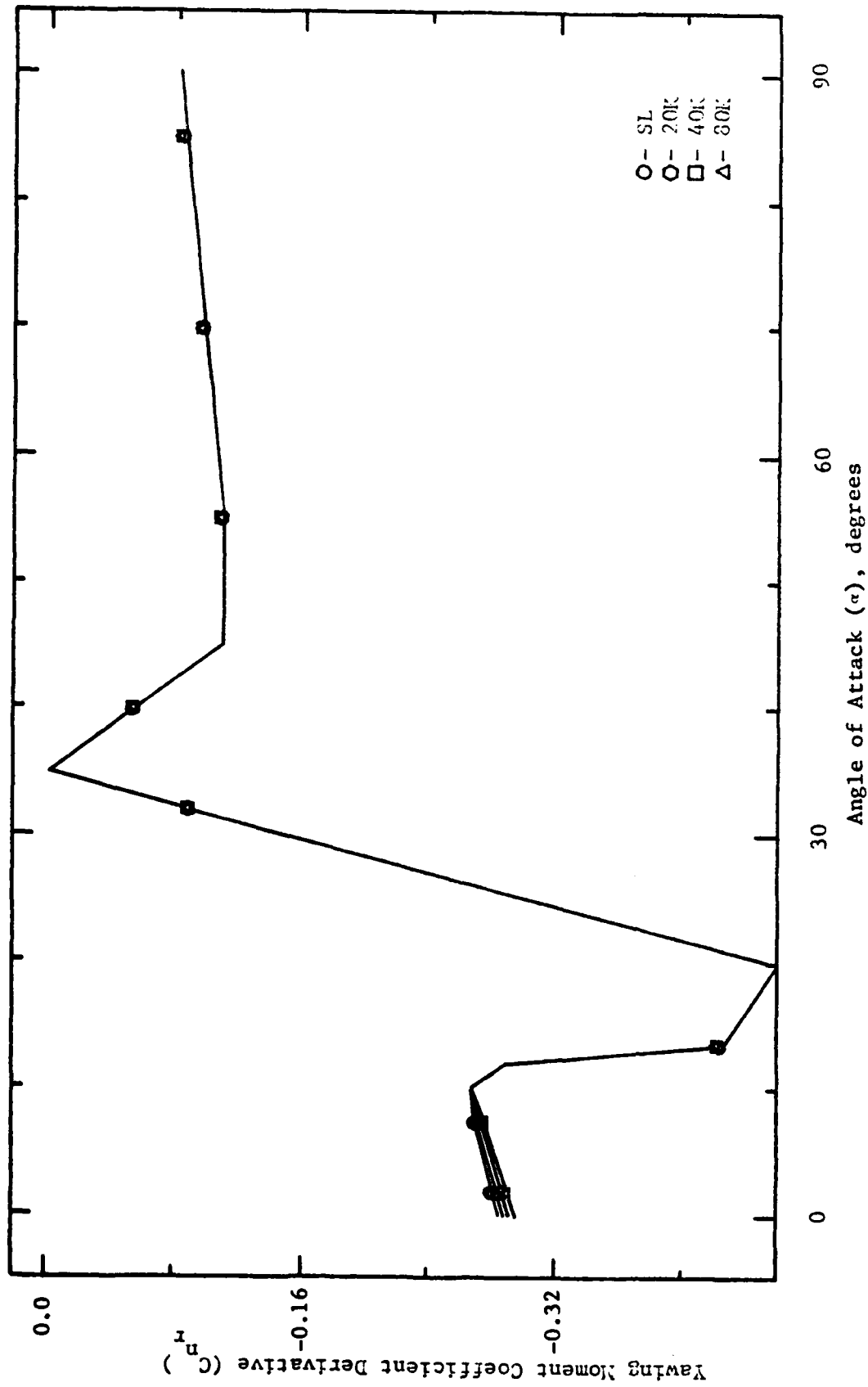


Figure 37. Production Phase Data:  $C_{n_r}$  vs  $\alpha$  for 0.3M

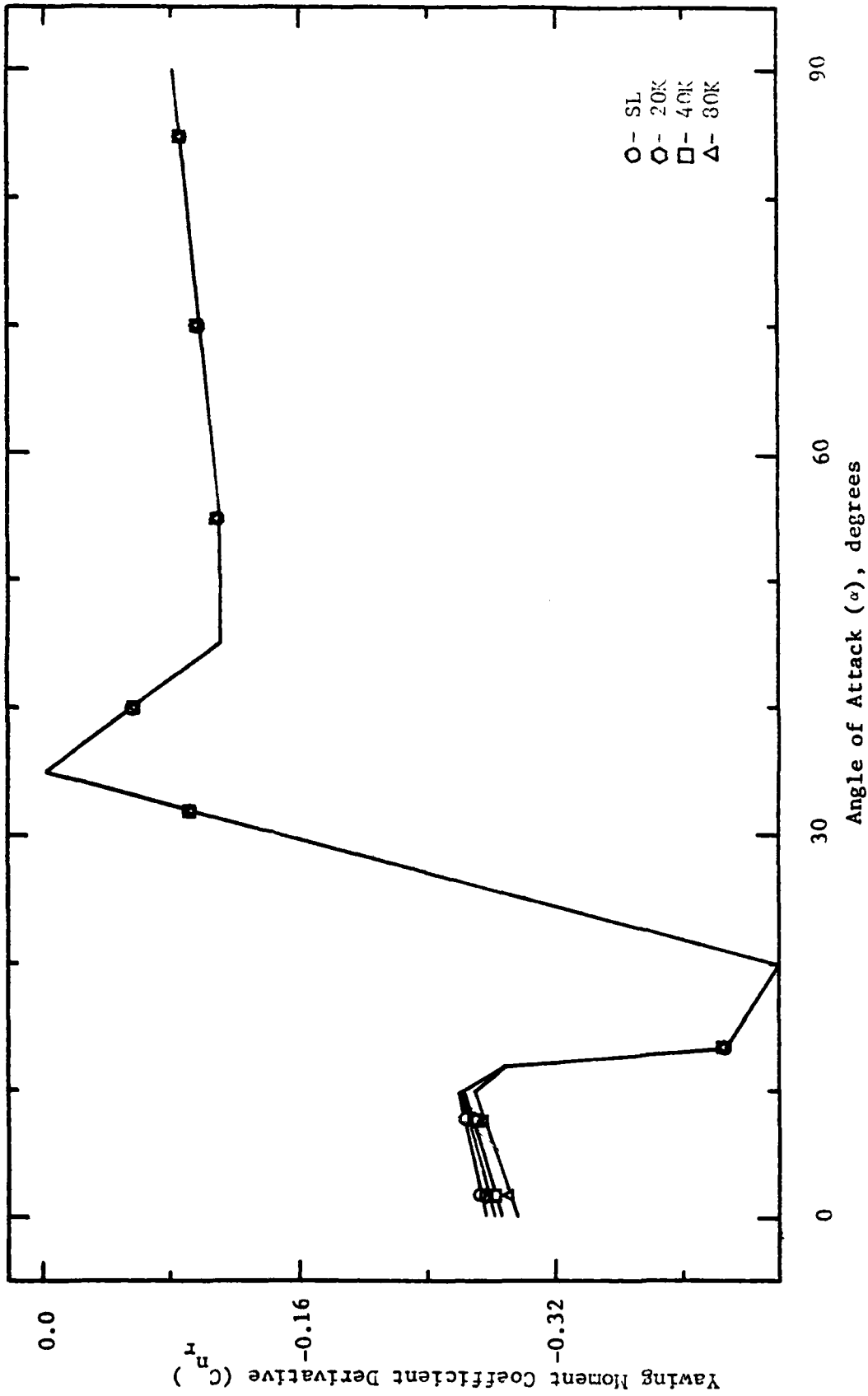


Figure 38. Production Phase Data:  $C_{n_r}$  vs  $\alpha$  for 0.6M

APPENDIX D: Derivation of the Relation for  $C_{i\Omega}$

When a model is tested on the rotary balance, it is mounted initially with the x axis of the body axis system aligned with the velocity vector (i.e., opposite the wind vector). Since this corresponds to an aircraft pointing along the gravity vector, the orientation of the y and z axes is arbitrary. The angle of attack ( $\alpha$ ) is defined as the angle between the x axis and the wind vector, and so it is zero in this initial mounting.

For testing, the model is set at an angle of attack and then rotated about an axis parallel to the wind vector. This rotation, when viewed in the body frame, is composed of a roll rate and a yaw rate. To find an expression for these rates in terms of the overall rotation rate,  $\Omega$ , it is necessary to do a 1-2 ( $\theta, \alpha$ ) axes rotation from the wind (inertial) axes frame to the body axis frame ( $\theta$  here is the rotation about the  $\hat{x}_1$  axis so:  $\dot{\theta} = \Omega$ ).

Designating the  $\hat{w}_i$  to be the wind axes frame unit vectors,  $\hat{i}_i$  to be the intermediate axes frame unit vectors, and  $\hat{b}_i$  to be the body axes frame unit vectors, the transformations become:

$$L_{iw} = \begin{pmatrix} 1 & 0 & 0 \\ 0 & \cos \theta & \sin \theta \\ 0 & -\sin \theta & \cos \theta \end{pmatrix} \quad (4)$$

$$L_{bi} = \begin{Bmatrix} \cos \alpha & 0 & -\sin \alpha \\ 0 & 1 & 0 \\ \sin \alpha & 0 & \cos \alpha \end{Bmatrix} \quad (5)$$

The overall rotation in the wind axes frame is:

$$\vec{\omega}^{b/i} = \alpha \hat{w}_1 \quad (6)$$

Using the transformation relation:

$$[\omega^{b/i}]_i = L_{iw} [\omega^{b/i}]_w \quad (7)$$

the rotation in the intermediate frame is:

$$\vec{\omega}^{b/i} = \alpha \hat{i}_1 \quad (8)$$

Transforming to the body frame:

$$\begin{aligned} [\omega^{b/i}]_b &= L_{bi} [\omega^{b/i}]_i \\ &= L_{bi} \begin{bmatrix} \alpha \\ 0 \\ 0 \end{bmatrix}_i \end{aligned} \quad (9)$$

so the rotation in the body frame is:

$$\vec{\omega}^{b/i} = \cos \alpha \hat{b}_1 + \sin \alpha \hat{b}_3 \quad (10)$$

Since the body rates are defined by:

$$\vec{\omega}^{b/i} = p \hat{b}_1 + q \hat{b}_2 + r \hat{b}_3 \quad (11)$$

the body rates become:



$$\begin{aligned} p &= \Omega \cos \alpha \\ r &= \Omega \sin \alpha \end{aligned} \quad (12)$$

or in non-dimensional form:

$$\begin{aligned} pb/2V &= (\Omega b/2V) \cos \alpha \\ rb/2V &= (\Omega b/2V) \sin \alpha \end{aligned} \quad (13)$$

The effect on the force and moment coefficients of the overall rotation rate must be the same as the sum of the effects of the body rates so:

$$C_{i\Omega} \Omega' = C_{ip} p' + C_{ir} r' \quad (14)$$

where  $\Omega'$ ,  $p'$ , and  $r'$  are nondimensional and:

$$\begin{aligned} C_{ik} &= \partial C_i / \partial (kb/2V) \\ i &= N, A, Y, l, m, n \\ k &= p', r', \Omega' \end{aligned} \quad (15)$$

Substituting for  $p'$  and  $r'$ :

$$C_{i\Omega} \Omega' = C_{ip} \Omega' \cos \alpha + C_{ir} \Omega' \sin \alpha \quad (16)$$

and dividing through by  $\Omega'$ :

$$C_{i\Omega} = C_{ip} \cos \alpha + C_{ir} \sin \alpha \quad (17)$$

Appendix E: Tabulations and Plots for Each  
Parameter/Mach Number/Data Set  
Combinations

Table III

Rotary Balance Data:  $C_1$  vs  $nb/2V$   
for  $8^\circ < \alpha < 90^\circ$

$\alpha$	$nb/2V$								
	<u>-0.4</u>	<u>-0.3</u>	<u>-0.2</u>	<u>-0.1</u>	<u>-0-</u>	<u>0.1</u>	<u>0.2</u>	<u>0.3</u>	<u>0.4</u>
8°	935	670	430	220	5	-235	-450	-690	-950
10°	850	585	380	195	5	-205	-395	-605	-860
12°	775	525	325	155	5	-160	-335	-530	-790
14°	695	450	265	130	5	-125	-265	-455	-690
16°	590	385	220	90	5	-95	-215	-385	-615
18°	450	315	175	80	0	-80	-170	-305	-500
20°	420	245	145	65	0	-80	-150	-235	-420
25°	200	75	15	-20	0	-20	-50	-125	-250
30°	-50	-185	-205	-140	0	115	180	140	15
35°	-240	-200	-105	-50	0	95	150	190	220
30°	-150	-255	-275	-150	-15	110	270	245	125
40°	65	70	125	100	95	10	-20	135	325
50°	160	195	145	50	35	25	40	70	145
55°	160	225	175	70	35	-5	15	125	75
60°	145	195	155	50	30	-5	-60	-45	100
70°	-15	110	85	-5	15	-5	-75	-95	25
80°	-250	-115	-45	-55	20	55	55	80	240
90°	-355	-245	-180	-60	15	100	180	230	370

Table IV

Rotary Balance Data:  $C_{1a}$  vs  $\alpha$  ( $8^\circ - 90^\circ$ )

$\alpha$	$C_{1a}$
$8^\circ$	-0.2306
$10^\circ$	-0.2060
$12^\circ$	-0.1843
$14^\circ$	-0.1595
$16^\circ$	-0.1364
$18^\circ$	-0.1085
$20^\circ$	-0.0923
$25^\circ$	-0.0422
$30^\circ$	0.0377
$35^\circ$	0.0611
$30^\circ$	-0.0011
$40^\circ$	0.0101
$50^\circ$	0.0096
$55^\circ$	0.0097
$60^\circ$	0.0063
$70^\circ$	0.0004
$80^\circ$	-0.0002
$90^\circ$	0.0006

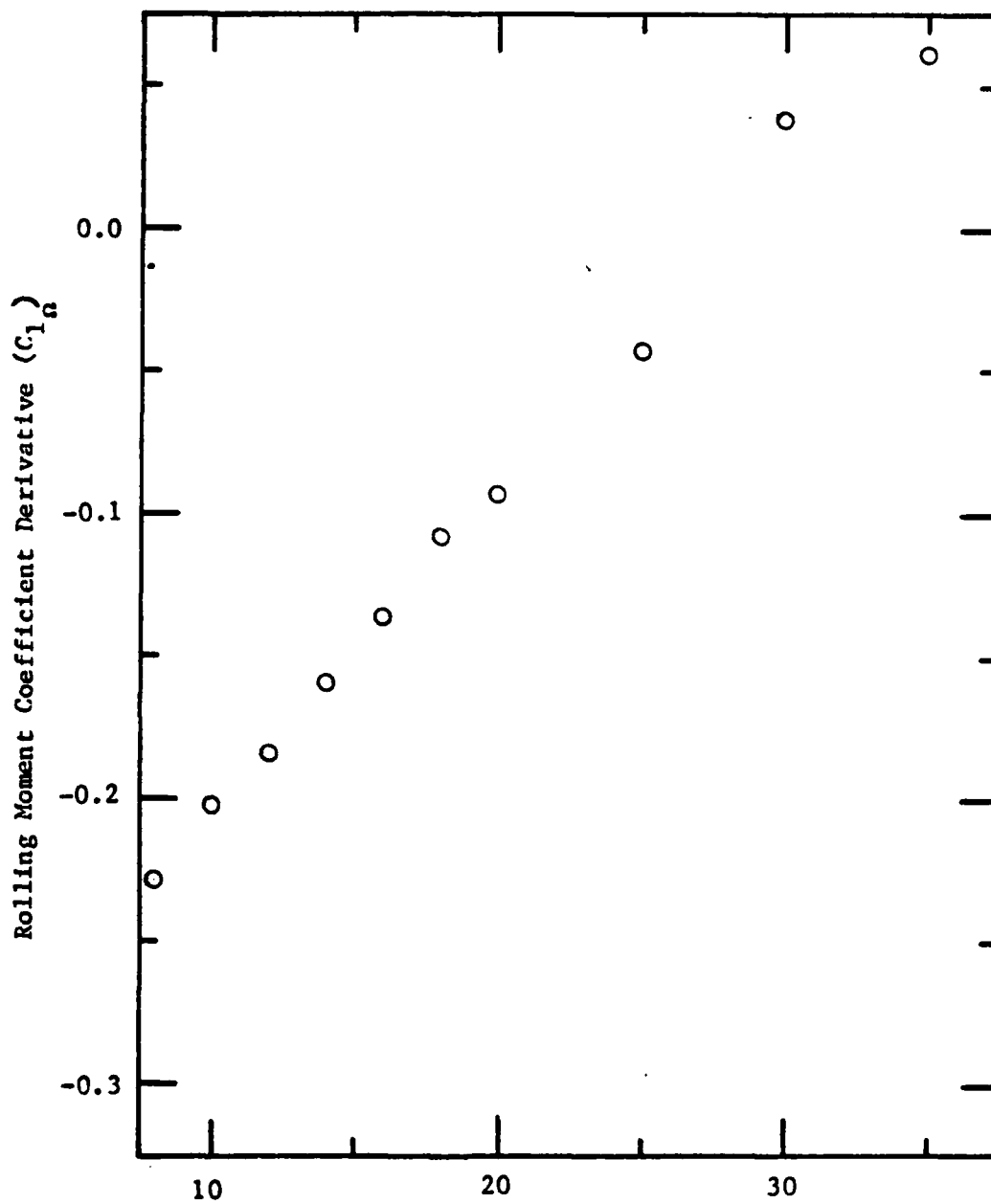


Figure 39. Rotary Balance Data:  $C_{l_{\dot{\alpha}}}$  vs  $\alpha$

Table V

Rotary Balance Data:  $C_n$  vs  $ab/2V$   
for  $8^\circ < \alpha < 90^\circ$

$\alpha$	$ab/2V$								
	<u>-0.4</u>	<u>-0.3</u>	<u>-0.2</u>	<u>-0.1</u>	<u>-0</u>	<u>0.1</u>	<u>0.2</u>	<u>0.3</u>	<u>0.4</u>
8°	375	275	170	50	-70	-185	-310	-435	-555
10°	435	320	195	55	-70	-195	-340	-480	-615
12°	475	365	230	70	-70	-220	-370	-530	-635
14°	500	395	250	95	-70	-245	-395	-555	-670
16°	560	445	285	110	-70	-265	-445	-605	-730
18°	620	500	330	140	-70	-280	-490	-645	-735
20°	635	535	355	155	-70	-280	-485	-650	-745
25°	665	550	380	190	-15	-245	-465	-615	-705
30°	680	510	330	160	-10	-180	-345	-510	-700
35°	700	460	300	160	25	-120	-265	-415	-680
30°	935	665	425	210	-15	-210	-440	-690	-995
40°	765	520	385	260	55	-125	-275	-430	-750
50°	920	620	455	360	375	135	150	55	-245
55°	1045	810	630	515	480	375	240	125	195
60°	875	690	685	565	475	310	350	300	90
70°	630	515	410	345	55	-95	-270	-420	-585
80°	475	275	160	120	30	-90	-150	-255	-460
90°	610	390	210	125	-10	-95	-185	-395	-590

Table VI

Rotary Balance Data:  $C_{n_a}$  vs  $\alpha$  ( $8^\circ - 90^\circ$ )

<u><math>\alpha</math></u>	<u><math>C_{n_a}</math></u>
$8^\circ$	-0.1174
$10^\circ$	-0.1320
$12^\circ$	-0.1436
$14^\circ$	-0.1527
$16^\circ$	-0.1691
$18^\circ$	-0.1819
$20^\circ$	-0.1865
$25^\circ$	-0.1850
$30^\circ$	-0.1712
$35^\circ$	-0.1593
$30^\circ$	-0.0013
$40^\circ$	0.0045
$50^\circ$	0.0384
$55^\circ$	0.0491
$60^\circ$	0.0482
$70^\circ$	0.0067
$80^\circ$	0.0012
$90^\circ$	0.0007

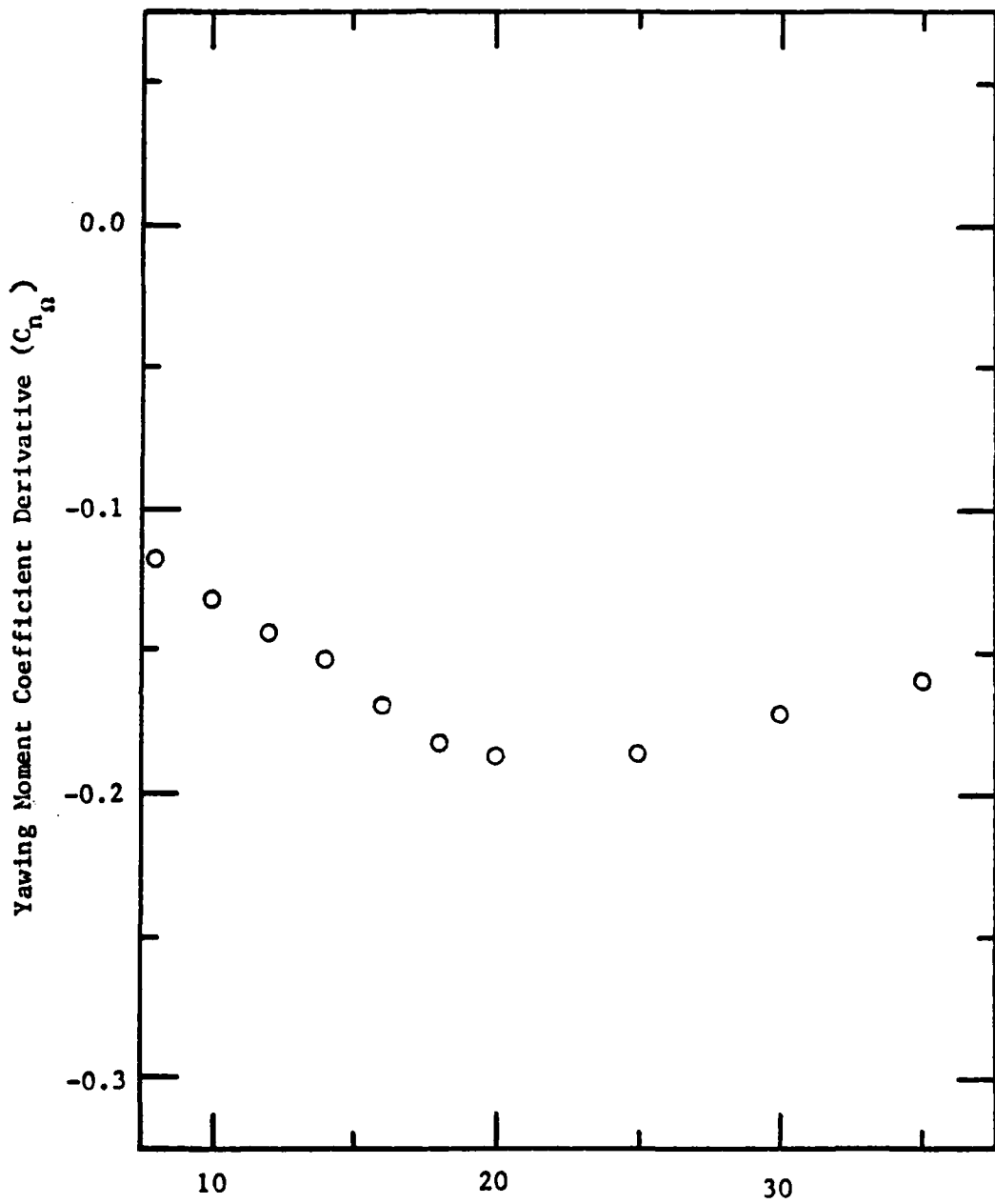


Figure 40. Rotary Balance Data:  $C_{n\dot{\alpha}}$  vs  $\alpha$



Table VII

Design Phase Data: Computation of  $C_{l_{\alpha}}$  vs  $\alpha$  ( $8^{\circ}$  -  $35^{\circ}$ )  
for 0.2M

$\alpha$	$C_{l_p}$	$C_{l_r}$	$C_{l_p} \cos \alpha$	$C_{l_r} \sin \alpha$	$C_{l_{\alpha}}$
$8^{\circ}$	-0.300	0.094	-0.297	0.013	-0.284
$10^{\circ}$	-0.302	0.110	-0.297	0.174	-0.278
$12^{\circ}$	-0.260	0.124	-0.254	0.026	-0.229
$14^{\circ}$	-0.203	0.138	-0.197	0.033	-0.164
$16^{\circ}$	-0.179	0.155	-0.172	0.043	-0.129
$18^{\circ}$	-0.173	0.143	-0.165	0.044	-0.120
$20^{\circ}$	-0.165	0.125	-0.155	0.043	-0.112
$25^{\circ}$	-0.105	0.156	-0.095	0.066	-0.029
$30^{\circ}$	-0.130	0.184	-0.113	0.092	-0.021
$35^{\circ}$	-0.170	0.194	-0.139	0.111	-0.028

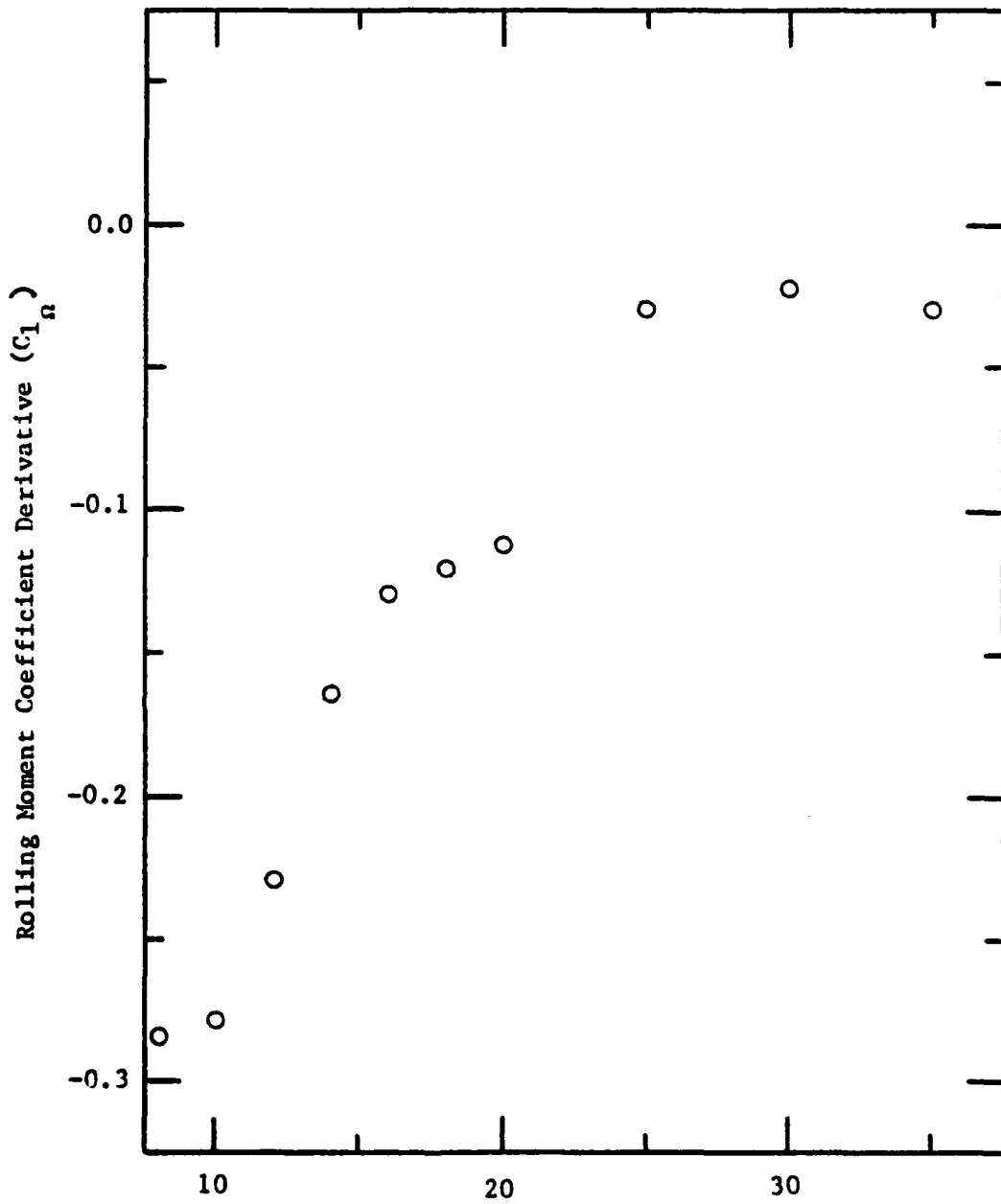


Figure 41. Design Phase Data:  $C_{1_n}$  vs  $\alpha$  for 0.2M

Table VIII

Design Phase Data: Computation of  $C_{n_{\alpha}}$  vs  $\alpha$  ( $8^{\circ}$  -  $35^{\circ}$ )  
for  $0.2M_{\alpha}$

$\alpha$	$C_{n_p}$	$C_{n_r}$	$C_{n_p} \cos \alpha$	$C_{n_r} \sin \alpha$	$C_{n_{\alpha}}$
$8^{\circ}$	-0.032	-0.386	-0.031	-0.053	-0.085
$10^{\circ}$	-0.008	-0.379	-0.007	-0.065	-0.074
$12^{\circ}$	0.022	-0.357	0.022	-0.074	-0.053
$14^{\circ}$	0.040	-0.343	0.039	-0.083	-0.044
$16^{\circ}$	0.046	-0.325	0.044	-0.090	-0.045
$18^{\circ}$	0.044	-0.308	0.042	-0.095	-0.053
$20^{\circ}$	0.036	-0.285	0.034	-0.097	-0.064
$25^{\circ}$	0.030	-0.190	0.027	-0.080	-0.053
$30^{\circ}$	0.012	-0.100	0.010	-0.050	-0.040
$35^{\circ}$	0.003	-0.100	0.002	-0.057	-0.055

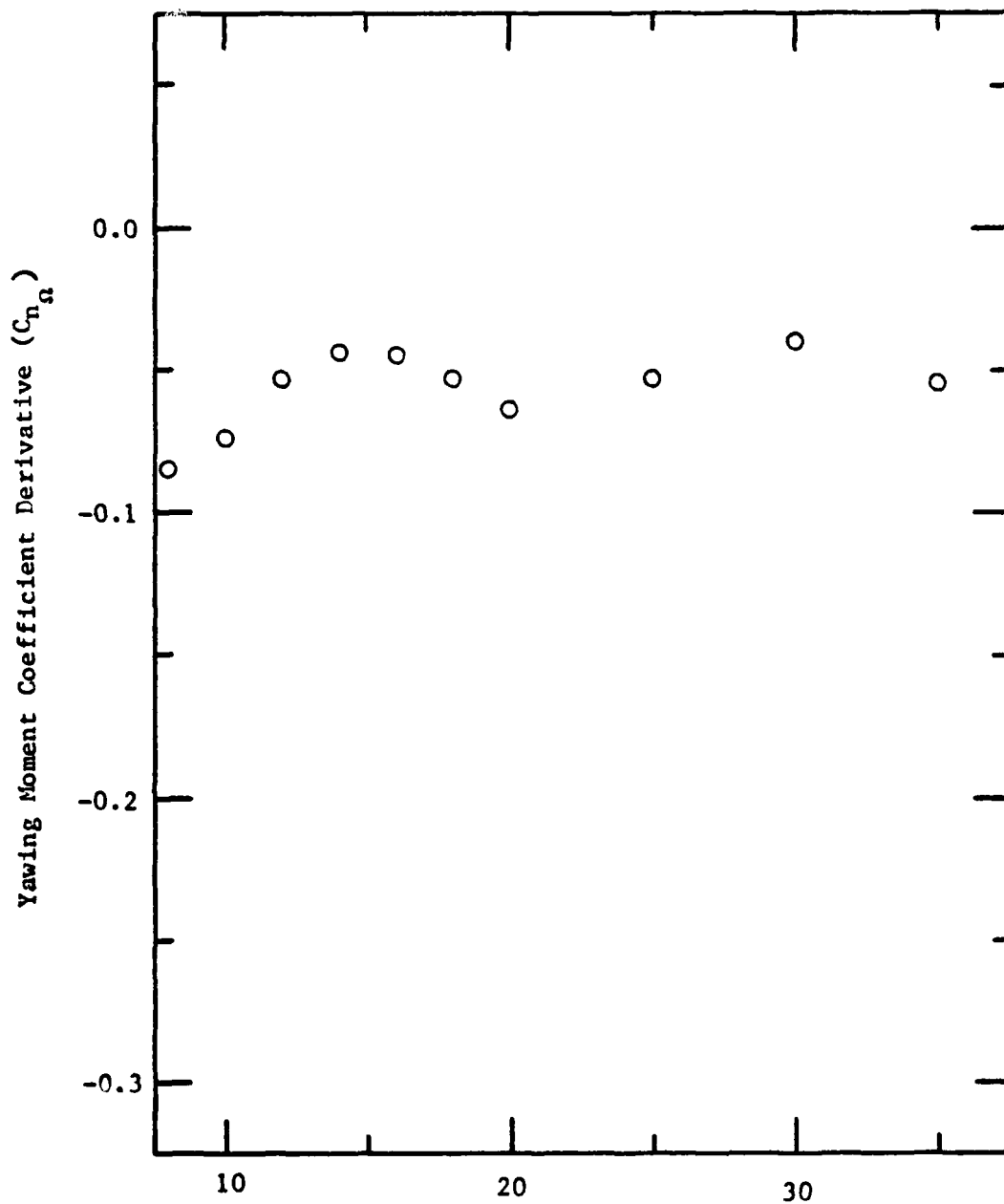


Figure 42. Design Phase Data:  $C_{n_\Omega}$  vs  $\alpha$  for 0.2M

Table IX

Design Phase Data: Computation of  $C_{1\Omega}$  vs  $\alpha$  ( $8^\circ - 35^\circ$ )  
for 0.6M

$\alpha$	$C_{1p}$	$C_{1r}$	$C_{1p} \cos \alpha$	$C_{1r} \sin \alpha$	$C_{1\Omega}$
$8^\circ$	-0.263	0.122	-0.260	0.017	-0.243
$10^\circ$	-0.253	0.142	-0.249	0.025	-0.224
$12^\circ$	-0.243	0.157	-0.238	0.033	-0.205
$14^\circ$	-0.238	0.170	-0.231	0.041	-0.190
$16^\circ$	-0.243	0.178	-0.234	0.049	-0.185
$18^\circ$	-0.253	0.183	-0.241	0.057	-0.184
$20^\circ$	-0.258	0.183	-0.242	0.063	-0.180
$25^\circ$	-0.166	0.170	-0.150	0.072	-0.079
$30^\circ$	-0.175	0.180	-0.152	0.090	-0.062
$35^\circ$	-0.195	0.190	-0.160	0.109	-0.051

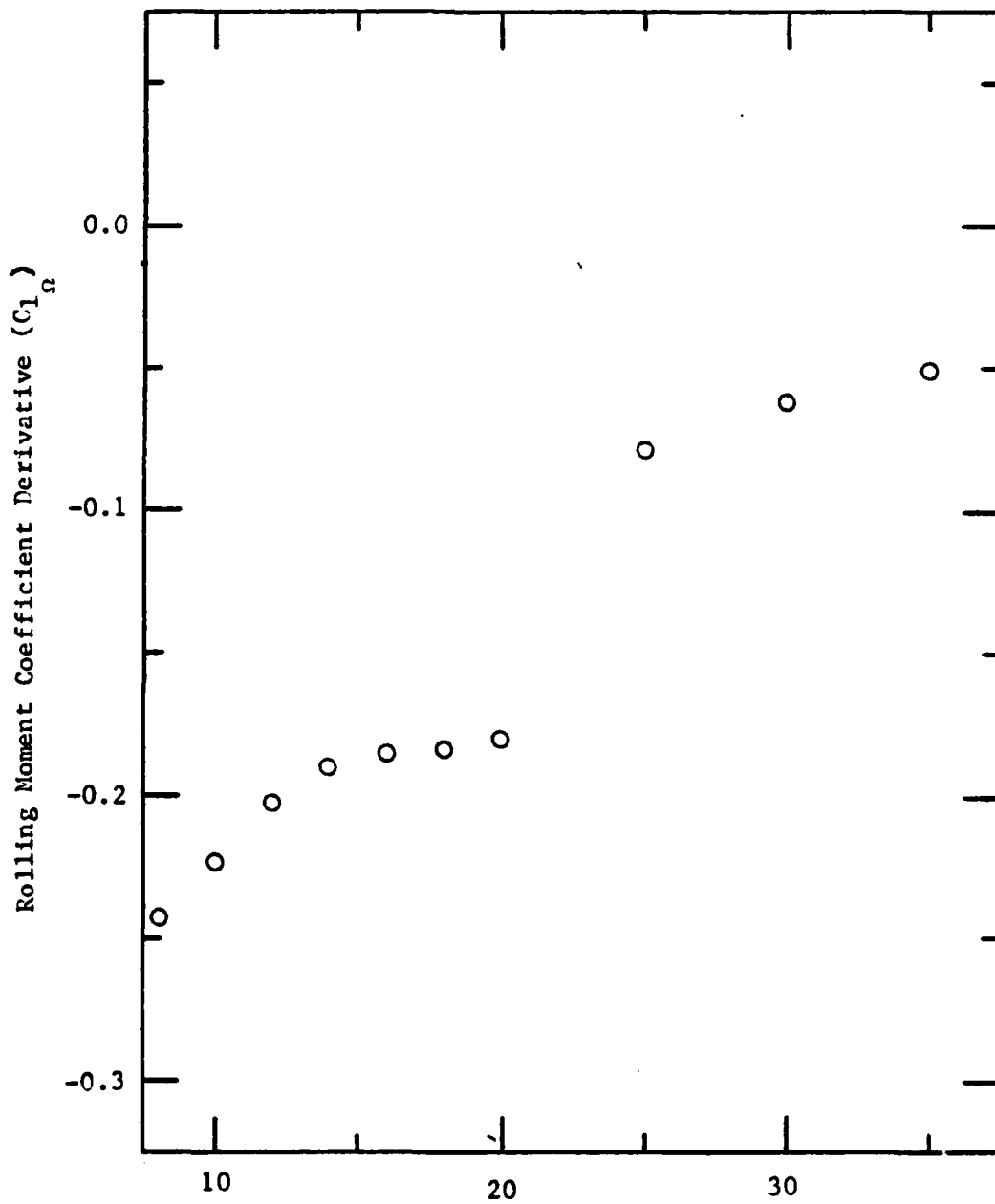


Figure 43. Design Phase Data:  $C_{1\Omega}$  vs  $\alpha$  for 0.6M

Table X

Design Phase Data: Computation of  $C_{n_{\Omega}}$  vs  $\alpha$  ( $8^{\circ}$  -  $35^{\circ}$ )  
for  $0.6M_{\Omega}$

$\alpha$	$C_{n_p}$	$C_{n_r}$	$C_{n_p} \cos \alpha$	$C_{n_r} \sin \alpha$	$C_{n_{\Omega}}$
$8^{\circ}$	-0.031	-0.276	-0.031	-0.038	-0.069
$10^{\circ}$	-0.001	-0.272	-0.001	-0.047	-0.048
$12^{\circ}$	0.014	-0.273	0.014	-0.057	-0.043
$14^{\circ}$	0.018	-0.275	0.017	-0.067	-0.049
$16^{\circ}$	0.018	-0.279	0.017	-0.077	-0.060
$18^{\circ}$	0.017	-0.272	0.016	-0.084	-0.068
$20^{\circ}$	0.014	-0.247	0.013	-0.084	-0.071
$25^{\circ}$	0.003	-0.174	0.003	-0.074	-0.071
$30^{\circ}$	0.000	-0.170	0.000	-0.085	-0.085
$35^{\circ}$	0.000	-0.170	0.000	-0.098	-0.098

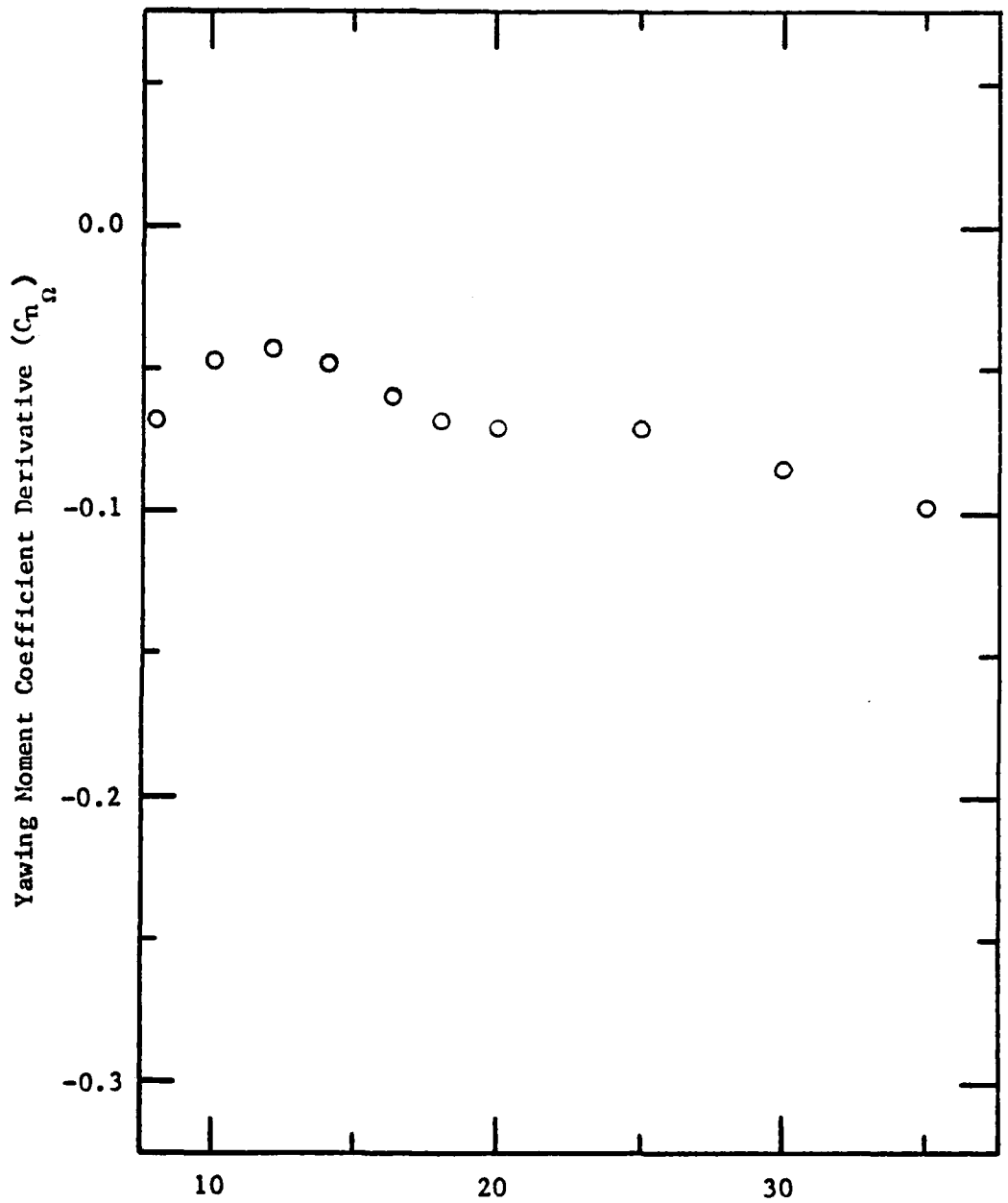


Figure 44. Design Phase Data:  $C_{n\dot{\alpha}}$  vs  $\alpha$  for 0.6M



Table XI

Production Phase Data: Computation of  $C_{1\alpha}$  vs  $\alpha$  ( $8^\circ - 35^\circ$ )  
for 0.3M

$\alpha$	$C_{1p}$	$C_{1r}$	$C_{1p} \cos \alpha$	$C_{1r} \sin \alpha$	$C_{1\alpha}$
$8^\circ$	-0.231	0.102	-0.229	0.014	-0.2146
$10^\circ$	-0.239	0.118	-0.235	0.020	-0.2149
$12^\circ$	-0.260	0.133	-0.254	0.028	-0.2267
$14^\circ$	-0.049	0.145	-0.047	0.035	-0.0125
$16^\circ$	-0.165	0.150	-0.158	0.041	-0.1173
$18^\circ$	-0.250	0.141	-0.237	0.043	-0.1942
$20^\circ$	-0.250	0.108	-0.234	0.036	-0.1980
$25^\circ$	-0.052	0.015	-0.047	0.006	-0.0408
$30^\circ$	-0.066	0.014	-0.057	0.007	-0.0502
$35^\circ$	-0.107	0.057	-0.087	0.032	-0.0550

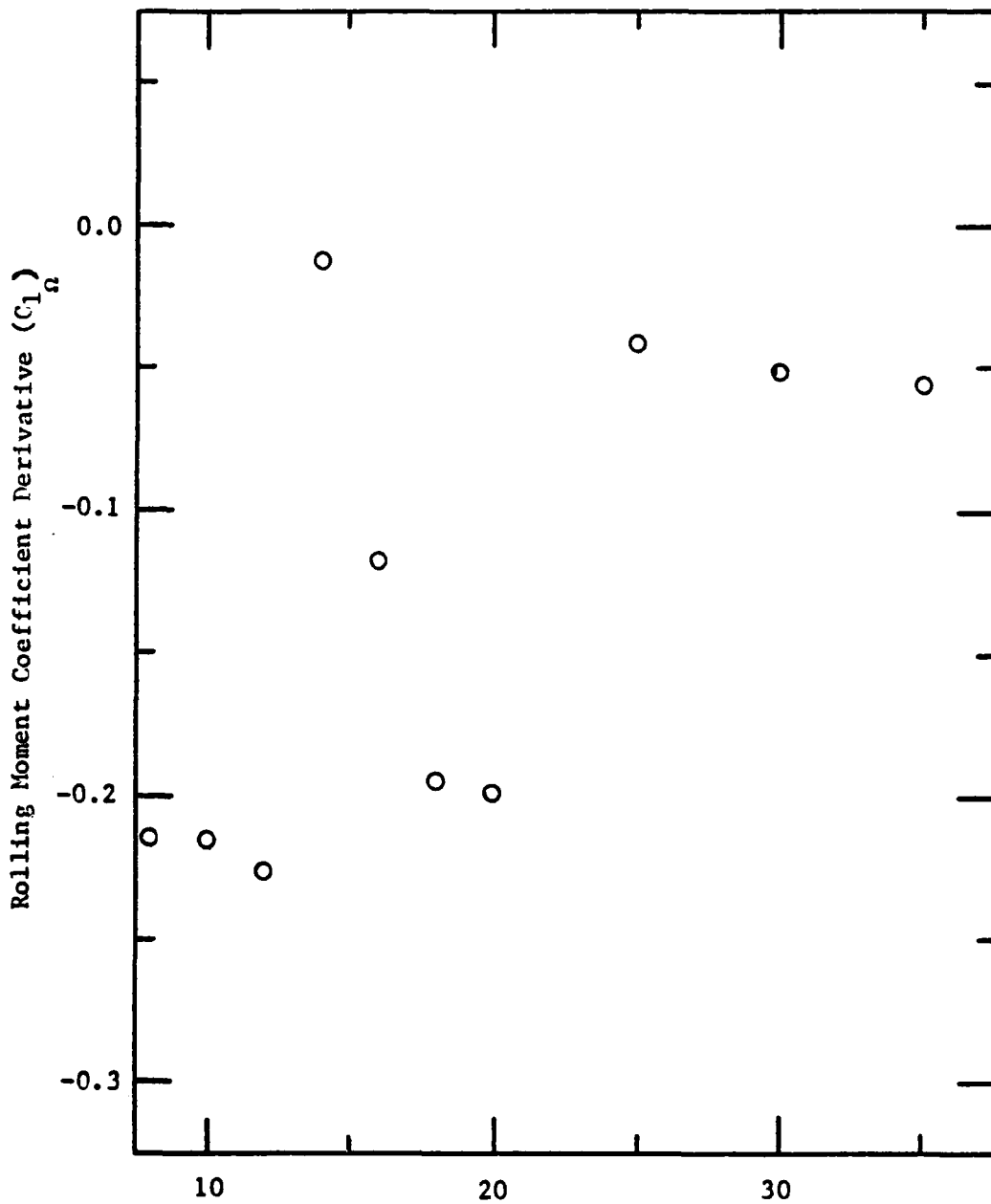


Figure 45. Production Phase Data:  $C_{1\alpha}$  vs  $\alpha$  for 0.3M

Table XII

Production Phase Data: Computation of  $C_{n\Omega}$  vs  $\alpha$  ( $8^\circ - 35^\circ$ )  
for 0.3M

$\alpha$	$C_{n_p}$	$C_{n_r}$	$C_{n_p} \cos \alpha$	$C_{n_r} \sin \alpha$	$C_{n\Omega}$
$8^\circ$	-0.033	-0.275	-0.032	-0.038	-0.0710
$10^\circ$	-0.023	-0.270	-0.022	-0.046	-0.0695
$12^\circ$	-0.019	-0.310	-0.018	-0.064	-0.0830
$14^\circ$	-0.027	-0.428	-0.026	-0.103	-0.1297
$16^\circ$	-0.049	-0.438	-0.047	-0.120	-0.1678
$18^\circ$	-0.073	-0.449	-0.069	-0.138	-0.2082
$20^\circ$	-0.103	-0.459	-0.096	-0.157	-0.2538
$25^\circ$	-0.113	-0.299	-0.102	-0.126	-0.2288
$30^\circ$	-0.083	-0.148	-0.071	-0.074	-0.1459
$35^\circ$	-0.021	0.000	-0.017	0.000	-0.0172

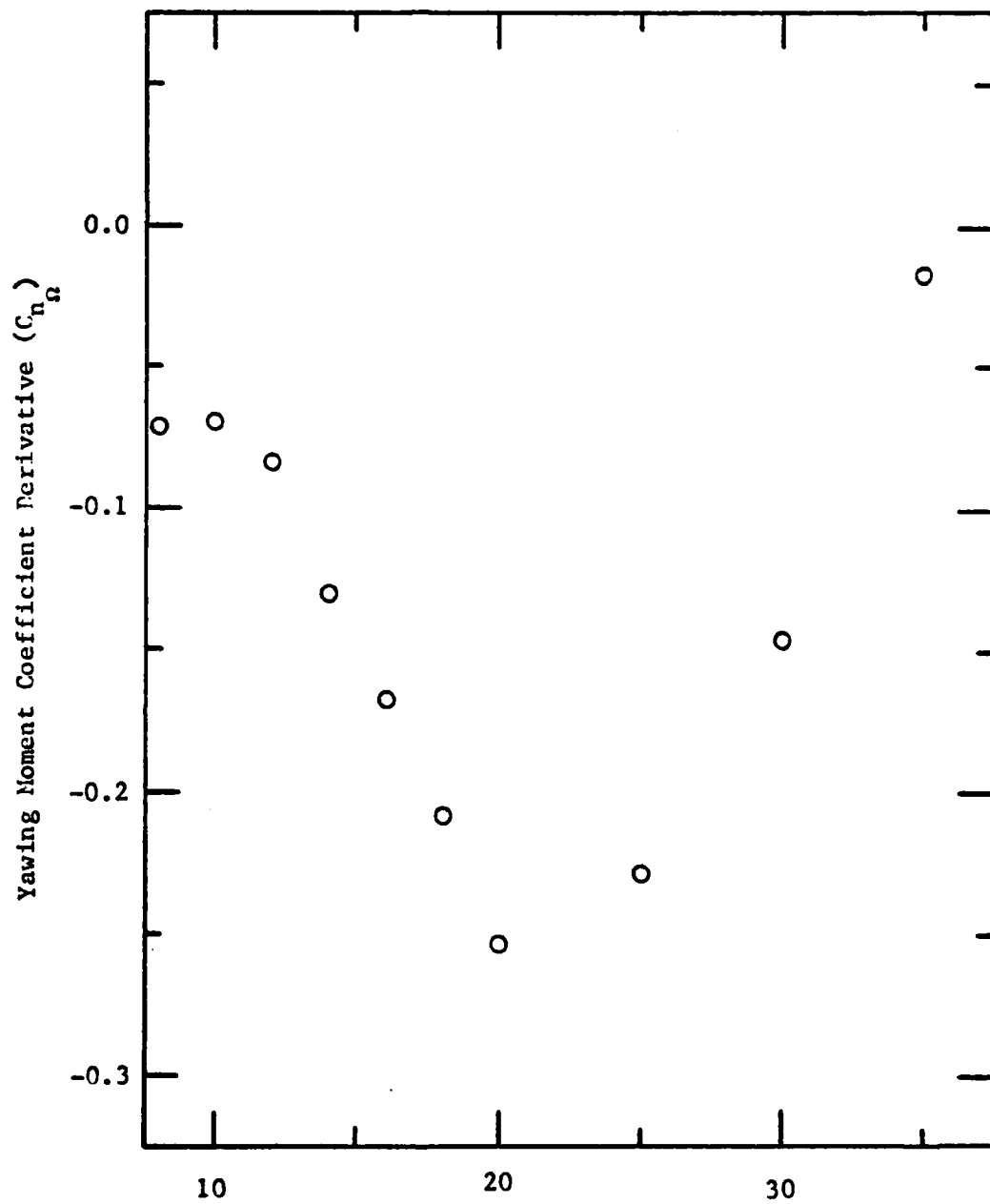


Figure 46. Production Phase Data:  $C_{n_\Omega}$  vs  $\alpha$  for 0.3M

Table XIII

Production Phase Data: Computation of  $C_{1\alpha}$  vs  $\alpha$  ( $8^\circ - 35^\circ$ )  
for 0.6M

$\alpha$	$C_{1p}$	$C_{1r}$	$C_{1p} \cos \alpha$	$C_{1r} \sin \alpha$	$C_{1\alpha}$
$8^\circ$	-0.260	0.125	-0.257	0.017	-0.2401
$10^\circ$	-0.250	0.139	-0.246	0.024	-0.2221
$12^\circ$	-0.113	0.155	-0.110	0.032	-0.0783
$14^\circ$	-0.125	0.165	-0.121	0.039	-0.0814
$16^\circ$	-0.147	0.173	-0.141	0.047	-0.0936
$18^\circ$	-0.189	0.160	-0.179	0.049	-0.1303
$20^\circ$	-0.251	0.124	-0.235	0.042	-0.1935
$25^\circ$	-0.053	0.017	-0.048	0.007	-0.0408
$30^\circ$	-0.066	0.014	-0.057	0.007	-0.0502
$35^\circ$	-0.108	0.057	-0.088	0.032	-0.0558

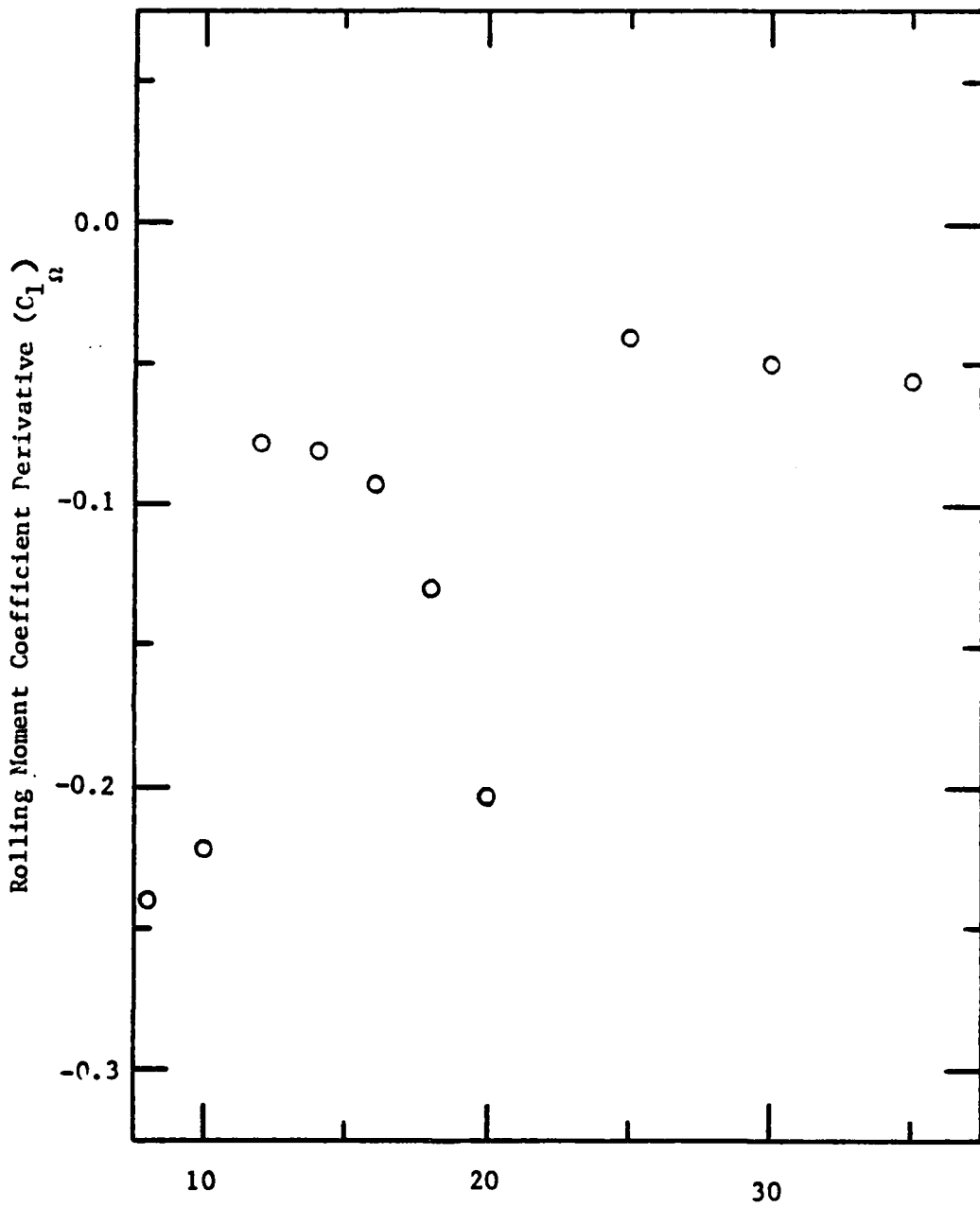


Figure 47. Production Phase Data:  $C_{1\Omega}$  vs  $\alpha$  for 0.6M

Table XIV

Production Phase Data: Computation of  $C_{n_{\Omega}}$  vs  $\alpha$  ( $8^{\circ}$  -  $35^{\circ}$ )  
for 0.6M

$\alpha$	$C_{n_p}$	$C_{n_r}$	$C_{n_p} \cos \alpha$	$C_{n_r} \sin \alpha$	$C_{n_{\Omega}}$
$8^{\circ}$	-0.040	-0.275	-0.040	-0.038	-0.0779
$10^{\circ}$	-0.001	-0.270	-0.001	-0.046	-0.0479
$12^{\circ}$	-0.015	-0.310	0.014	-0.064	-0.0498
$14^{\circ}$	0.014	-0.427	0.013	-0.103	-0.0897
$16^{\circ}$	-0.003	-0.438	-0.002	-0.120	-0.1236
$18^{\circ}$	-0.051	-0.449	-0.048	-0.138	-0.1873
$20^{\circ}$	-0.069	-0.459	-0.064	-0.156	-0.2218
$25^{\circ}$	-0.113	-0.300	-0.102	-0.126	-0.2292
$30^{\circ}$	-0.083	-0.150	-0.071	-0.075	-0.1469
$35^{\circ}$	-0.041	0.000	-0.033	0.000	-0.0336

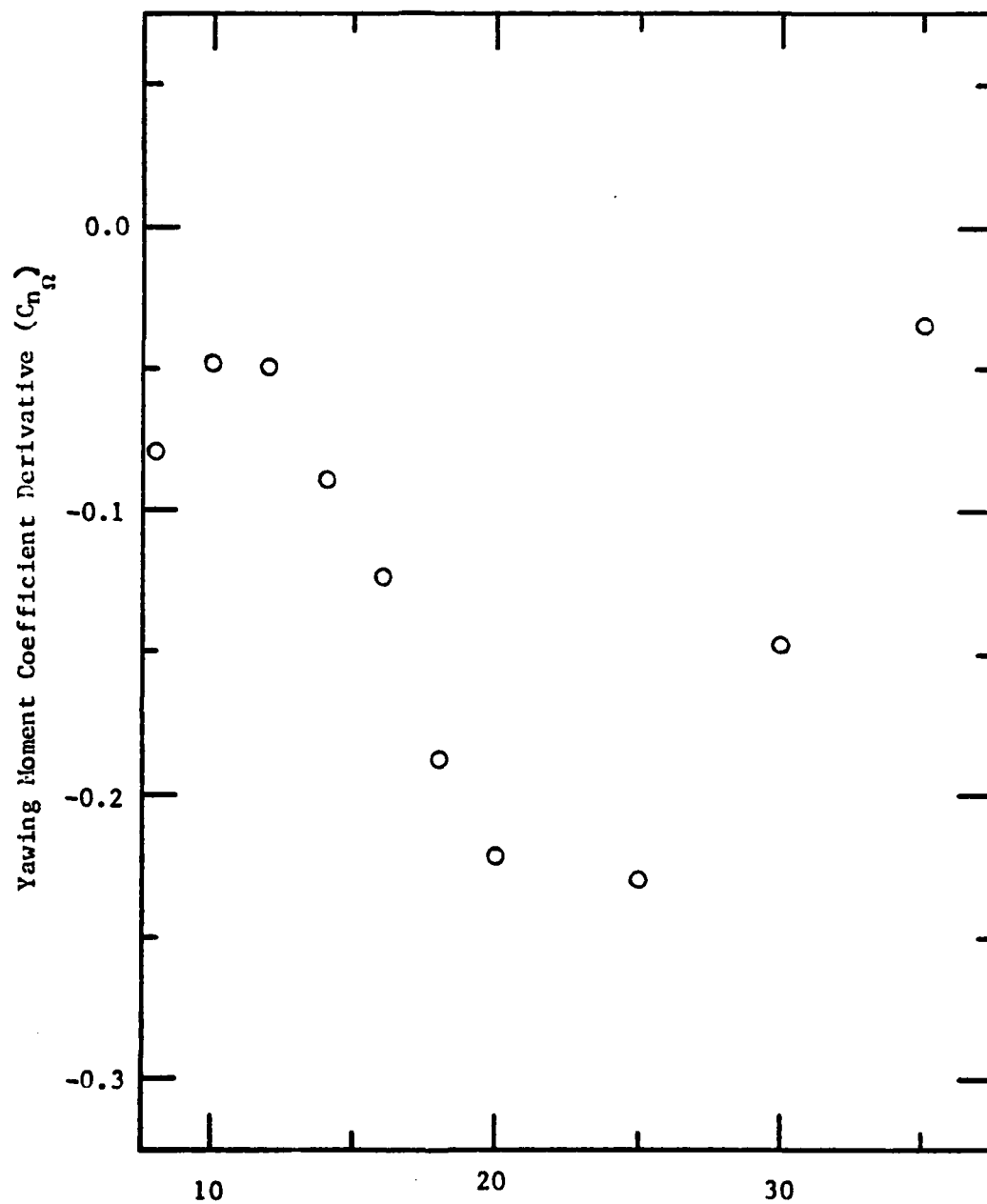


Figure 48. Production Phase Data:  $C_{n_\Omega}$  vs  $a$  for 0.6M



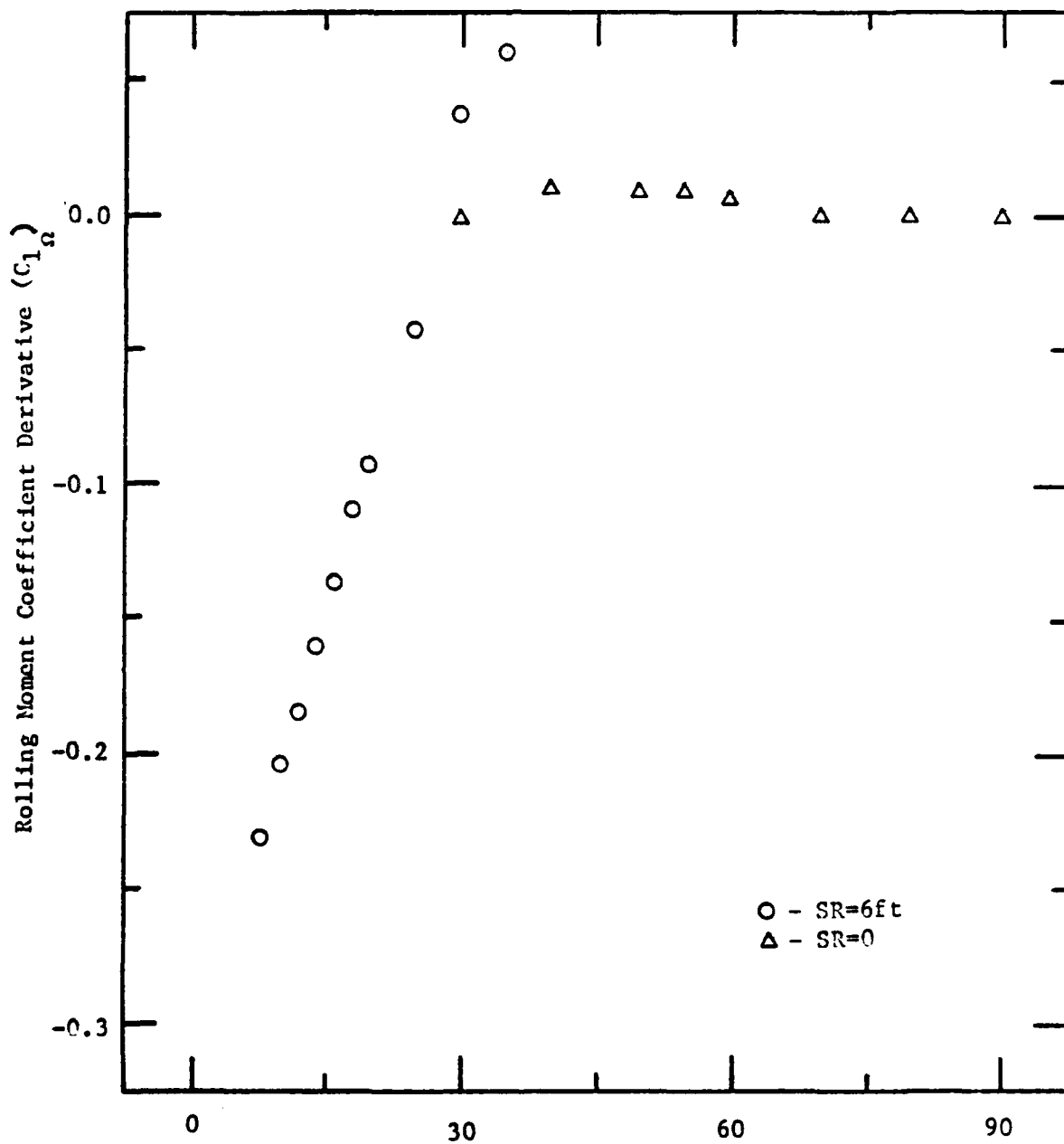


Figure 49. Rotary Balance Data:  $C_{1\Omega}$  vs  $\alpha$  ( $8^\circ$  -  $90^\circ$ )

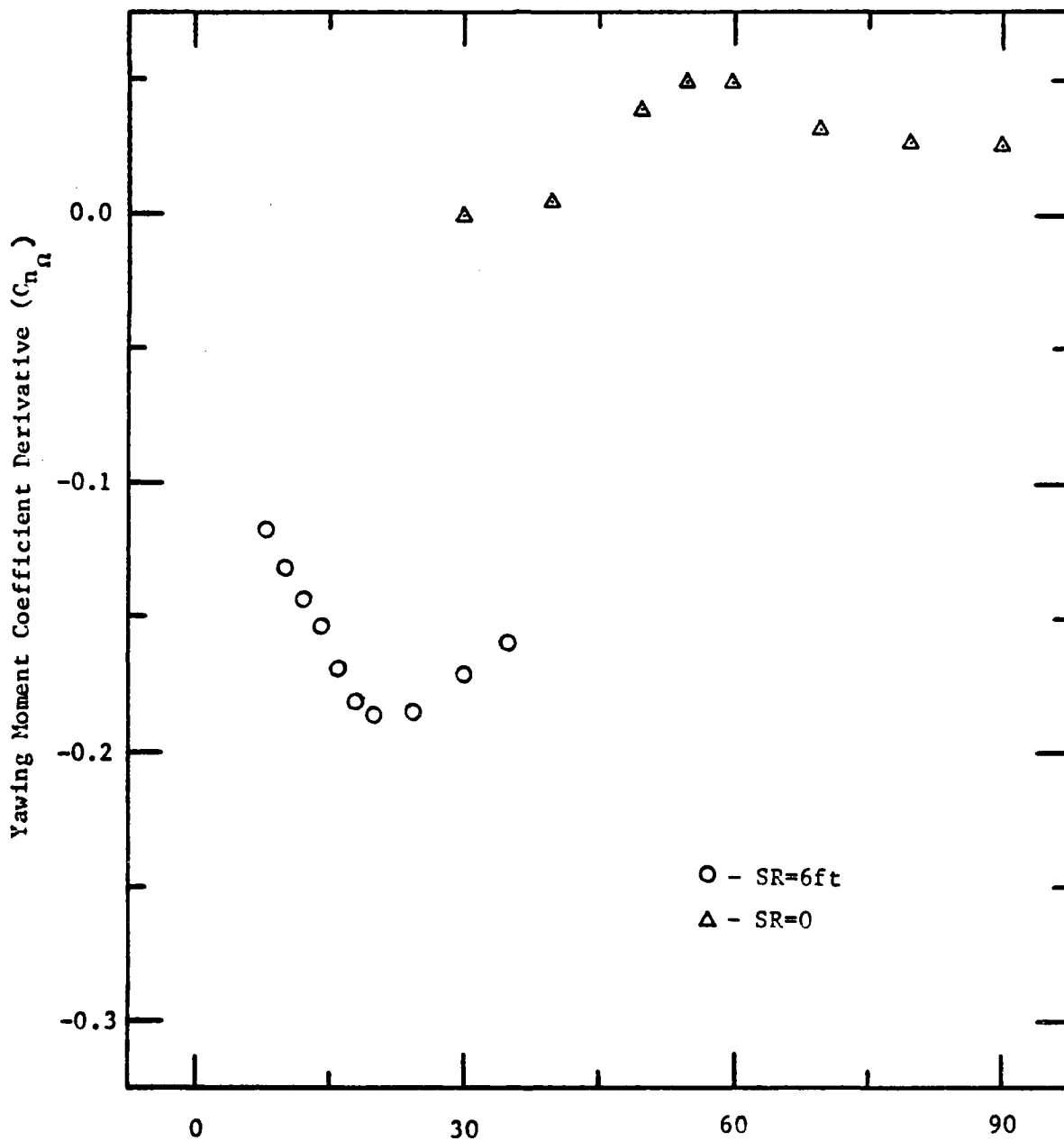


Figure 50. Rotary Balance Data:  $C_{n_{\Omega}}$  vs  $\alpha$  ( $8^{\circ}$ - $90^{\circ}$ )

AD-A136 913

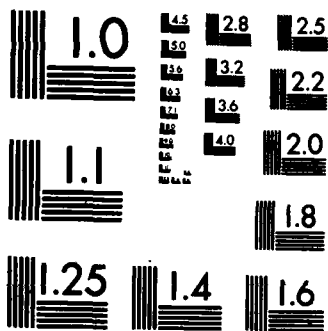
THE EFFECT OF CONSTANT VERSUS OSCILLATORY RATES ON  
DYNAMIC STABILITY DERIVATIVES<U> AIR FORCE INST OF TECH  
WRIGHT-PATTERSON AFB OH SCHOOL OF ENGI... M S LARSON  
DEC 83 AFIT/GAE/ENV/83D-11 F/G 20/4

2/2

UNCLASSIFIED

NL





MICROCOPY RESOLUTION TEST CHART  
NATIONAL BUREAU OF STANDARDS-1963-A

## Bibliography

1. Campbell, John P., and Marion O. McKinney. "Summary of Methods for Calculating Dynamic Lateral Stability and Response and for Estimating Lateral Stability Derivatives, Thirty-Eighth Annual Report of the National Advisory Committee on Aeronautics; Report 1098. Washington: Government Printing Office, 1954.
2. Burbage, Paul, et al. "The Battle for the Skies Over North Vietnam," USAF Southeast Asia Monograph Series, Volume I, edited by Lt Col Gordon Nelson and Major Norm Wood. Washington, D.C.: Government Printing Office, 1976.
3. Air Force Flight Dynamics Laboratory. USAF Stability and Control Datcom. Wright-Patterson Air Force Base, Ohio 45433: Air Force Flight Dynamics Laboratory, October 1960 (Revised August 1968).
4. Roskam, J. Methods for Estimating Stability and Control Derivatives of Conventional Subsonic Airplanes. Lawrence, Kansas: Roskam Aviation and Engineering Corporation, 1973.
5. Orlik-Rukemann, K.J. "Techniques for Dynamic Stability Testing in Wind Tunnels," Proceedings of the Fluid Dynamics Panel Symposium, AGARD Conference Proceedings No. 235. London: Technical Editing and Reproduction Ltd., 1978.
6. Bihrlé, William, Jr. "Spin Prediction Techniques," AIAA Journal of Aircraft, 20: 97-101 (February 1983). (AIAA Paper No. 80-1564).
7. McRuer, Duane., et al. Aircraft Dynamics and Automatic Control. Princeton: Princeton University Press, 1973.
8. Bisplinghoff, Raymond L., et al. Aeroelasticity. Cambridge: Addison-Wesley Publishing Company, 1955.
9. Etkin, Bernard. Dynamics of Atmospheric Flight. New York: John Wiley and Sons, Inc., 1972.
10. Barnhart, Billy. F-15 Rotary Balance Data for an Angle-of-Attack Range of 8 to 90 . NASA Contractor Report 3478, Prepared for Langley Research Center by Bihrlé Applied Research, Inc., Jericho, New York,

1982.

11. McDonnell Aircraft Company. F-15 Stability Derivatives Mass and Inertia Characteristics, Part III, Flexible Aerodynamic Coefficient and Stability Derivative Data. Report Number MDC A0502, Contract Number F33657-70-C-0300, McDonnell Aircraft Company, St. Louis, MO, 30 June 1970 (Revised 10 February 1972 and 10 May 1972).
12. Air Force Flight Dynamics Laboratory. "USAF Stability and Control Datcom," USAF WADC TR 60-261. October 1960 (Revised July 1963).
13. Wiggins, J.W. "Wind Tunnel Investigation at High Subsonic Speeds to Determine the Rolling Derivatives of Two Wing Fuselage Combinations Having Triangular Wings, Including a Semi-Empirical Method of Estimating the Rolling Derivatives," NACA RM L53 L18a, February 1954.
14. Wykes, John H., et al. "An Analytical Study of the Dynamics of the Spinning Aircraft, Part I," USAF WADC TR 58-381. December 1958.
15. McDonnell Aircraft Company. F/TF-15 Stability Derivatives, Mass and Inertia Characteristics, Flight Test Data Basis, Part II, Aerodynamic Coefficients and Stability and Control Derivatives. Report Number MDC A4172, Contract Number F33657-70-C-0300, McDonnell Aircraft Company, St. Louis, MO, 1 August 1976 (Revised 4 October 1979).

VITA

Michael Scott Larson was born on 8 February 1952 in Boulder, Colorado. He graduated from high school in St. Joseph, Missouri in 1970 and attended the United States Air Force Academy from which he received the degree of Bachelor of Science in Aeronautical Engineering in June 1974. Upon graduation, he entered Undergraduate Pilot Training and received his wings in July 1976. He then served as a T-37B instructor pilot in the 37th Flying Training Squadron, Columbus AFB, Mississippi until November 1979 and as a C-141 copilot in the 53rd Military Airlift Squadron, Norton AFB, California until December 1980. He then was assigned to the Ballistic Missile Office at Norton as a Project Officer until entering the School of Engineering, Air Force Institute of Technology, in June 1982.

Unclassified

SECURITY CLASSIFICATION OF THIS PAGE

REPORT DOCUMENTATION PAGE

1a. REPORT SECURITY CLASSIFICATION Unclassified		1b. RESTRICTIVE MARKINGS	
2a. SECURITY CLASSIFICATION AUTHORITY		3. DISTRIBUTION/AVAILABILITY OF REPORT Approved for public release; distribution unlimited	
2b. DECLASSIFICATION/DOWNGRADING SCHEDULE			
4. PERFORMING ORGANIZATION REPORT NUMBER(S) AFIT/GAE/ENY/83D-11		5. MONITORING ORGANIZATION REPORT NUMBER(S)	
6a. NAME OF PERFORMING ORGANIZATION School of Engineering Air Force Institute of Technology	6b. OFFICE SYMBOL (If applicable) AFIT/EN	7a. NAME OF MONITORING ORGANIZATION	
6c. ADDRESS (City, State and ZIP Code) Wright-Patterson AFB, Ohio 45433		7b. ADDRESS (City, State and ZIP Code)	
8a. NAME OF FUNDING/SPONSORING ORGANIZATION	8b. OFFICE SYMBOL (If applicable)	9. PROCUREMENT INSTRUMENT IDENTIFICATION NUMBER	
8c. ADDRESS (City, State and ZIP Code)		10. SOURCE OF FUNDING NOS.	
		PROGRAM ELEMENT NO.	PROJECT NO.
		TASK NO.	WORK UNIT NO.
11. TITLE (Include Security Classification) See Block 19			
12. PERSONAL AUTHOR(S) Michael S. Larson, Captain, USAF			
13a. TYPE OF REPORT MS Thesis	13b. TIME COVERED FROM _____ TO _____	14. DATE OF REPORT (Yr., Mo., Day) 1983 December	15. PAGE COUNT 104
16. SUPPLEMENTARY NOTATION Approved for public release: IAW AFR 150-47. Lynn E. W. CLAVER Dean for Research and Professional Development Air Force Institute of Technology (AFIT) Wright-Patterson AFB, Ohio			
17. COSATI CODES		18. SUBJECT TERMS (Continue on reverse if necessary and identify by block number)	
FIELD	GROUP	Stability Derivatives, Dynamic Lateral Stability, Rotary Balance, Spin Tunnel	
01	03		
19. ABSTRACT (Continue on reverse if necessary and identify by block number) Title: THE EFFECT OF CONSTANT VS OSCILLATORY RATES ON DYNAMIC STABILITY DERIVATIVES Thesis Chairman: Dr Robert Calico			
20. DISTRIBUTION/AVAILABILITY OF ABSTRACT CLASSIFIED/UNLIMITED <input checked="" type="checkbox"/> SAME AS RPT. <input type="checkbox"/> DTIC USERS <input type="checkbox"/>		21. ABSTRACT SECURITY CLASSIFICATION Unclassified	
22a. NAME OF RESPONSIBLE INDIVIDUAL Robert C. Calico, Dr		22b. TELEPHONE NUMBER (Include Area Code) 52362	22c. OFFICE SYMBOL AFIT/ENY



The purpose of this thesis was to determine whether or not there are phenomenological differences between dynamic derivatives calculated from F-15A rotary balance data and data from other sources.

To make this determination, two additional data sets were obtained: (1) the F-15A design phase stability derivative data, and (2) the F-15A production phase stability derivative data. The lateral dynamic derivatives were then compared through derivatives of the lateral moments with respect to the rotation rate about the velocity vector (wind vector).

The conclusion of the project was that differences exist between the data sets, but that the dominant characteristics were the same for all of the data sets; the differences in the data were not indicative of basic (phenomenological) differences in the data itself. Therefore, the contention that oscillatory rates affect determination of the dynamic derivatives was not substantiated by this study.

END

FILMED

2-84

DTIC